GOUGH ISLAND:

EVALUATION OF A FRACTIONAL CRYSTALLIZATION MODEL

and

AN EXPERIMENTAL STUDY OF THE PARTITIONING

OF A RARE EARTH ELEMENT IN THE SYSTEM DIOPSIDE/WATER

by

ROBERT A. ZIELINSKI

B.A. RUTGERS UNIVERSITY

(1967)

SUBMITTED TO THE DEPARTMENT OF EARTH AND PLANETARY SCIENCES

IN PARTIAL FULFILLMENT

OF THE REQUIREMENTS FOR THE

DEGREE OF

DOCTOR OF PHILOSOPHY

at the

MASSACHUSETTS INSTITUTE OF TECHNOLOGY

September, 1972

Signature of Author _____
Department of Earth and Planetary Sciences

Certified by _____
Thesis Supervisor

Accepted by _____
Chairman, Departmental Committee
on Graduate Students

GOUGH ISLAND:

EVALUATION OF A FRACTIONAL CRYSTALLIZATION MODEL

and

AN EXPERIMENTAL STUDY OF THE PARTITIONING

OF A RARE EARTH ELEMENT IN THE SYSTEM DIOPSIDE/WATER

by

ROBERT A. ZIELINSKI

SUBMITTED TO THE DEPARTMENT OF EARTH AND PLANETARY SCIENCES

IN PARTIAL FULFILLMENT

OF THE REQUIREMENTS FOR THE

DEGREE OF

DOCTOR OF PHILOSOPHY

ABSTRACT

Part 1

Gough Island is composed of an alkaline olivine basalt-trachyte series. A fractional crystallization model for the development of these rocks has been evaluated by correlating the geochemical trends of major and trace elements. Beginning with an alkali olivine basalt parent the major element abundances were used to determine the varying proportions of crystallizing minerals required to generate the various residual liquids. A least-squares computer model was used for this calculation. The modal proportions of cumulative minerals and trace element distribution coefficients were used to predict the trace element abundances in each rock type.

(Cont.)

Thesis Supervisor: F.A. Frey
Title: Associate Professor of Geochemistry

Three significant trace element trends are observed in Gough Island rocks: (1) increasing rare earth (RE) abundance and relative light RE enrichment with increasing major element differentiation, (2) marked Eu, Sr, and Ba depletions in late stage trachytes, (3) Cr and Ni enrichment in picritic basalt.

The trace element abundances predicted by the fractional crystallization model are in good agreement with these observed trends. A fractional crystallization process involving olivine, pyroxene, feldspar and apatite accounts for all the significant major and trace element trends observed in Gough Island rocks.

Part 2

The partitioning of Gd in the experimental system diopside/ water as a function of a number of variables including temperature, pressure, composition of the phases, time, grain size, solid/liquid ratio and Gd concentration has been investigated. The intention of the study was to investigate the feasibility of determining trace element partition coefficients by this technique. A radioactive tracer measurement was used to determine Gd concentration in the separated phases. Diopsides were first equilibrated with trace solution and reversability was tested by re-equilibrating Gd-doped diopsides with pure water.

Equilibration of Gd between the bulk of the diopside and the liquid was found to be limited by the slow rate of Gd diffusion in diopside, estimated at $D < 2 \times 10^{-15}$ cm^2sec^{-1} at 800°C. Depending on whether the diopside was previously synthesized or synthesized from an oxide mix during the experiment, Gd concentrations were zoned in the crystal such that higher concentrations existed at the edges or center, respectively. As a result, measurement of distribution coefficients as ratios of Gd bulk concentration in both phases led to erroneous and non-constant values. The applicability of the silicate/water system for studying distribution of Gd between two phases homogeneous in Gd, is considered invalid. This conclusion almost certainly holds for the other rare earths.

Information about the kinetics and mechanisms of Gd uptake in diopside is obtainable in such a system. Increasing pressure, temperature and decreasing grain size enhance uptake. Changing the composition of the aqueous solution indicated that possible mechanisms for Gd substitution included coupling of Gd^{+3} with H^+ or Na^+ with replacement of $2Ca^{+2}$ or substitution of $2Gd^{+3}$ for $3Ca^{+2}$ with formation of a cation vacancy. Conditions which increased the amount of leaching of diopside or the kinetics of its growth from an oxide mix increased the Gd uptake.

Thesis Supervisor: F.A. Frey
Title: Associate Professor of Geochemistry

Table of Contents

Part 1

Gough Island:

Evaluation of a Fractional Crystallization Model

Part 2

An Experimental Study of the Partitioning

of a Rare Earth Element in the System Diopside/Water

Part 1

Gough Island:

Evaluation of a Fractional Crystallization Model

Introduction

Gough Island is located near the Mid-Atlantic Ridge
230 miles south-southwest of Tristan Da Cunha. It has an
area of 32 square miles and a relief of 3000 feet. R.W.
Le Maitre (1960) has distinguished 5 stratigraphic units re-
ferred to as: (1) upper "basalts", (2) upper trachytes,
(3) middle "basalts", (4) lower trachytes, (5) lower basalts".
The term"basalt" includes all rocks with basaltic ferromag-
nesian minerals. The island is unusual in that 50% of the
surface area is trachyte. Le Maitre concluded that the is-
land was built up as a series of eruptive basalt-trachyte
cycles with possibly many more cycles represented in the
10,000 feet of submerged section (Le Maitre, 1960).

Rock specimens (28) were taken for a thorough petrolo-
gical study of the rock suite (Le Maitre, 1962). Rocks were
analyzed for major elements, mineralogies described and
mineral species analyzed by x-ray, optics and chemical tech-
niques. Rocks were classified on the basis of their alkali
contents. (See Table 1a.)

From picritic basalt to trachyte, compositions of whole
rocks and minerals varied in a manner consistent with a frac-
tional crystallization model. For example, whole-rock mag-
nesium, calcium and titanium abundances decrease steadily
while sodium and potassium increase. (See Table 1b) Le
Maitre concluded that the island was an alkali olivine ba-
salt-trachyte association, and that the rocks were related

Table 1a.

Rock Type	$Na_2O + K_2O$ (%)	Na_2O (%)
Picrite basalt	<3.5	–
Olivine basalt	3.5–5.0	–
Trachybasalt	5.0–8.5	–
Trachyandesite	8.5–10.5	–
Trachyte	>10.5	5.0–5.5
Aegerine-augite Trachyte	>10.5	>5.5

Table 1b. Chemical Analyses of Rocks

	Picrite G-121	Ol. Basalt G-13	Ol.-poor Basalt G-8	Trachybas. G-164	Trachyand. G-15
SiO_2	46.57	47.85	51.05	51.46	55.80
TiO_2	1.85	3.40	2.55	2.69	1.87
Al_2O_3	8.20	15.05	16.79	17.12	18.41
Fe_2O_3	1.20	3.44	3.85	2.96	3.07
FeO	9.75	7.23	5.26	6.05	3.78
MnO	0.14	0.10	0.12	0.15	0.09
MgO	19.65	8.51	4.30	4.03	2.13
CaO	9.43	8.00	8.97	5.94	5.07
Na_2O	1.56	2.90	3.26	4.06	4.57
K_2O	1.18	1.97	2.37	3.69	4.30
P_2O_5	0.26	0.29	0.34	0.26	0.23
H_2O+	0.11	0.59	0.84	1.09	0.34
H_2O-	0.12	0.47	0.66	0.26	0.26
F	0.04	-	-	-	-
Cl	-	-	-	-	-
Σ	100.06	99.80	100.36	99.76	99.92

Table 1b. Continued

	Trachyte G-114	Aeg-Aug Trachyte G-16	Aeg-Aug Trachyte G-149	Sodalite Trachyte G-19D
SiO_2	58.17	60.52	62.45	60.17
TiO_2	1.00	0.45	0.38	0.15
Al_2O_3	19.31	18.72	17.92	18.45
Fe_2O_3	1.98	2.67	2.06	3.32
FeO	3.45	2.85	3.11	2.53
MnO	-	0.19	0.16	0.23
MgO	1.05	0.52	0.09	0.04
CaO	1.84	1.87	1.17	1.44
Na_2O	5.05	5.83	6.47	7.52
K_2O	6.55	5.77	6.14	5.43
P_2O_5	0.36	0.19	0.09	0.04
H_2O+	0.84	0.32	0.16	0.31
H_2O-	0.50	0.07	0.27	0.30
F	0.07	-	-	-
Cl	-	-	0.03	0.38
Σ	100.17	99.97	100.50	100.31

by a mechanism of fractional crystallization with alkali
olivine basalt as the parent material.

The purposes of the present study were threefold. (1)
To measure whole-rock rare earth element (REE) abundances
of several Gough Island rocks in order to test a model of
fractional crystallization. Field relations and major ele-
ment variations of oceanic island rocks are often inter-
preted as a result of fractional crystallization. Yet some
trace element data (Frey et al., 1968), isotopic data (Gast
et al., 1964; Oversby and Gast, 1970), and rock type abun-
dances (Chayes, 1963) have not been interpreted as a result
of a simple fractional crystallization process. (2) To use
a least-squares computer analysis of mineral and bulk-rock
chemical compositions to calculate possible mineral addi-
tions or subtractions necessary to generate each rock type
in the proposed crystallization sequence. (3) To use min-
eral/liquid distribution coefficients for the rare earths
and other trace elements, and with computer results, to
estimate how much of each trace element was added or sub-
tracted from the system by fractional crystallization. Such
an estimate would predict trace element abundances in the re-
sidual liquids which crystallize to form the highly dif-
ferentiated rocks. Comparisons could then be made between
observed and calculated trace element abundances. General
agreement between the two would provide support for the frac-
tional crystallization model. Trace element data are useful

because trace elements are sensitive indicators of a wide range of chemical conditions. Abundances may parallel those of the major elements or respond to chemical conditions not affecting the major element content of a rock.

Sample Description

The rock samples chosen for this study were somewhat restricted by Le Maitre's sampling, but an effort was made to span the range of rock types observed at Gough Island. The sample identification numbers are Le Maitre's. In some cases, more detailed descriptions may be found in Le Maitre 1962.

G-121. A picrite basalt dike in the lower "basalt" map unit. In thin section there are abundant phenocrysts of olivine (Fa_{15}) and diopsidic augite set in a groundmass of pyroxene, feldspar (An_{67}) and opaques (Ilm_{75}).

G-13. A fine grained basalt flow of lower "basalt". Small amounts of phenocrysts of olivine (Fa_{21}), titanaugite, feldspar (An_{61}) and opaques (Ilm_{75}) set in a groundmass of similar mineralogy.

G-8. An olivine-poor basalt from a dike in the lower "basalt" unit. Phenocrysts of plagioclase (An_{57}) opaques (Ilm_{70}), titanaugite and some olivine in a fine-grained matrix of like mineralogy.

G-164. A trachybasalt flow in the lower "basalts". This rock type is the most abundant mafic unit on the island.

Olivine (Fa_{24}), titanaugite, feldspar (An_{54}) and opaques ($\sim Ilm_{66}$) are again the major phenocryst components and the intergranular groundmass consists of opaques, plagioclase laths, pyroxene, olivine and alkali feldspar.

G-15. A porphyritic trachyandesite from a dike in the lower "basalts". Abundant small phenocrysts of zoned plagioclase (An_{52}-An_{30}), olivine (Fa_{38}), titanaugite, ilmenite and and magnetite occur in an intergranular matrix of the same minerals plus alkali feldspar.

G-114. A vesicular trachyte flow of the lower trachyte unit. Some sporadic phenocrysts of feldspar (An_{26}) and alkali feldspar occur with smaller phenocrysts of olivine (Fa_{44}) opaques ($\sim Ilm_{50}$) and apatite. The rock matrix is mostly fine grained alkali feldspar plus traces of olivine and magnetite.

G-16. An aegerine-augite trachyte flow in the lower trachytes. Some sporadic phenocrysts of olivine (Fa_{62}), aegerine augite, alkali feldspar and magnetite are set in a matrix of alkali feldspar magnetite and olivine.

G-149. An aegerine-augite plug of upper trachyte. Phenocrysts are olivine ($Fa_{\sim 100}$), alkali feldspar ($Or_{35}Ab_{61}An_4$), opaques ($\sim Ilm_{20}$), aegerine-augite and apatite. Groundmass material is about 90% of the rock and is mostly alkali-feldspar.

G-19D. A sodalite-bearing aegerine-augite trachyte from the upper trachyte unit. Sodalite occurs as discrete crystals.

Texture and mineralogy similar to G-149.

Chemical analyses of the above rocks are taken from Le Maitre 1962 and reproduced in Table 1b.

Experimental Method

Determination of the rare earth elements (REE) was done using a neutron activation procedure after group chemical separation of the rare earths from the irradiated powdered rocks (Denechaud et al., 1970). Equipment utilized included a Ge(Li) detector of 26 cc active volume, a Ge(Li) low energy photon detector, and a pulse height analyzer of 10^5 counts-per-channel capacity. Resolution of the 26 cc was 2.5 Kev at the full width half maximum of the 661 Kev peak of Cs^{137}.

Errors in measuring peak areas were due to statistical uncertainties in the recording of radioactive decay events and in choice of background contributions. The size of this net error depended on the strength of individual peaks and the uniformity of background levels. Errors were compounded by the need for determination of a chemical yield factor which also involved peak area determinations and comparisons. Of the elements analyzed, error values fell into 3 groups: La, Eu, Ce, Sm, Tb, Lu±5-10%; Dy, Yb, Nd±10-20%, Gd±25%. Errors could be lowered by developing a RE separation of 100% chemical yield.

Missing values in the experimental results were due to

instrumental mishaps or problems in obtaining the use of
equipment. A more complete discussion of the experimental
technique is given in Appendix 1.

Results

The rare earth contents of the various rock types are
given in Table 2 and plotted normalized to chondrites in
Figs. 1 and 2. The figures indicate that all the Gough
Island rocks analyzed have RE distributions which are light-
rare-earth enriched relative to chondrites. The strong light
RE enrichment is characteristic of alkali olivine basalts.
In contrast, tholeiitic basalts dredged from the axis of the
Mid-Atlantic Ridge have distributions with light RE deple-
tions (Frey et al., 1968). It is this distinct difference
in trace element abundances between tholeiitic and alkali
olivine basalts which has been useful in understanding the
mechanisms of volcanic rock formation along ocean ridges
(e.g., Gast, 1968).

The basalts (Fig. 1) have similar relative RE distribu-
tions. Throughout the series the absolute abundaces of REE,
and the degree of light RE enrichment increases as the whole-
rock alkali content increases. The trends are consistent
with the hypothesis that the rocks are related by some mecha-
nism to a common parent. Similar trends have been noted for
rocks clearly related as in NW Germany (Herrmann, 1968),
Hawaii (Schilling and Winchester, 1966) and Siberia (Balashov

Table 2. Rare Earth Abundances (ppm)

	G-121 Picrite	G-13 Ol-Bas.	G-8 Ol-poor Bas.	G-164 Trachybas.	G-15 Trachyand.
La	13.8	24.0	49.2	62.4	115
Ce	21.2	37.8	90.4	109	-
Nd	15.9	32.3	-	60.6	-
Sm	2.92	5.13	10.4	10.2	15
Eu	1.19	1.78	3.05	3.5	4.9
Gd	2.5	5.25	5.10	7.69	12.3
Tb	0.23	0.59	1.01	0.93	-
Dy	2.37	3.65	7.0	6.58	-
Yb	0.65	0.84	2.0	1.75	3.5
Lu	0.20	0.36	0.61	0.47	-

Table 2. Continued

	G-114 Trachyte	G-16 Aeg-Aug. Trach.	G-149 Aeg-Aug. Trach.	G-19D Sodalite Trach.
La	130	112	135	223
Ce	165	152	164	503
Nd	79.4	70.2	130	149
Sm	13.1	10.6	15.2	23
Eu	5.2	1.87	0.98	0.50
Gd	-	5.6	11.6	17.8
Tb	2.1	1.3	2.0	3.0
Dy	-	6.4	10.1	-
Yb	2.2	3.2	5.18	7.0
Lu	0.8	0.59	0.75	1.2

Figure 1:   Chondrite-normalized rare earth contents of the
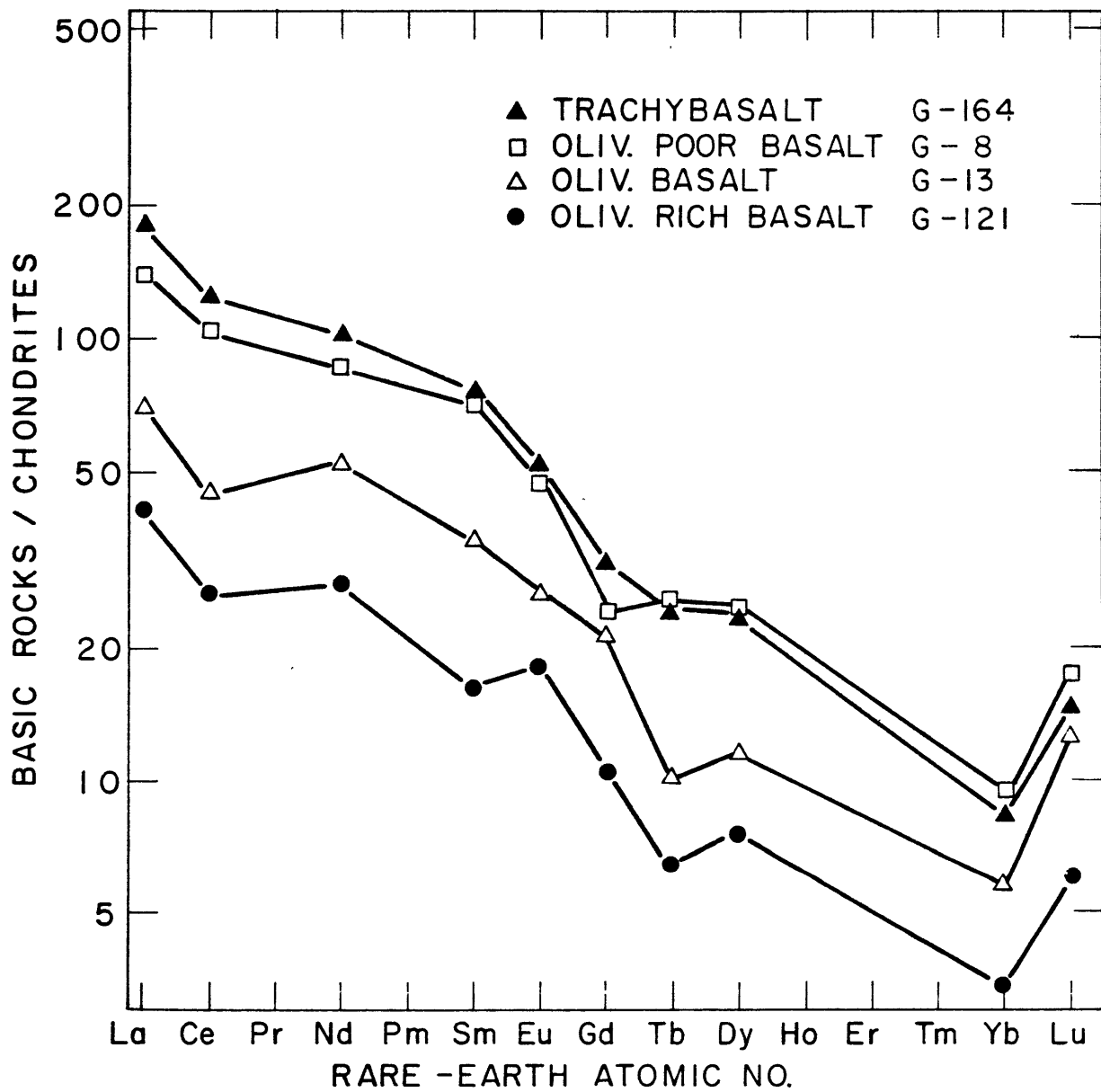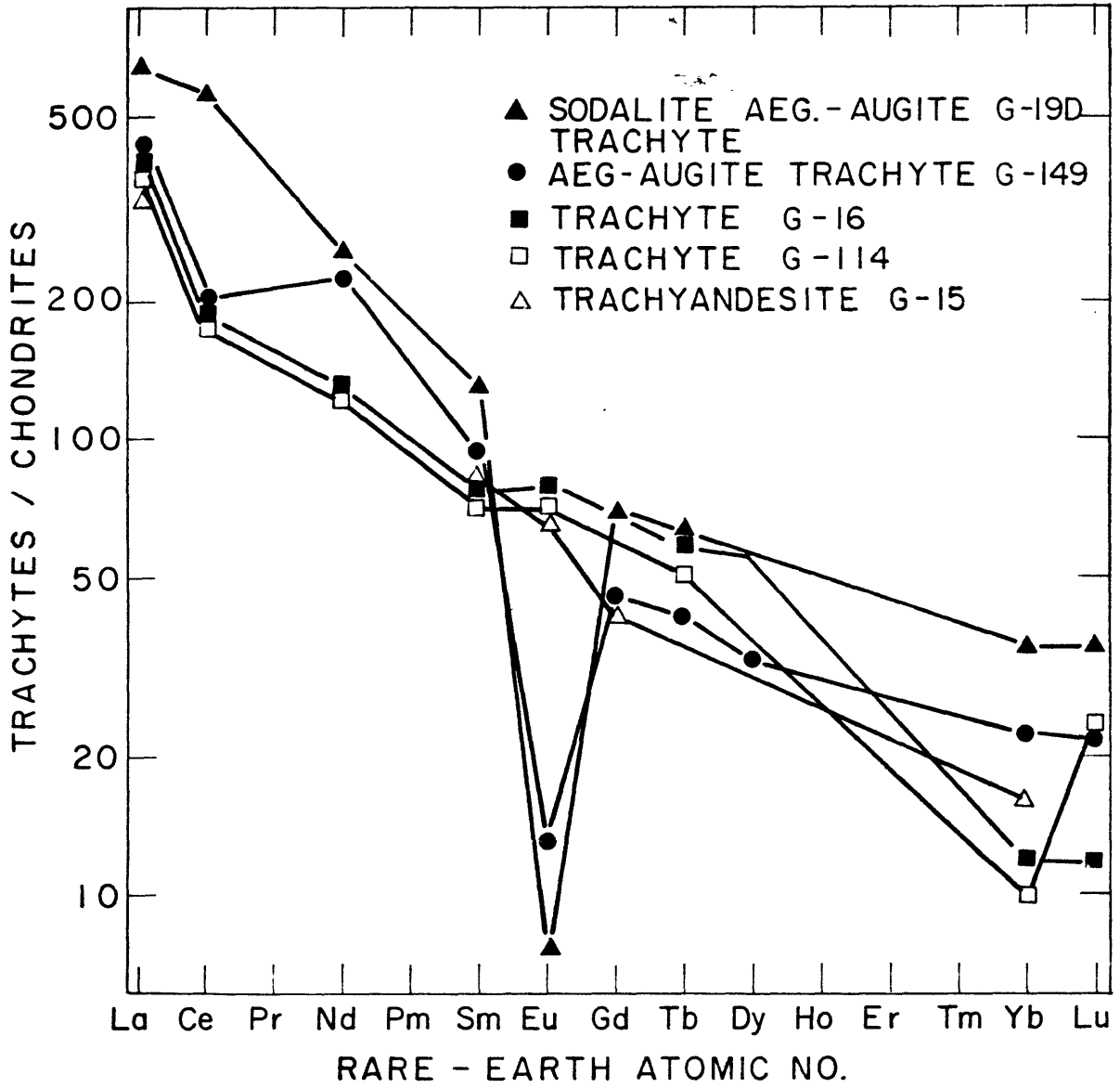
basic rocks of Gough Island.

Figure 2: Chondrite-normalized rare earth contents of the trachytic rocks of Gough Island.

and Nesterenko, 1960).

There is a marked depletion of Eu relative to the other rare earths in rocks at the very end of the crystallization sequence. The quantitative explanation of this negative anomaly in terms consistent with the overall mechanism relating the rock units is an important test of the fractional crystallization model.

Computer Analysis

The fractional crystallization model envisioned is that of a slowly crystallizing magma chamber. The separation of mineral phases is a means of generating a wide range of residual liquid compositions which can then erupt to the surface as trachybasalts, trachytes, etc. Traditionally petrologists approximated this process by manipulating oxides in addition-subtraction diagrams. Such graphical methods, while qualitatively informative, did not give unique solutions since data were often incomplete, biased, or applied in an unsystematic manner. A least-squares computer program recently developed (Bryan et al., 1969) and later modified (Wright and Doherty, 1970) provides a computational procedure which is a numerical equivalent of the graphical method. The computer program treats all the available data in a systematic fashion, and the best overall solution is generated. The inputs are weight percent of oxides in each mineral or rock used as a variable component, and oxides of the material

to be synthesized. Unknowns are the weight fractions of each
component which, when multiplied by the component compositions,
best approximate the material to be synthesized. Solutions
are generated for a matrix of linear equations in the form
A·X=B with the solution matrix X being that which minimizes
the differences between B=input and B*=calculated matrix.

Applications of this program to geological problems are
based on the concept of summing to a whole by the best com-
bination of constituent parts. (1) Matrix A may be the com-
positions of constituent minerals and B the whole rock com-
position. The solution matrix then represents weight frac-
tions of these minerals expected in the rock. Such a calcu-
lation is akin to a norm. (2) Matrix A may be the constitu-
ent rock compositions believed related to a common parent
(represented by matrix B). The solution matrix then gives a
non-geological estimate of weight fractions of each rock unit.
(3) Matrix A may be the compositions of any liquid, mineral
phases, wall rocks, etc. which are thought to contribute to
a particular product matrix B. Solutions for various weight
fractions may be positive, indicating additions to the system
(e.g. wall rock xenoliths) or negative, implying subtraction
from the system (e.g. crystal settling).

The Gough Island data included major element analyses of
rock types as well as optical, X-ray, and some chemical analy-
ses of constituent minerals. All but one of the rocks con-
sidered were fine-grained with only a few phenocrysts. The

rock chemical compositions were used as the compositions of
the liquid, and the analyzed phenocrysts were taken to repre-
sent compositions of removed mineral phases. The bulk of the
the cumulative minerals apparently remained in the magma
chamber, since cumulate rocks are not commonly exposed at
the surface. Using the alkali olivine basalt composition
and its mineral phenocryst compositions as matrix A, and
olivine-poor basalt composition as matrix B, one may calcu-
late the weight fractions of minerals subtracted via crystal
settling in order to change the liquid composition to olivine-
poor basalt. The same calculation may be repeated with olivine-
poor basalt and its phenocryst compositions in matrix A, trachy-
basalt composition in matrix B, and so forth through the dif-
ferentiation series. The numerical results of the computer
calculations are shown in Table 3 and represented graphically
in Fig. 3. Sums of squares of residuals (B-B*) are given as
well as the standard error in wt.%. A standard error indicates
the amount of scatter of values about the least-squares fit.
The data show that to go from alkali olivine basalt parent
liquid to picrite basalt significant amounts of olivine and
pyroxene have to be added. This is consistent with thin section
observations which show abundant olivine and pyroxene phenocrysts
in the picrite. Other rocks in the series are produced from
preceeding rock compositions via crystal subtraction.

The nature and relative abundances of separating mineral
phases as predicted by the computer program may also be

Table 3. Weight Fraction of Components from Computer Analysis

Picrite		Ol-poor Basalt		Trachybasalt		Trachyandesite	
Ol Bas	0.4670	Ol Bas	1.319	Ol-poor Bas	1.337	Trachybas	1.314
Fa_{21}	0.2718	Fa_{21}	-0.155	Fa_{21}	0.0249	Fa_{24}	-0.0734
Px	0.2710	Px	-0.019	Px	-0.1912	Px	-0.0141
An_{61}	-0.0029	An_{61}	-0.097	An_{57}	-0.1525	An_{54}	-0.1222
Ilm_{75}	-0.0130	Ilm_{75}	-0.034	Ilm_{70}	-0.0308	Ilm_{56}	-0.0477
						Kspar	-0.0259
$\Sigma(resid)^2$	0.272		0.862		0.993		0.0915
Standard error(wt.%)	0.253		0.506		0.504		0.145

Trachyte		Aeg-Aug Trach. G-16		Aeg-Aug Trach. G-149		Sodalite Aeg-Aug Trach.	
Trachyand	1.219	Trachyte	2.222	G-16	2.297	G-149	1.435
Fa_{38}	0.0283	Fa_{44}	-0.0965	Fa_{62}	-0.0677	Fa_{100}	0.0512
Px	-0.1622	Px	0.1024	Px	-0.0184	Px	-0.0010
An_{52}	-0.1229	An_{26}	-0.6700	An_{18}	-0.7971	An_4	-0.3317
Ilm_{56}	-0.0341	Ilm_{50}	-0.0521	Ilm_{20}	-0.0483	Ilm_{20}	-0.0558
Kspar	+-.0628	Kspar	-0.4628	Kspar	-0.3843	Kspar	-0.1771
						Sodalite	+0.0726
$\Sigma resid)^2$			1.310		0.778		0.0162
Standard error(wt%)			0.632		0.509		0.073

Figure 3: Graphical representation of computer results of wt. %

phenocrysts added or subtracted from parent liquid

to yield a particular rock type. Original magma

taken as olivine basalt is located between olivine-

poor and olivine-rich rocks.
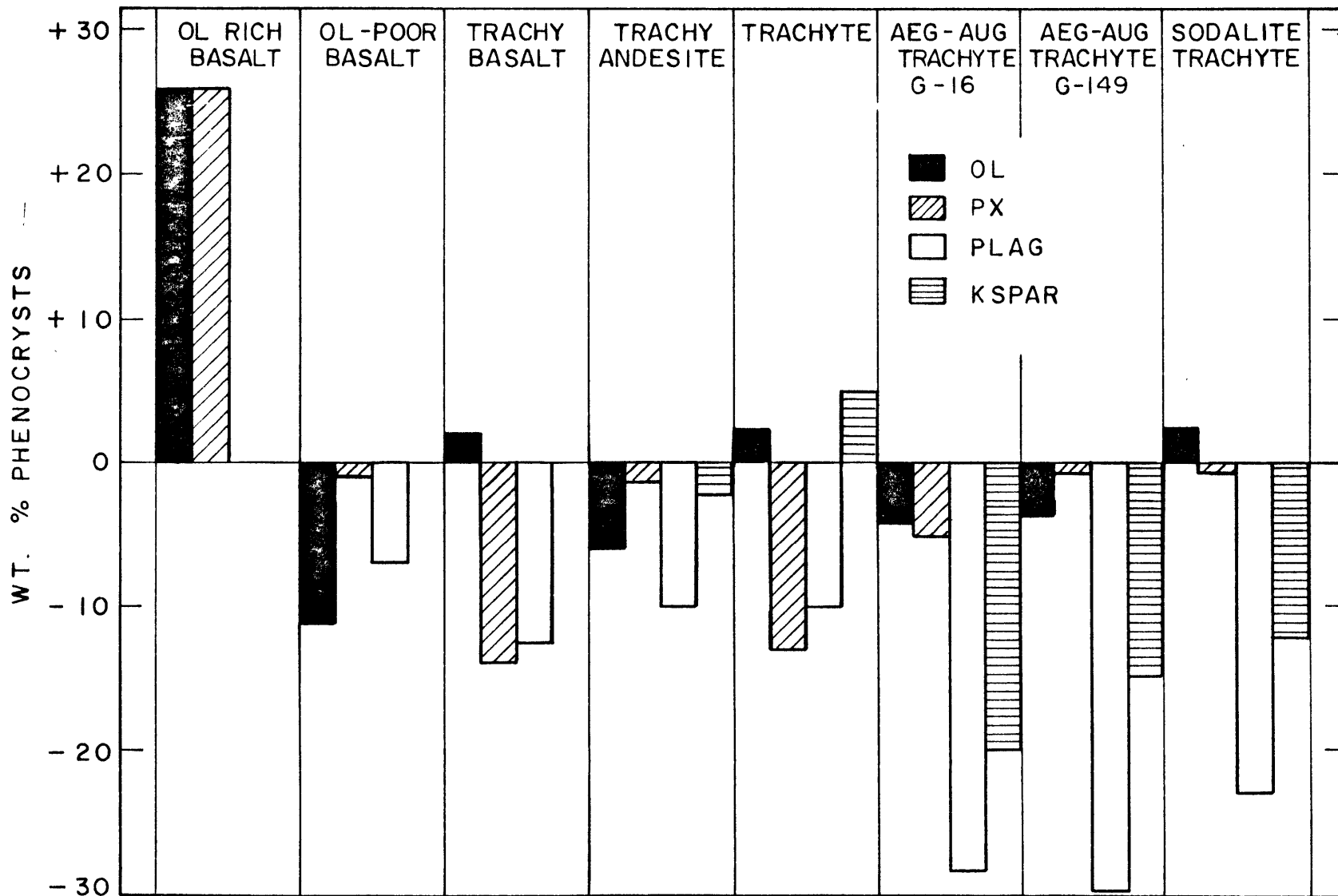
checked experimentally by melting experiments on the various

rock units. Such experiments give information on liquidus

phases, order of mineral crystallization and range of crystal-

lization temperatures.

A number of such melting experiments have been performed

under dry conditions at one atmosphere on a number of alkali

basalt series from Hawaii, Tristan da Cunha, the Hebrides

and Gough Island (Tilley, Yoder and Schairer, 1965 and 1966).

The results for the Gough Island sequence are reproduced in

Table 4. Some of the rocks studied (G-15, G-149) are iden-

tical to the ones of this study and all of the major rock

types are represented. A picrite from Tristan is also in-

cluded as the sample closest in composition to the Gough Is-

land picrite G-121.

Olivine is observed as the liquidus phase for the more

basic rocks, followed by clinopyroxene. This agrees with

the phenocryst content of the picrite and the observed oli-

vine depletion in later olivine-poor basalts and trachybasalts.

Plagioclase takes over as the liquidus phase at the trachy-

basalt-trachyandesite stage in agreement with the computer re-

sults. Later liquidus feldspars become more potassium rich

in the trachyte stage and this is reflected in the sizable

K-feldspar component in the computer output for the rocks.

Olivine takes the role of the latest crystallizing phase in

the more sialic rocks and the crystallization interval narrows

considerably. It should be noted that appearance of

Table 4. Melting Study Results

Rock Identification	Major Phases and Crystallization Temperatures (C°)
Ankaramite (Tristan de Cunha)	ol(1,235°)cpx(1,190°)Pl(1,145°)
Porphyritic olivine basalt G-111	ol(1,235°)cpx(1,180°)Pl(1,130°)
Trachybasalt G-97	ol(1,220°)cpx(1,180°)Pl(1,130°)
Trachybasalt G-95	Pl(1,170°)cpx(1,115°)ol(1,105°)
Trachyandesite G-15	Pl(1,155°)cpx(1,115°)ol(1,087°)
Trachyte	AlKf,cpx(1,025°)ol(1,000°)
Aeg-Augite Trachyte G-149	AlKf,(995°)cpx(965°)

plagioclase or alkali-feldspar on the liquidus is crucial to the postulation of a feldspar-rich separate as predicted by the computer and indicated by trace element evidence.

Dry-melting experiments done at one atmosphere on whole rocks rather than matrix separates are valuable as general indicators of crystallization trends. Correction for more realistic pressures and volatile contents probably do not affect the answers to a major degree, although water pressures in excess of 1000 bars can alter the order of crystallizing phases (Yoder and Tilley, 1962).

If one assumes that order of crystallization reflects the relative expected abundances of crystallizing phases, then agreement of melting data and computer results can be considered only generally good. This may be a function of the above errors in the   melting data, non agreement of analyzed rock types and/or errors in the computer data. Most probably there are contributions from all these sources, but the general agreement is nevertheless encouraging.

A negative solution value for a particular component in the computer results is interpreted as a loss of that component from the system of interest. In the case of dense phases such as olivine and pyroxene, this almost certainly takes place via gravitative settling. Phases such as feldspar may be quite close in density to that of the magma and may be removed by crystal floatation. The fact that no anorthitic rocks are found on Gough Island would tend to discredit the

floatation hypothesis. Recently, theoretical calculations
of silicate melt densities as a function of melt composition
and temperature have been carried out and seem to agree well
with experimental results (Bottinga and Weill, 1970). Simi-
lar calculations were performed on the Gough Island samples
for temperature just above the estimated liquidus temperatures
from Table 4. The results of these calculations are shown in
Table 5 and compared with estimated densities of feldspar
and alkali feldspar phenocrysts found in the various rock
units. Based on the theoretical calculations, feldspar crys-
tallizing from the more mafic rocks would be expected to
float, but in later rocks, when most of the feldspar is crys-
tallizing, the phenocrysts would sink. The float-sink boun-
dary being somewhere around trachybasalt-trachyandesite com-
positions. The calculations of Table 5 were performed for
dry melts. Addition of water to the system would tend to
make melts less dense than calculated and further enhance
crystal settling in late stage rocks.

Table 6 shows the results of norm-like calculations of
some rock compositions as in method (1). Only observed min-
erals were used as possible constituents in these computer
calculations. Comparisons with normative calculations are
possible if Ab+An+Or+Ne of the norms are compared to Plag+
Kspar of the computer model. The computer results for
weight fractions of observed minerals could be converted to
volume percent and compared with modes if the basalts were

Table 5. Density Calculations

Rock	Calc. Melt Density (gm/cm^3)	Est. Feldspar Density (gm/cm^3)
Picrite G-121	3.11	2.71
Ol-Basalt G-13	2.97	2.71
Ol-poor Basalt G-8	2.85	2.71
Trachybasalt G-164	2.81	2.70
Trachyandesite G-15	2.69	2.70
Trachyte G-114	2.59	2.69
Aeg-Trachyte G-16	2.57	-
Aeg-Trachyte G-149	2.53	2.60
Sod. Trachyte G19D	2.56	-

Table 6. Computer Generated Wt.-% Compared to Normative Values

	Picrite		Ol-Bas		Ol-poor Bas	
	Calc	Norm	Calc	Norm	Calc	Norm
Ol	0.30	0.35	0.13	0.11	0.02	0.00
Px	0.39	0.29	0.21	0.18	0.27	0.24
Kspar + Plag	0.26	0.31	0.56	0.59	0.64	0.66
Mag-Ilm	0.06	0.05	0.09	0.12	0.09	0.10

	Aeg-Aug Trachyte		Sodalite Trachyte	
	Calc	Norm	Calc	Norm
Ol	0.00	0.01	0.00	0.00
Px	0.04	0.04	0.07	0.04
Kspar + Plag	0.92	0.91	0.89	0.91[a]
Mag-Ilm	0.07	0.04	0.04	0.05

[a](includes sodalite)

not so fine-grained. See Appendix 2 for more discussion of the computer program.

Calculated REE Distribution

The rare earth content of successive rocks (liquids) in the crystallization scheme was calculated according to two models of trace element partitioning.

The first of these is referred to as the total equilibrium model and assumed complete equilibrium partitioning of trace elements between liquid and crystallizing solid phases. Concentration of trace elements in the two phases are presumed uniform and equal to the equilibrium values for the system. Under these conditions, one may derive an expression for the concentration in successive liquids starting with the simple mass balance expression (2)

$$C_i F + C_i{}^S (1-F) = C_i{}^O \tag{2}$$

C_i = concentration of trace i in liquid phase

$C_i{}^S$ = concentration of trace i in solid phase

$C_i{}^O$ = original concentration of trace i in the system

F = weight fraction of remaining liquid

rearranging equation (2) leads to an expression for $C_i / C_i{}^O$

$$\frac{C_i}{C_i{}^O} = \frac{1}{F + K_i{}^{S/L}(1-F)} \tag{3}$$

$K_i{}^{S/L}$ = solid/liquid distribution coefficient for i

C_i^0 is taken as the concentration of rare earth in the preceeding rock unit. The weight fraction F of liquid remaining after each step is obtained from the computer results by dividing the computed weight fraction of liquid into 1.0. Since more than one mineral phase is crystallizing during each step, $K_i^{S/L}$ is an average of individual mineral/liq. distribution coefficients (Table 8) weighted according to their proportion in the total solid phase, as obtained from the computer data.

The second model for trace element partitioning is referred to as the Rayleigh or surface equilibrium model. Only the surfaces of crystallizing phases are considered to be in equilibrium with a coexisting liquid. Such a process can lead to zoning of the trace element in solid phases with complex crystallization histories. The ratio C_i /C_i^0 under the surface equilibrium condition is given in (4) where the notation is the same as above (Gast, 1968).

$$C_i \ /C_i^0 = F^{K_i^{S/L}-1} \tag{4}$$

Generally speaking, the surface equilibrium model is more efficient for enriching trace elements in the preferred phase. The natural situation is probably some combination of the above models.

Table 7 shows a comparison of RE abundances calculated by the above two models and the measured values. Agreement is generally better using the Rayleigh model. Figure 4 plots

Table 7. Comparison of Calculated and Observed REE Abundances

	Ol-poor Bas G-8			Trachybas G-164			Trachyand G-15		
	Tot	Ray	Obs	Tot	Ray	Obs	Tot	Ray	Obs
La	30.96	31.08	49.2	40.1	40.4	62.4	51.5	52.0	115.0
Ce	48.95	49.06	90.4	63.4	63.7	109.0	81.5	82.2	-
Nd	41.5	41.6	-	52.5	52.7	60.6	66.3	67.4	-
Sm	6.55	6.57	10.4	8.08	8.16	10.2	10.2	10.4	15.0
Eu	2.17	2.18	3.05	2.51	2.55	3.5	2.85	2.93	4.9
Gd	6.67	6.71	5.10	8.10	8.23	7.69	10.17	10.39	12.3
Tb	0.748	0.751	1.01	0.90	0.92	0.93	1.13	1.16	-
Dy	4.61	4.64	7.0	5.53	5.59	6.58	6.90	7.00	-
Yb	1.06	1.07	2.0	1.26	1.28	1.75	1.57	1.60	3.5
Lu	0.45	0.46	0.61	0.53	0.55	0.47	0.66	0.69	-

Table 7. Continued

	Trachyte G-114			Aeg-Aug Trachyte G-16			Aeg-Aug Trachyte G-149		
	Tot	Ray	Obs	Tot	Ray	Obs	Tot	Ray	Obs
La	61.7	62.4	130.4	78.4	85.0	112.0	100.4	117.3	135.0
Ce	97.5	98.6	164.7	123.8	134.3	152.0	159.1	186.0	164.0
Nd	78.0	79.5	79.4	81.9	85.1	70.2	86.8	92.6	130.0
Sm	11.9	12.2	13.14	11.8	12.1	10.6	11.9	12.2	15.2
Eu	3.07	3.18	5.2	2.31	1.97	1.87	1.73	1.20	0.98
Gd	11.7	12.0	-	13.9	15.1	5.6	16.9	19.6	11.6
Tb	1.30	1.34	2.1	1.45	1.56	1.30	1.66	1.88	2.0
Dy	7.79	8.04	-	8.65	9.27	6.40	9.89	11.1	10.1
Yb	1.79	1.83	2.2	2.46	2.72	3.2	3.5	4.3	5.18
Lu	0.75	0.79	0.80	1.09	1.24	0.59	1.66	2.05	0.75

Table 7. Continued

Sodalite Trachyte G-19D

	Tot	Ray	Obs
La	138.6	161.3	223
Ce	220.0	258.9	503
Nd	119.7	128.6	149
Sm	16.4	16.9	23
Eu	1.66	1.14	0.50
Gd	23.2	27.1	17.8
Tb	2.28	2.60	3.0
Dy	13.5	15.3	-
Yb	4.8	5.9	7.0
Lu	2.3	2.8	1.2

Figure 4: Agreement of observed and calculated (Rayleigh) values of rare earth contents of the various Gough rocks (two pages).
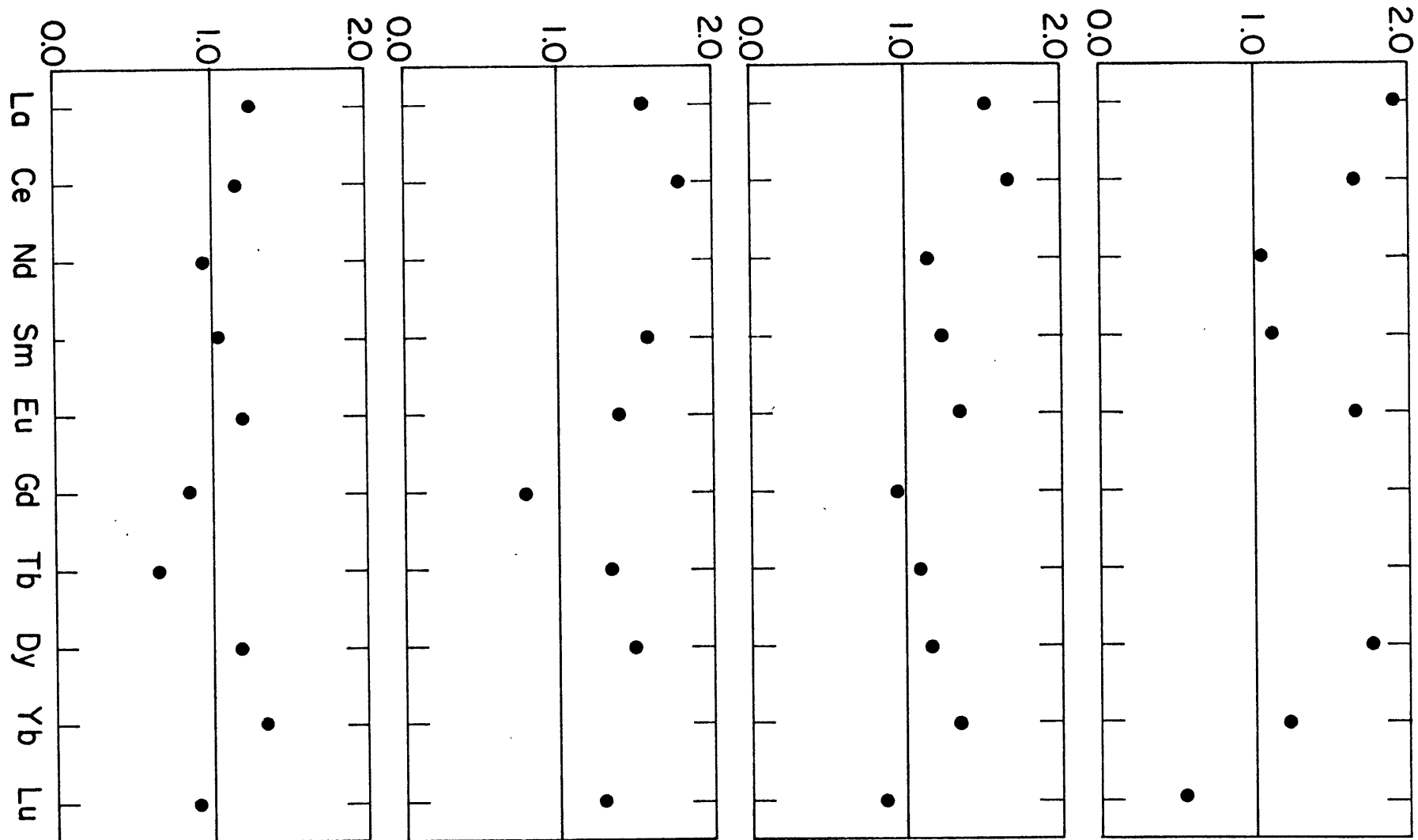
OBS / CALC

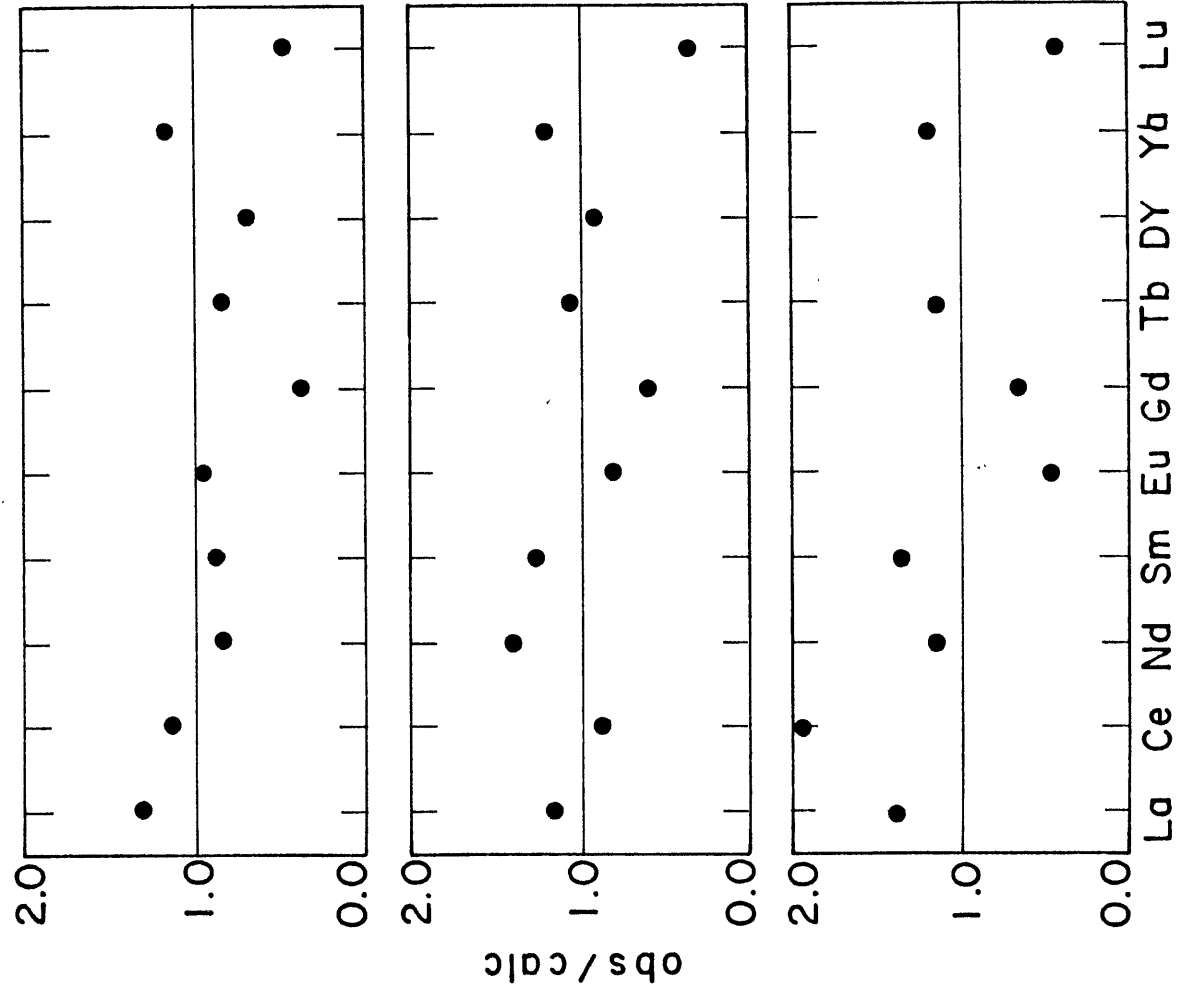OL-RICH BASALT   OL-POOR BASALT   TRACHYBASALT   TRACHYTE

AEG-AUG TRACHYTE

AEG-AUG TRACHYTE
G-16

G-149

SODALITE TRACHYTE
G-19D

La Ce Nd Sm Eu Gd Tb DY Yb Lu

obs/calc

the observed/calculated (Rayleigh) ratios for the various

rock types. In most cases, agreement is within a factor of

two.

The observed negative europium anomaly occurs in the cal-
culated values since the crystallization of large amounts of

sodic plagioclase and potassium feldspar is required by the

major element chemistry. Feldspar is known to preferentially

accept Eu over the other rare earths and recent work indicates

that the degree of Eu enrichment increases as the An content

of the plagioclase decreases (Schnetzler and Philpotts, 1970a).

This variation of Eu distribution coefficient has been used

in the calculations. The data indicate that Eu is preferen-

tially enriched in a potassium feldspar $(Ab_{19} \; An_{6.5} \; Or_{74.5})$

compared to sodic plagioclase (Schnetzler and Philpotts, 1970a).

Crystallization of large amounts of feldspar, as noted in the

trachytic rocks will cause negative Eu anomalies in the re-

sidual liquids.

Table 8 lists the distribution coefficients used in the

calculations. These values were not measured on phenocryst

matrix separates from the Gough rocks because of the limited

amounts of samples available and the general scarctiy of pheno-

crysts. Rather, they represent literature values for pheno-

crysts of similar composition taken from basaltic rocks. Such

values are often taken to represent equilibrium partitioning

of a trace element between phases having homogeneous distri-

butions of trace elements. As has been noted (Albarede and

Table 8. REE Distribution Coefficients

	Ol/Liq.	Cpx/Liq.	Plag/Liq.	Kspar/Liq.	Ap/Liq.
La	0.01	0.10	0.12	0.05	52
Ce	0.009	0.12	0.11	0.05	52
Nd	0.007	0.26	0.11	0.03	81
Sm	0.006	0.38	0.11	0.02	90
Eu	0.006	0.39	0.6 → 1.4	1.2	50
Gd	0.007	0.46	0.10	0.01	60
Tb	0.01	0.50	0.10	0.006	69
Dy	0.01	0.58	0.10	0.006	69
Yb	0.01	0.60	0.10	0.012	37
Lu	0.01	0.60	0.10	0.012	30

and Bottinga, 1972; Schnetzler and Philpotts, 1970a) non-homogeneity of trace element distributions is likely in natural systems and measured values of distribution coefficients may be ratios of average concentrations. Crystals may represent a series of frozen-in surface equilibrations between the growing crystal and a changing melt. Also, the distribution coefficient may vary in response to changes in temperature pressure or composition of the phases. Zoning of major elements in Gough minerals was not pronounced, but this may have little bearing on the behavior of trace elements. The chosen values for distribution coefficients are therefore taken as best guesses for average values over the period of crystallization of the phases.

There is some uncertainty regarding the applicability of D.C. data obtained from other rocks crystallizing under different conditions. The variations of distribution coefficients with changing pressure, temperature and composition of phases are incompletely understood. It is encouraging that the relative pattern of RE D.C. for a mineral remains the same for many analyzed rocks (Schnetzler and Philpotts, 1970a). The absolute values of such distribution coefficients may vary by a factor of ten or more. In some cases the direction of this variation has been correlated with mineral composition changes although a true causal relationship has not been proven.

Selection of realistic distribution coefficients is most

important for clinopyroxene which is an important host for REE. The trend of decreasing Ca and increasing Fe may cause significant changes in rare earth distribution coefficients (Schnetzler and Philpotts, 1970a). As additional D.C. data becomes available the calculations can be improved by incorporating the effects of pyroxene composition changes.

Apatite occurs as a phenocryst phase only in the trachytic rocks of Gough Island. As seen from the distribution coefficient data (Nagasawa, 1970), apatite takes up large amounts of REE when it crystallizes from a liquid. The calculations included crystallization of small amounts (1 wt %) of apatite in the aegerine augite trachytes. Bulk chemical analysis of whole rocks indicated that the P_2O_5 content increased gradually from 0.29 wt % in the alkaline olivine basalt to 0.36 wt % in trachyte. In later rocks, P_2O_5 content dropped sharply to 0.04 wt % implying removal from the liquid as apatite. The increase of P_2O_5 prior to apatite crystallization is not consistent with the percentage increase expected in the diminishing liquid phases by simple concentration (Anderson and Greenland, 1969). Computer calculations indicate that when the trachyte stage is reached, only 35% of the original liquid remains. P_2O_5 content should have increased from 0.29 wt % to something near 1 wt %. Removal of 1 wt % apatite from the residual liquids at the aegerine-augite trachyte stage is equivalent to removal of 0.15 wt% P_2O_5 from the original liquid. This is about half

of the original alkali olivine basalt P_2O_5 content.

If the RE abundances in the alkali olivine basalt parent G-13 were 10% higher, agreement between calculated and observed distributions would be improved. This amount of variation is within expected experimental error and expected natural inhomogeneities of a basalt flow (Haskin et al., 1971). Small errors in the beginning of the calculation are magnified since each calculated distribution of whole-rock RE abundance is used as the basis for calculated values of later rocks. Other errors arise from the fact that since all rock samples contained some phenocrysts (∿5%) they were not representative of true liquids. Solidified minerals would have acted as dilutents and the observed rare-earth abundances would be lower than expected if the rock were 100% liquid. Since all rocks had about the same amount of phenocrysts, this effect is probably not too important. A prime source of error for the calculated abundances probably arises from the uncertainty in solid-liquid distribution coefficients. Newer values can be readily incorporated into the calculations. Probable error sources in the computer data which is used to compute F and $K_i^{S/L}$ are discussed in appendix 2.

Other Trace Element Data

The fractional crystallization model for Gough Island rocks is further supported by other trace element variations.

Ba, Sr, Ni and Cr were measured by LeMaitre using emission spectra.

The strontium content of the early rocks shows gradual enrichment through trachyandesite and a sharp depletion in later rocks. Distribution coefficient data indicate a high preference of Sr for plagioclase. The Sr D.C. varies with plagioclase composition (Schnetzler and Philpotts, 1970b). Figure 5 shows the correlation of Eu and Sr depletions in the liquid with onset of extensive feldspar crystallization. The ordinate is a measure of the Eu anomaly observed in the whole-rock patterns. Sr is normalized to a non-anomalous rare earth. Points represent experimental values and triangles show positions of calculated hypothetical points when definite amounts of feldspar have been removed.

Barium concentrations show a similar gradual increase through trachyandesite and then a precipitous decrease. Barium is almost exclusively taken into alkali feldspar with a solid/liquid D.C. value of about 6. Appearance of alkali feldspar as a crystallizing phase correlates with the sharp Ba decrease in the liquid (Fig. 3, Table 9).

Concentrations of Ni and Cr decrease sharply in early rocks and remain fairly constant through the rest of the series. This is consistent with removal of these elements into olivine and pyroxene; the major crystallizing phases at early stages of fractional crystallization.

Quantitative comparisons of calculated and observed

Table 9. Sr, Ca, Cr, and Ni Abundances in Gough Island Rocks

	Picrite	Ol-poor Bas	Trachybas	Trachyand	Trachyte	Aeg-Aug Trachyte
Sr_{Obs}	450	1000	1100	1100	250	N.D.
Sr_{Calc}	330	700	700	700	450	0
Ba_{Obs}	340	700	1200	1200	600	N.D.
Ba_{Calc}	310	840	1075	1200	950	0
Cr_{Obs}	1250	100	45	5	N.D.	N.D.
Cr_{Calc}	1363	0	0	0	0	0
Ni_{Obs}	465	90	45	5	N.D.	N.D.
Ni_{Calc}	371	0	0	0	0	0

N.D. = indicates not detected

Figure 5: Correlation of europium anomalies and Sr depletions

in Gough rocks. Eu/Eu* = 1.0 indicates no anomalous

behavior of Eu compared to the other rare earths.

Sr values normalized to a non-anomalous rare earth.

Points are experimental values and triangles show

positions of calculated values when definite amounts

of feldspar have been removed.
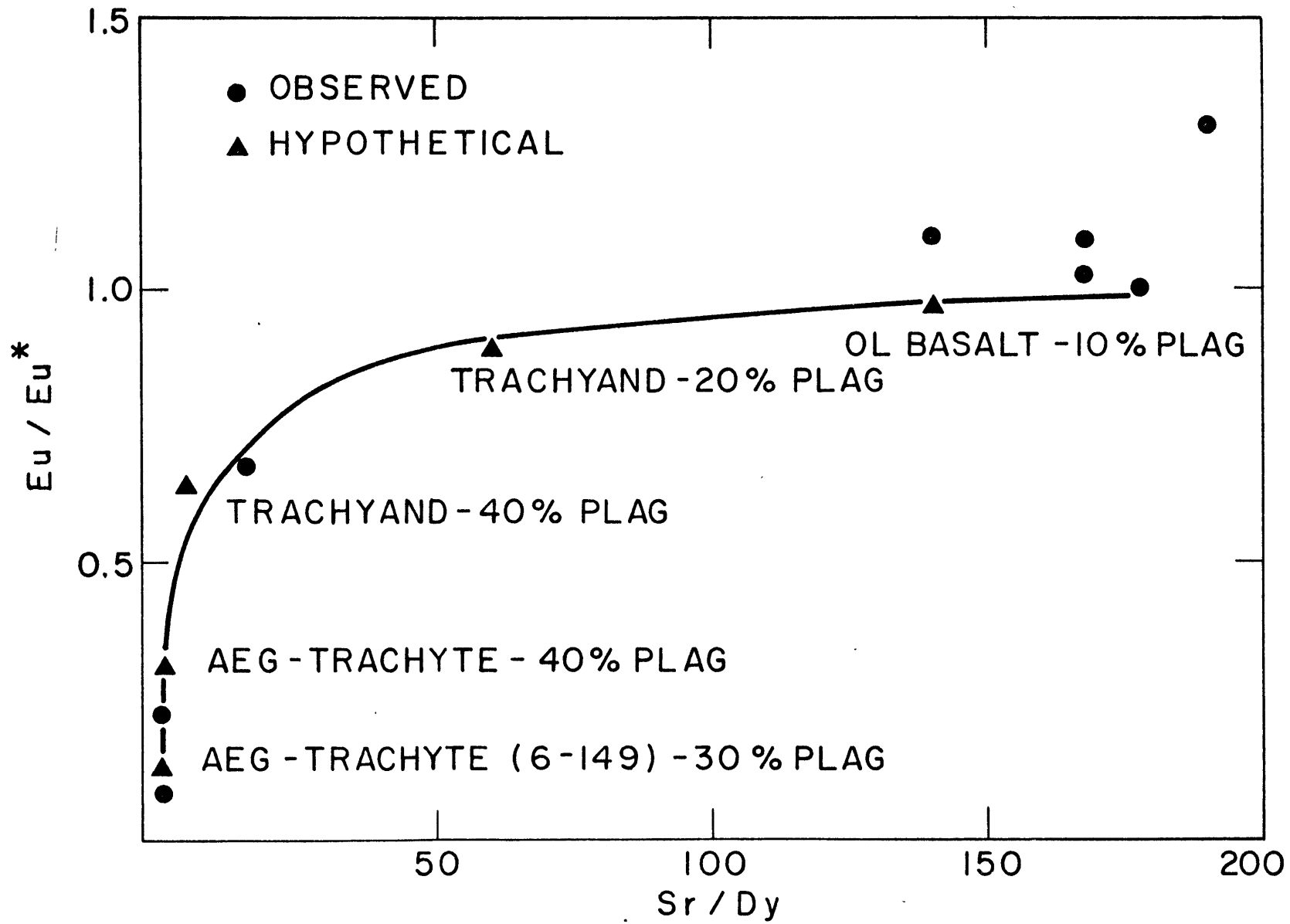
concentrations of these elements are presented in Table 9. Calculations are of the same nature as those used for the rare earth elements. Distribution coefficient data used are from Schnetzler and Philpotts (1970b) and Gast (1968). In Table 9 it is clear that the observed and calculated trends for Sr, Ba, Cr and Ni are similar. The absolute abundances do not agree as well as the data for REE. In part the discrepancy may result from analytical uncertainties of the emission spectrographic data for Sr, Ba, Cr and Ni.

Conclusions

A computer model which approximates fractional crystallization of a magma has been developed based on major element variations of Gough Island rocks. The model is consistent with calculated norms and the petrographically observed crystallization sequence of minerals.

Several significant trace element trends are observed in the Gough Island rocks.

1. The REE increase in abundance in the sequence from alkali-olivine basalt to trachyte. The light REE become increasingly more abundant than the heavy REE.

2. Eu, Sr and Ba are severely depleted in some trachytes (e.g. Eu/Eu* =0.07).

3. Cr and Ni are enriched in the picrite basalt.

All of these trends are predicted by the fractional crystallization model. This model is consistent with both

major and trace element data.

The model does not explain the isotopic variations dis-
cussed by Oversby (1969), and Oversby and Gast (1970). They
concluded that mantle heterogeneity and tholeiitic basalt
wall rock contamination were important in affecting the Pb
and Sr isotopic data of Gough Island rocks. The success of
the model in predicting trace element abundances implies that
fractional crystallization was the dominant mechanism for
generating trace element abundances.

A criticism of the fractional crystallization model is
that no cumulative rocks were obtained by LeMaitre except
for the picrite basalt. The observation that 50% of the is-
land surface is trachyte implies that large amounts of cumu-
lative rocks must be present if the fractional crystalliza-
tion model is valid. In part this may be a result of sam-
pling difficulties. More likely the cumulative rocks are
present at depth within the volcanic pile (Cann, 1968).

Suggestions for Future Work

The purpose of this investigation has been to study the
feasibility of using computer-generated solutions for testing
major and minor element correlations for a series of rocks
believed related by a fractional crystallization model. Cer-
tainly the amount of input data required is large, error
sources many, and the influence of many variables on the final
solutions poorly understood. With these problems in mind, it

would be foolish at this time to attach strict quantitative significance to the generated solutions. Nevertheless, many of the elemental and mineralogical variations predicted by this approach agree in a qualitative and semi-quantitative way with the observed situations. It is believed that further more sophisticated studies along this line are justified and will become more informative with improvement of input data. The following section outlines the concerns when planning future studies of this nature.

1) An area must be chosen for study which contains a sequence of basaltic rock types clearly related in space and time to a common source of origin. The area should be relatively unaffected by weathering and metamorphism. The choice of an oceanic island minimizes problems of possible crustal contamination of magmas. Tight geological control of sampling and thorough understanding of field relations are required.

2) Petrological investigations should include complete major element analysis of whole rocks and minerals. Optical and X-ray analysis of minerals should be supplemented with electron microprobe data when possible. Thorough petrographic descriptions of mineral phases, textures, modes should also be included.

3) Efforts should be made to continually upgrade estimates of distribution coefficients based on new analytical and experimental data.

4) Whole-rock analyses of trace elements such as REE, Sr, Ba, Rb, Cr, Ni, Zr, V should be carried out by the most sensitive methods available. Such trace elements can be particularly informative of the fractionation process since they often associate with particular phases such as Eu, Sr in feldspar, Ba, Rb in orthoclase, Ni in olivine, Zr, V in liquid. When possible, trace element analyses on separated minerals-matrix would eliminate the dependence on theoretical values for D.C.

5) Melting relationship studies should be done on the rock units to see which phases appear on the liquidus and to determine the order of mineral crystallization. This information could be compared to the computer results.

6) Isotopic studies on the rock units would lend extra evidence to their relationship to a common parent.

7) The computer program of Wright and Doherty should be utilized with weighing factors, error ranging and other options to simulate more complicated, but perhaps more realistic, magma generation processes. One particularly interesting option allows for specifying the sign of solution values. If one postulates the formation of different liquid compositions in a compositionally stratified magma column, then possible positive input of material could result from crystals which have settled out of higher levels. A set of mineral components of the computer input could contain two plagioclase compositions. One phenocryst composition would be constrained

to a negative solution value indicating it had settled out of the layer of interest, while another plagioclase, constrained as a positive solution, would be assumed to have settled in from a higher level. This could be repeated for other phases until the number of phases = number of oxides at which point the problem has only one solution.

The type of investigation described above would probably require the joint efforts of a number of specialists, all with a clear idea of the problem at hand and of their role in its solution. The conclusions of this study depended very heavily on the previous work of Roger LeMaitre and his associates who made a creditable attempt to bring together the type of data described. Unfortunately, studies of similar scope are difficult to find. The key to a convincing solution to problems of rock petrogenesis must be in this type of broad spectrum approach and it is hoped that such studies will be forthcoming in the future.

Appendix 1

Sample Preparation and Irradiation

Samples and standards were irradiated in pneumatic tube facilities of the M.I.T. reactor at a flux of $2 \times 10^{13} n/cm^2$ sec for times of one or two hours. Flux monitor experiments indicated that the neutron flux was constant over the area occupied by the samples which is equivalent to the size of the four dram polyethylene vial used as a container.

Rocks were submitted for irradiation as 0.5 grams of 200 mesh powder. Powder was packaged in one of two ways: 1) in one dram polyethylene snap-top vials which were heat sealed before irradiation, 2) in short lengths of $\frac{1}{4}$" I.D. polyethylene tubing which were heat sealed by pinching closed with needle-nosed pliers after heating the ends. Usually, two rock samples plus a standard were irradiated in each "run".

It was necessary to calculate expected activities of samples after irradiation and after cooling time, which was usually about 5 hours. Sample calculations were done for a hypothetical 1 gram aliquot of noritic gabbro for which chemical analyses were available. Oxide weight percents were recalculated to elemental weight percents. The pertinent equations are the following:

$$A_{tirr} = A_{sat} (1 - e^{-\frac{.693\ tirr}{t\frac{1}{2}}})$$

$A_{t_{irr}}$ = activity after irradiation (millicuries)

t_{irr} = duration of irradiation

$t^{\frac{1}{2}}$ = half life of nuclde produced

A_{sat} = equilibrium or saturation activity of nuclide

$$A_{sat} = n \cdot \sigma \cdot \phi \cdot a$$

σ = cross section of target nuclides for thermal neutrons (barns = $10^{-24} cm^3$)

ϕ = flux of neutrons (neutrons/cm^2sec)

n = number of target atoms = $\frac{Nm}{M}$

N = avogadro's number

m = weight of target element (grams)

M = molecular weight of target element

a = molecular abundance of target isotope

The equation for activity after decay:

$$A_D = A_{t_{irr}} \cdot e^{-\frac{.693 t_D}{t^{\frac{1}{2}}}}$$

A_D = activity after decay

t_D = decay time

Results of these calculations are given in Table 1[1] for t_{irr} = 1 hr t_D=5 hrs. Most of the initial activity after irradiation is from the short-lived nuclides which have been able to approach their saturation activities during t_{irr}. These same nuclides decay away quickly during t_D and the activities of the longer lived nuclides begin to dominate.

Table 1[1]. Stravjo Noritic Gabbro

element	wt%
SiO_2	52.79
TiO_2	1.12
Al_2O_3	13.79
Fe_2O_3	1.91
FeO	8.13
MnO	0.09
MgO	8.34
CaO	8.84
Na_2O	3.12
K_2O	1.48
P_2O_5	0.29
H_2O	0.32

Element	wt. grms.	Nuclide	b(Barns)	$t_{\frac{1}{2}}$(sec)	A_{sat}(mc)	At_{irr}(mc)	A_D(mc)
Si	0.246	^{31}Si	0.11	9432	9.72	2.25	0.59
Ti	0.00685	^{51}Ti	0.14	348	0.326	0.326	0
Al	0.0731	^{28}Al	0.23	138	197	197	0
Fe	0.0768	^{59}Fe	1.2	3.88×10^6	1.67	0	0
Mn	0.0007	^{56}Mn	13.3	9300	55	13	3.41
Mg	0.050	^{27}Mg	0.03	570	2.01	1.99	0
Ca	0.0632	^{49}Ca	1.1	528	1.01	1.0	0
Na	0.0231	^{24}Na	.13	5.4×10^4	40.6	1.82	1.44
K	0.0123	^{42}K	1.1	4.46×10^4	7.2	0.396	0.30
						$\Sigma = 218$	$\Sigma = 5.74$

Preparation of Standard Solutions

Standard solutions were made up from aqueous stock so-
lutions of rare-earth chlorides according to Table 2[1]. Stock
solutions were prepared in concentrations such that aliquots
of the order of one milliter could be diluted to 250 ml in a
standard solution; 0.5 ml of which would then approximate
the rare-earth content of a typical rock. Table 3[1] repeats
the type of calculations done in Table 1[1] for the prepared
0.5 ml of standard solution irradiated with the powdered
rocks.

Chemical Separation of the Rare Earth Group

The solution of the Ge(Li) detectors allows one to ir-
radiate a rock and simply measure the many resolved peaks on
an energy-vs.-channel number spectrum. Although there are
often some problems with overlapping peaks and high back-
grounds, these problems can be partially solved using comp-
ton suppression and peak ratios for pure elements. The al-
ternative is to chemically separate elements or groups of
elements from one another before counting. Corrections must
then be made for chemical yields if quantitatively accurate
numbers are desired.

The chemical separation technique was employed in this
study. Chemical separation of the rare earth elements from
the rest of the rock constituents was performed after irradi-
ation and the addition of 2 ml of non-radioactive rare earth

chloride carrier solution of the composition shown in Table 4^1. The chemical procedure used has been described in detail (Haskin, Wildeman, Haskin, 1968) and involves sodium peroxide fusion of the rock plus carrier followed by a series of pH controlled precipitations culminating in a purified rare earth oxalate precipitate.

After counting, bulk chemical yield determinations of the rare earth group were performed by titrating with EDTA followed by a back titration with Cu^{+2} using PAN indicator (Cheng, 1958). Values for chemical yields determined in this way gave yields of the order of 50-60%. Such bulk chemical yields are valid if one assumes that the chemical operations do not fractionate the rare earths. To test this assumption, chemical yields were determined for each rare earth element using a reirradiation technique.

This technique requires two assumptions: a) the carrier solution is fractionated during chemistry in the same manner as the rare earths contained in the rock, b) the carrier solution is much more concentrated than the rare earths in the rock. Assumption (a) is presumed valid by chemical theory and comparison of the last columns in Tables 2^1 and 4^1 show that the carrier is always at least ten times more concentrated than the standard (average rock) solution.

The chemically treated rock-plus-carrier is submitted for irradiation with a companion sample containing the equivalent amount of carrier added to the rock before chemistry

Table 2[1]. Makeup of Standard Solutions

Element	Stock Soln meg/ml	μgrm/ml (x10^{-3})	ml stock used / 250 ml std	μgrm/0.5ml std.
La	0.05695	7.95	1.0	15.9
Ce	0.06126	8.60	3.0	51.5
Pr	0.06291	8.85	1.0	17.7
Nd	0.06356	9.16	4.0	73.3
Sm	0.06494	9.75	0.1	1.95
Eu	0.06283	9.56	0.1	1.91
Gd	0.06581	10.35	1.0	20.7
Tb	0.06411	10.20	0.1	2.04
Dy	0.06509	10.60	0.5	10.6
Ho	0.06488	10.60	0.02	0.04
Er	0.06795	11.35	2.0	45.4
Tm	0.06778	11.50	0.5	11.5
Yb	0.06541	11.35	0.05	1.135
Lu	0.06508	11.41	0.02	0.456

Table 3^1. Activity Calculations for Standard

Element	wt (μgrams)	Nuclide	σ(barns)	$t_{\frac{1}{2}}$(secs)	A_{sat}(mc)	At_{irr}(mc)	A_D(mc)
La	15.9	^{140}La	8.9	1.44×10^5	0.297	0.005	0.0046
Pr	17.7	^{142}Pr	19	6.95×10^4	0.448	0.015	0.0125
Sm	1.95	^{153}Sm	210	1.69×10^5	0.156	0.0023	0.0011
Eu	1.9	^{152m}Eu	2800	3.31×10^4	5.55	0.405	0.278
Dy	10.6	^{165}Dy	2700	8.35×10^3	12.5	3.25	0.72
Ho	0.042	^{166}Ho	100	9.8×10^4	.005	0	0
Er	45.4	^{171}Er	9	2.7×10^4	0.118	0.010	0.006
Lu	0.456	^{176m}Lu	23	1.33×10^4	0.029	0.025	0

$$\Sigma = 3.72 \qquad \Sigma = 1.03$$

Table 4[1]. Carrier Solution of the Rare Earths

Elements	Meq/2ml carrier	μgrm/2ml (×10^{-3})
La	0.01199	1.66
Ce	0.006448	0.903
Pr	0.006622	0.934
Nd	0.006690	0.963
Sm	0.006836	1.03
Eu	0.006614	1.01
Gd	0.006928	1.09
Tb	0.006748	1.07
Ho	0.006788	1.12
Er	0.01431	2.39
Tm	0.01427	2.41
Yb	0.01377	2.38
Lu	0.01370	2.40

was performed (2 ml). Comparison of the subsequent radio-
active samples is that of carrier before and after chemistry.
Yields for each element are then computed by comparing equi-
valent peaks in the two samples.

The results of a typical chemical yield experiment are
shown in Table 5[1]. Yields are higher for the middle rare
earths and lower at each end. A bulk chemical yield titra-
tion would probably give a value around 50%. This type of
fractionation effect during chemistry has been reported be-
fore (Denechaud, 1969) and its cause linked to iron inter-
ference during the final rare-earth oxalate precipitation.
Clearly, improvements are necessary to increase overall
yield and decrease fractionation. A procedure utilizing
ion exchange resins would seem a likely possibility.

Counting Procedures and Schedules

Conceptually, the calculation of the concentration of
some element in a sample is very straightforward and reduces
to the simple proportional relationship:

$$\frac{\text{conc element in sample}}{\text{conc element in std}} = \frac{\text{peak area of element's radiation in sample}}{\text{peak area of element's radiation in std.}}$$

As long as conditions of analysis are kept constant, and sam-
ple and standard have similar elemental makeup, the calcula-
ted concentration in the sample should agree well with re-
sults of other analytical techniques. In order to insure

Table 5[1]. Chemical Yield Determination

Element	Sample/Std (%)
La	40
Ce	41
Nd	60
Sm	68
Eu	63
Tb	62
Ho	61
Er	56
Yb	38
Lu	38

identical analytical conditions, the following effects and corrections must be considered.

Geometry Considerations

Geometry effects fall into two main types: a) irradiation geometry, and b) counting geometry.

It is crucial that both the standard and sample receive the same neutron flux during irradiation. In order to check this, the neutron flux in the pneumatic tube facility can be checked for lengthwise and radial variations using strategically placed bits of flux monitor material of constant weight. If the flux is uniform, all should give the same activity when counted; within the statistical fluctuations of radioactive decay (see below). Such an experiment has been performed at the M.I.T. reactor and fluxes were shown to be uniform. Care should also be taken such that the arrangement of samples in the holder does not lead to excessive shielding of one sample by the others.

The sample-detector geometry must remain identical for standard and sample. This is especially critical if the samples are close to the face of the detector. Changes in distances perpendicular to the detector face are more important than shifts in a plane parallel to the detector face. The intersection of the detector with the solid angle described by the sample determines what fraction of the sample activity is actually counted. A quantitative discussion of the magnitude of these effects has been described (Denechaud, 1969).

A special sample holder was built for these experiments
which was designed to fasten onto the detector head and pro-
vide reproducible   holder-detector face distances. The
sample holder was designed to accommodate 1 dram snap top
polyethylene vials which could be placed into a number of care-
fully-machined grooved slits at various distances from the
detector.

Samples and standards were counted as known volumes of
REE-HCl solutions contained in the above mentioned vials.
Possible variances in sample shape or absorbancy were there-
fore minimized. Self absorbancy differences between sample
and standard can lead to errors if analytical gamma ray peaks
are of low energy (<100KeV).

Peak Area Calculations

Radiations from the samples were stored according to
energy in a 4096 channel pulse-height analyzer and displayed
as a γ-ray spectrum. Prior to counting, the gain was ad-
justed such that a calibration standard of ^{137}Cs had its
661.6 KeV peak stored in channel number 1323, giving a cali-
brated spectrum of 2 channels/KeV. The linearity of the am-
plification was usually good, but was checked with a series
of other standards of varying energies to give a calibration
curve which could then be used to identify peaks in the sam-
ple and standard spectrums.

The total number of counts recorded under a particular
peak served as the raw data and could be obtained in the

form of paper tape readout or magnetic tape storage for use with computer programs which would analyze peaks. The data presented in this paper was obtained using hand-plotted peaks and hand-calculated backgrounds and peak areas. This technique, while much more time consuming, allowed for careful scrutiny of peak shapes, peak overlaps, background inconsistencies and allowed for more options in the calculation of "corrected" peak areas than were available in current computer programs.

The calculation of a peak area from the raw data required 1) the selection of where the peak began and ended, and 2) the subtraction of contributions from background compton scattering events. To aid in these determinations data for each peak was plotted.

Selection of peak limits was usually straightforward and represented the points between which the recorded activities were above backgound levels. Once the flanking positions were chosen, a straight line was drawn between them with all counts falling below the line taken as background. Once peak limits and baselines were selected, the total number of counts within the limits was summed and background contributions calculated by multiplying the number of channels by an average background. The "corrected" peak area was then the total counts less background.

Consistency of peak area calculations between sample and standard is the important rule. Often it was desirable to

compare constant fractions of peaks rather than whole

peak areas, especially if one suspected possible overlap-

ping interferences from neighboring peaks. Denechaud

(1969) suggests using half-peak areas in these cases, using

only the portion of the peak within which the recorded

counts are greater than half the peak height (full width

half maximum). This method was used for some of the area

calculations.

If the sample and standard differ greatly in composition

and/or concentration of elements, peak shapes may differ due
                                                    or higher
to peak broadening in the higher background/concentration

samples. Such broadening may be due to instrumental gain

shifts or generally poorer resolution at high count rates.

In such cases, fractional peak area calculations would be

erroneous and whole peak areas are required.

Decay Corrections

Since standard and sample were not counted at the same

time, it was necessary to apply a further correction to the

"corrected" peak areas. This correction takes into account

the fact that radioactive decay is occurring throughout the

counting intervals. Net activities had to be corrected to

those expected if the sample and standard were counted at

the same point in time. The pertinent equation is

$$A = A_{o}e^{-\lambda t}$$

A = corrected activity

A_O = measured activity

t = decay time = time interval between midpoints of

counting intervals

λ = decay constant = $\dfrac{.693}{t_{\frac{1}{2}}}$

$t_{\frac{1}{2}}$ = half life of nuclide of interest

Using this equation, the activity of the first-counted

specimen can be corrected to its activity if counted with

the second-counted specimen. Conversely, the inverse of the

above equation, a hypothetical growth relationship, can be

used to correct the other way.

A further complication arises if the counting periods

are comparable to the half life of the decaying species. In

this case the activity changes markedly during the counting

period and a dead time correction must be applied (Löw, 1964).

The most serious example of this was the case of 165 Dy of

2.31 hour half-life counted for 0.5 hours. The calculated

error in taking the activity as that at the midpoint of the

counting interval leads to an error of less than $\frac{1}{4}$% for the

peak area. With shorter half-life species this source of

error can become appreciable.

Counting Schedule

Depending on the half-lives of the rare-earths to be

analyzed and the relative importance of interfering activities

and background levels, a counting schedule was devised which

would allow the best measurement of the most elements. The schedule and chosen analytical peaks are shown in Table 6[1].

Error Analysis

The process of radioactive decay is a statistical phenomenon. The probability of obtaining x disintegrations in time t from No radioactive atoms may be expressed by a bimodal distribution law

$$S(x) = \frac{No!}{(No-x)!\,x!} \; P^x (1-P)^{No-x} \tag{1}$$

P   = probability of an atom decaying in time t

1-P = probability of an atom not decaying in time t

S(x) = probability of x atoms decaying in time t

From the above equation (1) it is possible to derive expressions for expected distributions of time intervals between disintegrations, the average expected disintegration rate and the expected standard deviation is given as:

$$\sigma = \sqrt{Me^{-\lambda t}} \tag{2}$$

where M is the average disintegration rate. When λt is small and the number of counts is large, this reduces to (3)

$$\sigma = \sqrt{M} \tag{3}$$

where M = number of counts recorded.

The Poisson and Gaussian distributions are just modifications of the basic bimodal law, given certain assumptions that are usually valid for radioactive decay; $\lambda t \ll 1$,

Table 6[1]. Counting Schedule

Nuclide	Count Set	Peak Energy (KeV)
^{140}La	III,IV	328.8, 487.0
^{141}Ce	IV	145.4
^{147}Nd	III	531.0
^{135}Sm	II	103.2
^{152}Eu	I,IV	121.8, 344.4
^{153}Gd	IV	97.4
^{160}Tb	III,IV	298, 879.3
^{165}Dy	I	94.7
^{169}Yb	IV	177.2
^{175}Yb	III	282.6
^{177}Lu	III	208.4

I = same day   III = 2 weeks
II = 3 days   IV = 40 days

No>>1. This is the case, when a large number of atoms are counted for times which are short compared to their half-lives. The Gaussian distribution is symmetrical about M and for large M, so is the Poisson. Both of these cases reduce to (3).

Errors in estimation of baselines can be critical. The total counts attributed to background are the result of graphical approximation and not subject to a statistical analysis. The more points on either side of the peak through which to draw a background line, the more reliable the approximation. The background error may then be approximated by the statistical uncertainty of the counts used as reference points for the background. The percent contribution of this background error estimate to the total error estimate will depend upon the size of the integrated peak. For a strong peak sitting on flat background, peak area and background errors should both be small. The advantage of using peak fractions rather than whole-peak areas was discussed above. This practic reduces m, the total number of counts and increases statistical uncertainty in the peak area to a point where it is comparable to baseline uncertainty. A list of expected uncertainties for the various analytical peaks is given in column 1 of Table 7[1].

The uncertainties in column 1 of Table 7[1] are for each measured peak. In the calculation of the elemental concentration in the sample, peaks of sample and standard are

compared and their individual errors combined to obtain the
net error for the calculated concentration in the sample
(column 2, Table 7[1]). As mentioned above:

$$\text{conc in sample} = \frac{(\text{counts in sample peak})(\text{conc in standard})}{(\text{counts in standard peak})}$$

In the case of Eu, each measured peak has an uncertainty
of ±2%. The error of concentration in the standard is as-
sumed to be significantly smaller. The net error for the
conc in the sample is given by the combination of error for-
mula for a quotient.

$$\frac{\sigma^{(\frac{x}{y})}}{x/y} = \sqrt{(\frac{\sigma x}{x})^2 + (\frac{\sigma y}{y})^2} \tag{4}$$

$$= \sqrt{(2\%)^2 + (2\%)^2}$$

$$= \pm 2.8\%$$

Each sample concentration must be multiplied by a chemi-
cal yield factor to obtain its absolute concentration in the
starting material. The determination of the chemical yield
involved peak analysis and comparisons as before, and the
chemical yield error would be expected to be similar to the
error of the measured sample. Equation 4 is valid for a com-
bination of errors by multiplication so the % error for the
final product is given as:

$$\% \text{ error of absolute conc} = \sqrt{(2.8\%)^2 + (2.8\%)^2}$$

$$\rightleftharpoons \pm 4\%$$

Table 7[1]. Error Estimates

Element	net est. error for analyzed peak (%)	error for conc. of sample (%)	error for absolute yield (%)
La	±2	±2.8	±4
Ce	±5	±7	±10
Nd	±10	±14	±20
Sm	±5	±7	±10
Eu	±2	±2.8	±4
Gd	±15	±21	±30
Tb	±5	±7	±10
Dy	±8	±11.5	±16
Yb	±8	±11.5	±16
Lu	±5	±7	±10

These errors are reported in column 3 of Table 7^1. The errors in column 3 are assumed minimum errors and do not take into account differences in counting geometry, sample geometry, or neutron flux. Every effort was made to minimize the sources of error and they are believed small compared to the error sources mentioned above.

Additional errors arise in the preparation and pipetting of standard solutions. Each individual rare earth chloride stock solution was checked by titration procedures and found to have possible concentration errors of ±0.5%. Errors in pipetting of stock solutions ranged from ±0.2-0.5%. Errors in pipetting from standard solution flask into irradiation vial were ±0.2%. The combinational formula for error addition gives a net error from these effects of ±0.6% for each element. Inclusion of this error in the previous calculations would raise the final europium error to ±4.07%, a small increase.

From Table 7^1 it is obvious that one cannot expect better precision than ±5-10% for most rare earths using the analytical scheme of this investigation. The elimination of a re-irradiation step would improve matters somewhat, but this is possible only when separation of the rare earth group is 100% complete.

Details of Elemental Analysis

Lanthanum - There are several strong, easily identifiable peaks

attributed to the 40 hr ^{140}La isotope persisting up to two weeks after irradiation. The peaks used for analysis were at 328.8 and 487.0 KeV and were counted $\sim$3 days after irradiation. They were also detectable in the subsequent counting group at the two-week interval and provided a check between count sets. The closest interfering peaks in the second count set of 3 days are at 307.8 ^{169}Yb, 344.4 ^{152}Eu, 432.5 ^{140}La, 531.2 ^{147}Nd and posed no problem of overlap.

Cerium - The 145.4 KeV peak of 33 day ^{141}Ce is observable throughout the counting period and is the only analytical peak for this element. Fortunately there are few interferences except a very weak 4.21 day ^{175}Yb at 144.8 KeV which has decayed off by the 40 day count set. The previous chemistry has removed contributions from ^{59}Fe of 142.5 KeV which would otherwise require correction as a major interference.

Neodynium - This element has two peaks of importance from its 11.1 day ^{147}Nd isotope, but only the weaker of the two at 531 KeV is free from interference. It is counted during count set 3 at the two-week interval. Increased efficiency of larger Ge(Li) detectors and longer irradiation times and counting times allowed somewhat lower estimates of uncertainty for this peak than previously reported (E.B. Denechaud, 1969).

Samarium - Analytical peaks of 47 hr ^{153}Sm are at 69.7, 103.2

KeV with the latter being the strongest and cleanest. Optimum counting time was at the 3 day interval. Later counts contain significant contributions from 242 Day ^{153}Gd of the same energy. Luckily, the strength of the samarium peaks in early counts overwhelm any Gd contribution. Both samarium peaks, because of their low energies, reside on a high and irregular background and some error in assigning background is inevitable.

Europium - Irradiation of europium results in the product.on of 12Y ^{152}Eu and its metastable isomer 9.3 hr ^{152m}Eu. The contribution of these two isomers to the europium activity enables Eu peaks to be observed at all times during counting. In the first set, less than 24 hours after irradiation, the peaks are strong and dominated by the short lived isomer. It is difficult to use the standard decay equation when the contribution of both isomers is important, so analytical measurements were made when one or the other activity dominated the decay, i.e. count set one for 9.3h and count set four for 12Y decays. The peaks used were at 121.8 and 344.4 KeV. There are some minor interferences from 118.2 KeV of ^{169}Yb and 337.1 KeV of ^{160}Tb, but these are usually resolvable with the detector and small overlaps are minimized by taking half-peak areas according to the method of Denechaud.

Gadolinium - This element presents some analytical problems.

It has three weak peaks from 242 day ^{153}Gd at 97.4, 103.2 and 69.7 KeV. The latter two coincide with ^{153}Sm peaks and the peak at 97.4 just barely rises above a background which is raised by nearby and partly overlapping peaks from 91 KeV ^{147}Nd and 93.6 KeV ^{169}Yb. Counting must be done at the 40 day count set or later. Interferences can be reduced by using the low energy Ge(Li) (Leps) detector which has better resolution but much lower efficiency, and use of half-peak integration.

Terbium - There are many peaks from 72.1 day ^{160}Tb which become prominent in the spectra after a couple weeks, but most are interfered with by other peaks or are too weak. The best combination of strength and isolation is shown by the 298.5 KeV peak. There is possible interference from 12 yr 296 KeV ^{152}Eu. The contribution from this weak Eu peak is small but may be corrected for if one choses to count a ^{152}Eu standard to get peak ratios between the 296 and some other clean Eu peak. Counting this "clean" peak in the sample then allows calculation of the 296 contribution. The efficiency of the large 26cc Ge(Li) detector gave a reasonable number of counts (a few thousand) in count set 3 for the 879.3 KeV ^{160}Tb peak which turns out to be free from interferences. Some minor amount of Scandium comes through the chemistry to give a 889.3 KeV ^{44}Sc peak, but this is far enough away to pose no problem, likewise for the ^{159}Eu 873.7 KeV. This peak should give at least as good a number as the 298.5 KeV.

Dysprosium - It is important to count the 2.31 hr ^{165}Dy peak of 94.7 KeV on the first day before it decays. This may be done with either the 26cc Ge(li) or Leps. The latter is probably preferable since the sample is quite active and resolution is better. The Leps also helps minimize possible low energy background inconsistencies due to ^{176m}Lu 85.4 KeV and ^{153}Sm 89.5 KeV.

Holmium - The 80.6 KeV peak of 27 hr ^{166}Ho was found to be of too low intensity to use above the intense low energy background levels during early counting. Also many interfering peaks, among which 74.7 KeV and 83.4 KeV of ^{153}Sm are important, make resolution difficult.

Erbium - The peak from 7.52 hr ^{171}Er at 308.4 KeV is the largest but still below the level of the background levels encountered.

Thulium - Intensity of the 58 KeV analytical peak was not great enough, nor could a reasonable separation from surrounding peaks be expected if one were visible.

Ytterbrium - The analysis for this element was made using the 282.6 KeV peak of the 4.21 day Yb^{175} during count set 3. This peak is free from interferences at this period with the nearest problems being ^{159}Eu 248.1 KeV and 298.5 ^{160}Tb. In some cases the 177.2 KeV peak of 32 day ^{169}Yb was measured during count set 4 at 40 days after irradiation. This peak is also free

of interferences at this time.

Lutecium - There is one important peak of 6.7 day ^{177}Lu at 208.4 KeV which is most favorable for counting after two weeks. Possible interferences are from 198 KeV ^{169}Yb and 215.6 KeV ^{160}Tb but the resolution of the system eliminates problems of overlap.

Appendix 2

Computer Program

Theory of Least Squares Calculation

A system of linear algebraic equations is defined as overdetermined when the number of equations exceeds the number of unknowns. In theory, there are $K!/n!(K-n)!$ solutions to a system of K equations in n unknowns, each solution utilizing only n/K of the data (Chayes, 1969). The least squares method of solution to such a system is attractive because it uses all of the available data to chose the one possible solution satisfying the criteria of a minimization of residuals. Mathematically, this is expressed as the solution, such that the quantity $S = \Sigma(B*-B)$ is minimized. B* is defined as the product matrix of the least-squares solution matrix, X, and matrix A. B is the original input matrix which is to be approximated.

Matrix A consists of the weight % of K oxides in n phases. Matrix B has dimensions K,1 and the solution matrix X the dimensions n,1. The matrix expression $A \cdot X = B$ represents a shorthand notation for the K equations of mass balance in the system.

In matrix notation, the least-squares solution matrix is obtained by a) premultiplication of both sides of the equation by the transposed matrix (rows and columns interchanged) of A=A'

$$A'AX = A'B \tag{5}$$

followed by b) premultiplication of both sides of 5 by the inverse matrix $[A'A]^{-1}$

$$X = [A'A]^{-1}A'B \tag{6}$$

A least-squares matrix calculation subroutine is commonly available in programming manuals (IBM 360A-CM-03X) as well as descriptions of input format and mathematical theory.

Limitations of the Program

The application of the above computational technique to the testing of geologic models is restricted by its intractability. Because of the complex interactions of all of the components of the A matrix in yielding a least squares solution, it is nearly impossible to decide a priori how an input component or group of components should be changed to improve the fit. One is dealing with a minimum in an n-dimensional surface of sums of squares of residuals and the n-dimensional error functions describing deviations from this minimum. As yet, the mathematics of such a calculation are too complex to program. A partial solution to this problem has been devised (Wright and Doherty, 1970) and is described in a later section.

Assuming that the input data are correct, one is faced with the philosophical problem of treating the minimum in the residual-surface as the true best solution. Clearly, a complex surface may have many minima and the smallest errors in input data may lead to the selection of a minima different from the true situation. This situation may be aggravated when sets

of input vectors are very similar (Gordon Goles, personal communication). The magnitude of this effect remains to be tested.

The analytical errors attached to analyses of major element compositions of rocks may vary considerably with the element of interest, yet the program used in the original study contained no subroutine for weighting of input data. Such weighings would constrain the final solution to give best fits for the oxide compositions most reliably measured. The selection of weights should not be arbitrary but based on some consistent scheme. Selection of weight values and the effect on solution values is discussed below.

At its present stage of development, the computer analysis of major element data as a tool for predicting rock petrogenesis must remain in the role of supportive evidence. If one relies on the computer calculations to generate hypothess, general confusion is likely to result. Our imprecise knowledge of the relationship between goodness of fit and the real world situation and our poor understanding of the affects of erroneous input data on the final answers remain serious obstacles. The more reasonable approach depends on field, petrographic and experimental evidence as the principle sources of data for petrological hypothesis, with computer studies serving as useful corroborative evidence. A successful hypothesis would require the support of a computer study, but the degree of agreement required remains unclear.

Program Improvements

Subsequent to the original investigation, a least-squares program was developed to specifically deal with some of the problems discussed in the preceding section(Wright and Doherty, 1970). Some of the original data was rerun on this program to check for inconsistencies and enhance interpretation of original results.

The new program allowed for an approximation of the sensitivity of residuals to changes in the solution matrix. In this scheme, each solution value is incremented by a fixed amount and a new solution set calculated. This is continued until the residuals of the new solution set violate arbitrarily fixed limits. (One residual changes by .01 or the average of all residuals changes by more than .03.) The best solution set which does not violate the conditions is then printed. This procedure is repeated for each solution value and called error ranging. Such a restricted trial-and-error testing of the effect of solution variations gives a qualitative feel for reliability of each of the components of the solution matrix. Such a procedure approximates errors induced by using the other components to compensate for changes in a particular solution.

Input oxide analyses are weighted according to the relative standard deviations of analyses on suites of analyzed Hawaiian basalts. Additional options useful for petrologic calculations (restricting signs of solutions, calculating

compositions of mineral solid solutions) were also included but not utilized in this study.

The computer result comparison was carried out in three stages, 1) exact duplication of original calculations on the new program 2) recalculation using weighted oxide inputs, 3) error ranging on solutions.

The results of phase (1) were surprising. The two programs gave slightly different solutions, given the same input data. Some results of this comparison are shown in Table 8[1]. The method of calculation is the same for both programs and the small discrepancies in solutions are probably due to some differences in numerical rounding. This same result has been found by other investigators (Ian Gibson, personal communication).

Weights used for phase (2) are taken from Wright and Doherty with the exception of P_2O_5, MnO which were given lower weights. SiO_2 = 1.40, Al_2O_3 = 1.70, FeO = 1.70, MgO = 2.00, CaO = 2.20, Na_2O = 2.90, K_2O = 4.00, TiO_2 = 2.50, P_2O_5 MnO = 9.9. Results for this data set are also shown in Table 8[1]. As expected, sums of squares of residuals are somewhat larger because of more allowed scatter in the weakly weighted points. In effect, the weighing restraints impose extra conditions on the best-fit, the results of which lead to small deviations from the non-weighted solution.

Error ranging was performed on solution sets for the weighted and non-weighted cases. Those solutions with large

Table 8[1]. Program Comparisons

Ol Bas → Picrite G-13 → G-121	Bryan	Wright	Wright (weighted)
G-13	.4670	.4623	.5119
Fa_{21}	.2718	.2739	.2634
Px	.2710	.2727	.2663
An_{61}	-.0029	.0020	-.0269
Ilm_{75}	-.0130	-.0108	-.0145
$\Sigma (resid.)^2$	.272	.361	.443

Ol Bas → Ol Poor Bas G-13 → G-8	Bryan	Wright	Wright (weighted)
G-13	1.318	1.328	1.2684
Fa_{21}	-.155	-.159	-.1458
Px	-.019	-.022	-.0133
An_{61}	-.097	-.108	-.0739
Ilm_{75}	-.034	-.039	-.0351
$\Sigma (resid.)^2$	.862	1.362	1.482

Ol Poor Bas → Trachybas G-8 → G-164	Bryan	Wright	Wright (weighted)
G-8	1.337	1.353	1.458
Fa_{21}	.0249	.0320	.030
Px	-.1912	-.2060	-.2475
An_{59}	-.1525	-.1529	-.2143
Ilm_{70}	-.0308	-.0294	-.0379
$\Sigma (resid.)^2$	.993	1.36	1.754

Trachybas → Trachyand G-164 → G-15	Bryan	Wright	Wright (weighted)
G-164	1.314	1.382	1.3091
Fa_{24}	-.0734	-.0761	-.0728
Px	-.0141	-.0351	-.0168
An_{54}	-.1222	-.1592	-.1235
Ilm_{66}	-.0477	-.0582	-.0504
Kspar	-.0259	-.0395	-.0273
$\Sigma (resid.)^2$	.0915	.821	.914

Table 8[1]. Continued

Trachyand → Trachyte G-15 → G-114	Bryan	Wright	Wright (weighted)	Trachyte → Aeg-Aug Trachyte G-114 → G-16	Bryan	Wright	Wright (weighted)
An_{52}	-.1229	-.1206	-.1458	An_{26}	-.6700	-.4598	-.3486
Ilm_{56}	-.0341	-.0335	-.0392	Ilm_{50}	-.0521	-.0392	-.0342
Kspar	.0628	-.0649	-.0558	Kspar	-.4628	-.3375	-.2730
$\Sigma(resid.)^2$	.1306	.170	.293	Ap	-.0099	-.0223	-.0149
				$\Sigma(resid)^2$	1.310	3.03	3.34

Aeg-Aug → Aeg-Aug Trachyte G-16 → G-149	Bryan	Wright	Wright (weighted)	Aeg-Aug Trachyte → Sodalite Trachyte G-149 → G-19D	Bryan	Wright	Wright (weighted)
G-16	2.297	2.2784	1.9977	G-149	1.435	1.2612	1.3590
Fa_{62}	-.0677	-.0723	-.0619	Fa_{100}	.0512	.0367	.0434
Px	-.0184	-.0311	-.0152	Px	-.0010	-.0135	-.0077
An_{18}	-.7971	-.7924	-.6149	An_4	-.3317	-.2307	-.2868
Ilm_{20}	-.0483	-.0490	-.0352	Ilm_{20}	-.0558	-.0370	-.0464
Kspar	-.3843	-.3831	-.2898	Kspar	-.1771	-.1174	-.1506
Ap	-.0073	-.0123	-.0107	Sod.	+.0726	+.0741	+.0740
$\Sigma(resid.)^2$	.778	.977	1.176	$\Sigma(resid.)^2$	.0162	.0615	.088

error ranges relative to their original values were considered
least critical in determining the degree of fit. Solution
ranges are displayed for the non-weighted and weighted cases
as a function of rock type in Figure 1[1].   In most cases,
the solution for the liquid phase is the most critical to the
fit. Ranging patterns are not very different for the two cases.
Uranium in the absence of zircon, and phosphorous in the ab-
sence of apatite concentrate very efficiently in the melt
during crystallization. Accurate determinations of these ele-
ments would provide an independent estimate of wt. fractions
of liquid remaining for each calculation step.

Error ranging was also performed on the major oxides.
This was done by solving a matrix equation of the form $A \cdot X = B$
in which the A matrix was in the transposed form of the ori-
ginal A matrix. Rows of the tranposed matrix had the labels
of mineral and liquid constituents and the columns ($\leq$ number
of rows) had the labels of major oxides. Matrix B contained
the pertinent solution set of wt % minerals and liquid from
Table 3. Ranging was performed on the solution set of this
new matrix equation in order to get an idea of the oxides most
critical to the fit. The order of sensitivity of the oxide
solution values is shown in Table 9[1]. Na_2O, K_2O, Al_2O_3 con-
sistently show high degrees of sensitivity while FeO shows
consistent low sensitivity. Sodium and potassium have large
weighing factors indicating difficulty of analysis and are
also the elements most subject to volatile transport.

Figure 1[1]: Error ranging on solution values for weighted and
non weighted results using program of Wright and
Doherty. Values expressed as % of the solution
value. Small error ranging indicates sensitivity
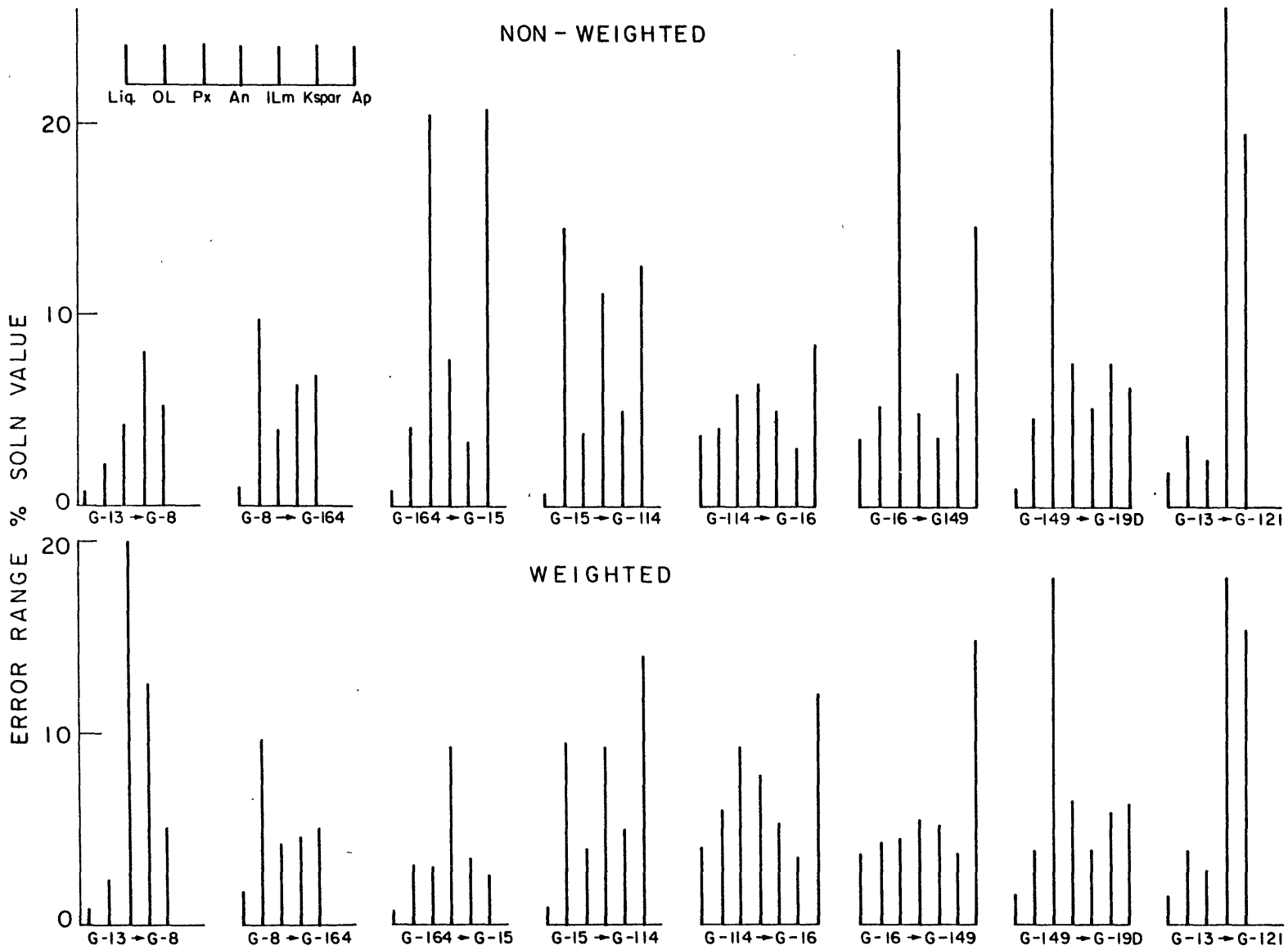of degree of fit to a particular solution value.

Table 9[1]. Oxide Ranging

Order of Sensitivity (#1 = most sensitive)

	G-13→ G-121	G-13→ G-8	G-8→ G-164	G-164→ G-15	G-15→ G-114	G-114→ G-16	G-16→ G-149	G-149→ G-19D
SiO_2	4	4	3	4	2	4	4	6
Al_2O_3	2	1	2	3	4	2	3	1
FeO	5	5	6	6	7	7	7	7
MgO	1	3	4	5	5	5	5	2
CaO	3	2	5	7	6	6	6	4
Na_2O			1	1	1	1	1	3
K_2O				2	3	3	2	5

G-121 Picrite Basalt

G-13 Olivine Basalt

G-8 Ol-poor Basalt

G-164 Trachybasalt

G-15 Trachyandesite

G-114 Trachyte

G-16 Aeg-Aug Trachyte

G-149 Aeg-Aug Trachyte

G-19D Sodalite Trachyte

Erroneous input values for the two elements are therefore possible and the efect on the least squares fit important.

References

Albarede, F., Bottinga, Y., Kinetic disequilibrium in trace element partitioning between phenocrysts and host lava. Geochim. Cosmochim. Acta 36 141-156 (1972).

Anderson, A.T., Greenland, L.P., Phosphorous fractionation diagram as a quantitative indicator of crystallization differentiation of basaltic liquids. Geochim. Cosmochim. Acta 33, 493-506 (1969).

Balashov, Y.A., Nesterenko, G.V., Distribution of the rare-earths in the traps of the Siberian platform. Geochem. Intern. 2, 672-679 (1966).

Bottinga, Y., Weill, D.F., Densities of liquid silicate systems calculated from partial molar volumes of oxide components. Am. J. Sci. 269, 169-182 (1970).

Bryan, W.B., Finger, L.W., Chayes, F., Estimating proportions in petrographic mixing equations by least squares approximation. Science 163, 926-927 (1969).

Cann, J.R., Bimodal distribution of rocks from volcanic islands, Earth and Planetary Sci. Letters 4, 479-480 (1968).

Chayes, F., Relative abundance of intermediate members of the oceanic basalt-trachyte association, J. Geophys. Res. 68, 1519-1534 (1963).

Chayes, F., A least-squares approximation for estimating the amounts of petrographic partition products. Min. et Pet. Acta 14, 111-114 (1968).

Cheng, K.L., EDTA titration of micro quantitites of rare earths. Chemist-Analyst 47, 93 (1958).

Denechaud, E.B., Helmke, P.A., Haskin, L.A., Analyses for the rare-earth elements by neutron activation and Ge(Li) spectrometry. Radioanal. Chem. 6, 97-113 (1970).

Frey, F.A., Haskin, M.A. Poetz, J.A., Haskin, L.A., Rare earth abundances in some basic rocks. J. Geophys. Res. 73, 6085-6097 (1968).

Gast, P.W., Trace element fractionation and the origin of tholeiitic and alkaline magma types, Geochim. Cosmochim. Acta 32, 1057-1086 (1968).

Haskin, L.A., Wildeman, T.R. Haskin, M.A., An accurate procedure for the analysis of the rare earths by neutron activation. J. of Radioanalytical Chem. 1, 337-348 (1968).

Haskin, L.A., Helmke, P.A., Paster, T.P., Allen, R.O., Rare earths in meteoritic, terrestrial and lunar matter. In Activation Analysis in Geochemistry and Cosmochemistry (ed. A.O. Brunfelt, E. Steinnes) 201-218 (1971).

Le Maitre, R.W., The geology of Gough Island, South Atlantic. Overseas Geol. Mineral. Resources (G. Brit.) 7, 371-380 (1960).

Le Maitre, R.W., Petrology of volcanic rocks, Gough Island, South Atlantic. Bull. Geol. Soc. Am. 73, 1309-1340 (1962).

Löw, K., Dead time corrections on measurements of shortlived activities. Nucl. Inst. and Methods 26, 216-218 (1964).

Nagasawa, H., Rare earth elements in zircon and apatite in acidic volcanic and igneous rocks, Earth and Planetary Sci. Letters 9, 359-364 (1970).

Onuma, N., Higuchi, H., Wakita, H., Nagasawa, H., Trace element partition between two pyroxenes and the host lava. Earth and Planetary Sci. Letters 5, 47-51 (1968).

Oversby, V.M., Lead isotopic compositions in recent volcanic rocks from islands in the Atlantic Ocean and from the troilite phase of iron meteorites. Ph.D. thesis, Columbia University (1969).

Oversby, V.M., Gast, P.W., Isotopic composition of lead from oceanic islands. J. Geophys. Res. 75, 2097-2114 (1970).

Schilling, J.G., Winchester, J.W., Rare-earths in Hawaiian basalts. Science 153, 867-869 (1966).

Schnetzler, C.C., Philpotts, J.A., Partition coefficients of rare earth elements and barium between igneous matrix aterial and rock-forming mineral phenocrysts - I. In: Origin and distribution of the elements (ed. L.H. Ahrens), p. 929-938. New York: Pergamon Press 1968.

Schnetzler, C.C., Philpotts, J.A., Partition coefficients of rare earth elements between igenous matrix material and rock-forming mineral phenocrysts - II. Geochim. Cosmochim. Acta 34, 331-341 (1970a).

Schnetzler, C.C., Philpotts, J.A., Phenocryst-matrix partition coefficients for K, Rb, Sr and Ba with applications to anorthosite and basalt genesis. Geochim. Cosmochim. Acta 34, 307-323 (1970b).

Tilley, C.E., Yoder, H.S., Schairer, J.F., Melting relations of volcanic tholeiite and alkali-rock series, Carnegie Inst. Wash. Y.B. 64, 69-82 (1965).

Tilley, C.E., Yoder, H.S. Schairer, J.F., Melting relations of
volcanic rock series. Carnegie Inst. Wash. Y.B. <u>65</u>, 260-269
(1966).

Wright, T.L., Doherty, P.C., A linear programming and least
squares computer method for solving petrologic mixing problems.
G.S.A. Bull. <u>81</u>, 1995-2008 (1970).

Yoder, H.S., Tilley, C.E., Origin of basalt magmas: An experi-
mental study of natural and synthetic rock systems. Jour. Pet.
<u>3</u>, 342-532 (1962).

Part 2

An Experimental Study of the Partitioning

of a Rare Earth Element in the

System Diopside/Water

Introduction

The understanding of trace element migrations under the influence of geologic processes can provide useful information about rock petrogenesis. Trace elements may be sensitive indicators of environmental conditions operative during the formation of a rock body which are not reflected in the major element abundances. Improvement of analytical techniques in recent years has led to a large body of trace element analyses of geologic and biologic materials. The rare earth elements are of particular interest as trace elements because of their widespread distribution throughout much of the biosphere and lithosphere and because of their geochemical coherency as a group.

Initial analyses of geologic materials for rare earth elements revealed that geological processes fractionated rare earths compared to a supposed primitive abundance pattern for chondritic meteorites. Similar rare-earth distributions among a series of rocks was taken to indicate similar geologic histories. Whole-rock rare earth abundances were found to be weighted averages of individual mineral rare earth abundances.

At the same time, the mathematics of trace element distributions during various solid-liquid equilibria such as partial melting or fractional crystallization was being developed. Semi-quantitative predictions of these distributions as a function of degree of melting or crystallization were found to agree with trends observed among geologically related rocks such as at Gough Island (Zielinski and Frey, 1970) and the Skaergaard (Wager

and Mitchell, 1951). Crucial to these calculations was the ac-
curate assignment of distribution coefficients.

The equilibrium distribution of a trace element between two
coexisting phases should be expressible as a constant which is
equal to the ratio of the trace element concentrations in each
phase. This is the so-called Berthelot-Nernst distribution law
and the constant is called the distribution coefficient (D.C.).
The law requires homogeneous distribution of trace throughout
the phases and therefore is also called the homogeneous distribu-
tion law. The existence of such a distribution coefficient can
be proven thermodynamically simply by assuming that at equilibri-
um the activity of the trace element is the same in both phases
and that the trace concentrations are small enough that dilute
solution theory (Henry's law) is obeyed. According to Henry's
law, activity = constant.concentration. Equating activities
then lead to a concentration ratio equal to a constant = D.C.

The distribution coefficient is not an absolute constant
but a constant in the sense of an equilibrium constant, i.e., it
varies with temperature, pressure and composition of the phases.
Figure 1 is a compilation of current distribution coefficient
data measured on separated clinopyroxene-rock matrix fractions
of a series of basaltic rocks (Schnetzler and Philpotts, 1970;
Onuma et al., 1968; Masuda and Kushiro, 1969). The overall
similarity of D.C. distributions is taken to indicate equilibri-
um in these systems. The absolute magnitudes of the distribution
coefficients are seen to vary over a factor of ten, probably
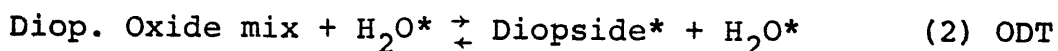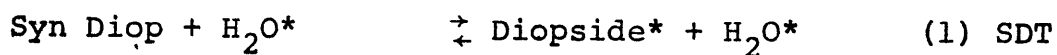under the influence of the above variables or kinetics (Albarede

Figure 1: Summary of existing measured clinopyroxene/liquid

distribution coefficients.
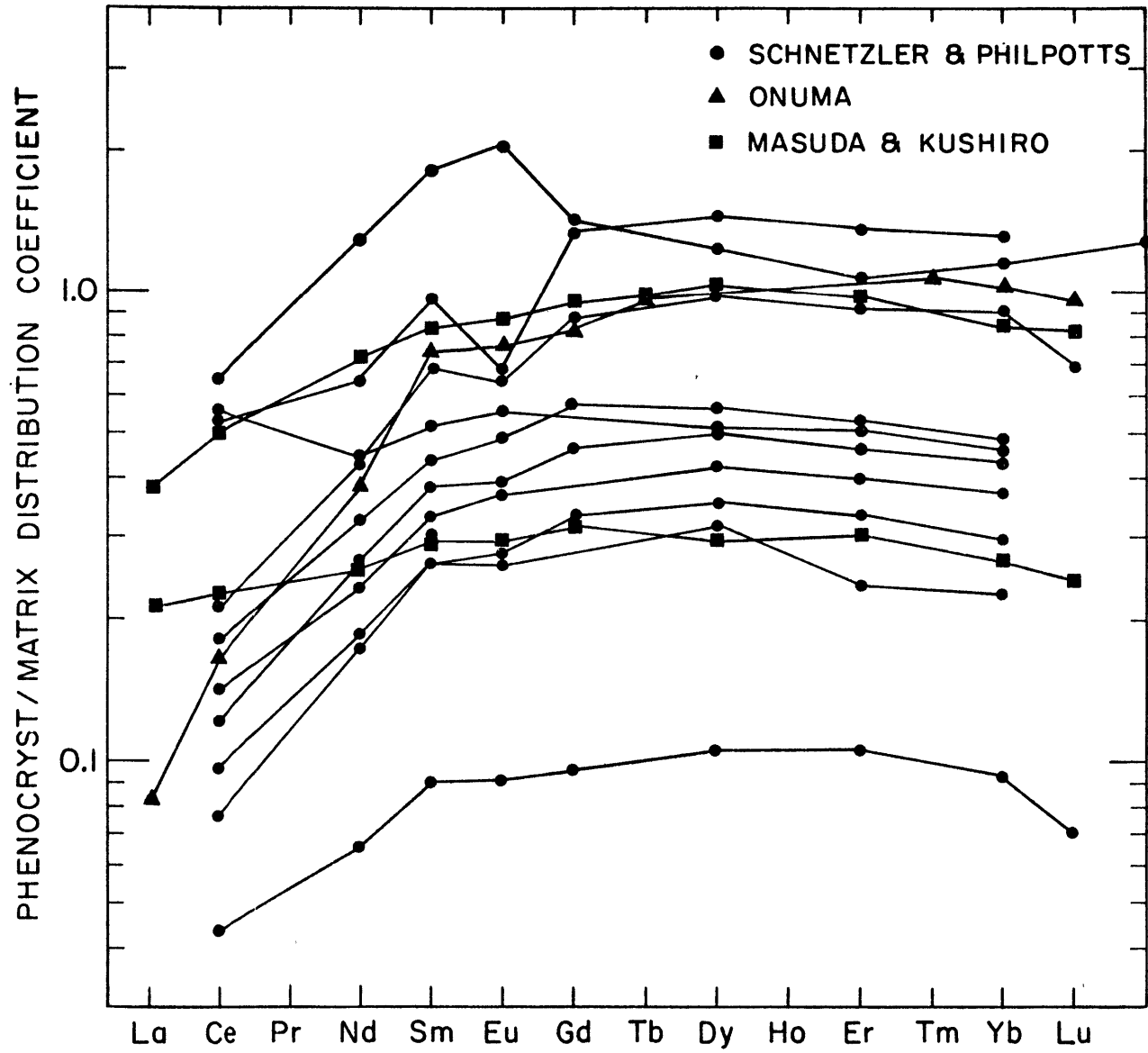
and Bottinga, 1972). Unfortunately these variables are covarient in nature and it is impossible to isolate the influence of each. An experimentally controlled situation is required for such information. Knowledge of the relative importance of each of the variables temperature, pressure, composition of the phases might lead to an independent means of estimating pertinent distribution coefficients in situations where physical separation of phases is impractical or impossible.

This study represents an attempt to measure and describe the partitioning of a rare earth ion Gd^{+3}, as a radioactive tracer, in the system diopside-water. Experimental conditions were controlled in such a way as to measure the degree of equilibrium or non-equilibrium in the system as well as the effect of each of the above variables. Gadolinium was chosen because of its central position in the rare earth group and because of its availability as a ^{153}Gd tracer of long half-life. Diopside was chosen because of the ease and completeness of its synthesis under hydrothermal conditions and because of its ubiquity in igneous and metamorphic rocks. The system mineral-water was chosen to facilitate separation of the phases. Direct comparison with natural mineral-water interactions such as metamorphic or hydrothermal situations was intended. Indirect analogy with mineral-melt equilibria was implied.

Partitioning of Gd in the diopside-water system was studied according to the following reactions.

$$\text{Syn Diop} + H_2O^* \rightleftharpoons \text{Diopside}^* + H_2O^* \qquad (1)\ \text{SDT}$$

$$\text{Diop. Oxide mix} + H_2O^* \rightleftharpoons \text{Diopside}^* + H_2O^* \qquad (2)\ \text{ODT}$$

SDT, ODT products + $H_2O \overset{\rightarrow}{\leftarrow}$ Diopside* + H_2O*   (3) SDTR, ODTR

*contains radioactive gadolinium tracer.

Reaction #1, the SDT type, starts with previously synthe-
sized diopside (see preparation methods below) and an aqueous
solution of gadolinium tracer. In reaction #2, diopside is syn-
thesized from a stoichiometric mixture of oxides as the parti-
tioning is occurring. Finally reaction #3 represents reversals
of reactions 1, 2 by re-equilibrating products of the first two
reactions with pure water.

Starting Materials

Diopsides were synthesized from a stoichiometric mix of
spec-pure oxides. Prior to mixing, each of the oxides was fired
to constant weight and stored in a desicator. The mix was ground
under acetone in an agate mortar and later ground as a dry powder.
The mix was then redried and stored in air-tight containers.

Gadolinium carrier and non-radioactive stock solutions were
prepared from spec-pure Gd_2O_3. Gadolinium tracer was obtained as
99% purity ^{153}Gd, half-life 242 days, specific activity 2.21
mc/mg Gd. All gadolinium solutions were diluted to the appropri-
ate concentrations with distilled, deionized water and acidified
with reagent grade HCl.

Stock solutions of $CaCl_2$ and NaCl were prepared from spec
pure $CaCO_3$ and NaCl. Oxalic acid for CO_2 runs was reagent grade.

Experimental Method

Diopside was prepared from the starting mix in two ways.

1) Diopside was crystallized from an oxide melt at one atmosphere in a vertical, platinum wire resistance furnace calibrated with a platinum-rhodium thermocouple. 2) Diopside was grown hydrothermally during the course of experimental runs described below. The purity of the products was checked optically and by x-ray and found to be free of glass and other phases. Some tridymite <1% was observed in the hydrothermal runs and probably represents precipitation of leached silica.

Hydrothermal experiments were performed in externally heated cold-seal type stellite steel bombs 12 inches long with internal bores of $11\frac{1}{4}$" x $\frac{3}{4}$". Bombs were positioned in the furnaces such that the end of the bore hole "sample chamber" was in the "hot spot" of the furnace. The temperature gradients over the lower 1" of the sample chamber were usually less than 2° as measured by chromel-alumel thermocouples. During experiments, a thermocouple was placed in an outside well drilled so as to be adjacent to the inner bore. Temperature differences for the well and inner bore were measured to be usually less than 4°C. During experiments temperatures were read using a Leeds and Northrup potentiometer. Temperatures were controlled by Harrel proportional temperature controllers linked with 100 ohm ceramic-shielded platinum resistance sensors. Total variation in temperatures during experiments was less than ±2°C.

The pressure medium was water except in a few cases where argon was used. Pressures were attained using Haskel air driven water pumps and read off Bourdon-tube pressure gauges. Variations in pressure readings usually were less than ±3%.

Experiments were contained in clean, annealed platinum cap-
sules 3.6 cm long, 3.0mm O.D. x 2.8 mm I.D. In some experiments
gold or silver - palladium alloy capsules of similar dimensions
were used. Liquid solutions containing tracer were added using
a microliter syringe. Weights of liquid and solid starting ma-
terials were recorded as well as the loaded capsule weight and
the weight after being crimped and micro-arc-welded shut (approx.
0.1 mg wt. loss during welding). Loaded bombs were placed in
pre-heated furnaces and usually attained run conditions within
$\frac{1}{2}$ hour. Capsules were small enough so that two could be placed
side by side in the sample chamber. Unless otherwise stated,
most experiments were performed at 800°C and 1 kb pressure, well
in the stability field of diopside.

At the termination of an experiment, bombs were allowed to
cool in air and were then immersed in a water quench bath with
total quench time approximately five minutes. Recovered capsules
were cleaned, dried and reweighed to check for possible leaks.
Any weight change greater than ±0.5 mg was considered a leak and
the experiment was discarded. Ends of the capsule were snipped
and the contents rinsed into a nalgene dish with a solution of
0.01 M $GdCl_3$ carrier. The large excess of non-radioactive Gd in
the carrier was used in order to exchange with any Gd tracer
which might have been adsorbed on solid surfaces. Independent
experiments verified the efficiency of this procedure. Gd^{+3} ion
is strongly adsorbed at room temperature and presence of carrier
solution was intended to minimize loss by adsorption of tracer
during the separation procedures. The opened capsule was also

submersed in the exchanger solution. Capsule and contents remained in this bath for $\frac{1}{2}$ hour although final results were independent of immersion time or amount of agitation during immersion.

Run products and additional rinsings of the nalgene dish were transferred by eye-dropper to two 15 ml conical centrifuge tubes and centrifuged at 3000 rpm for 10 minutes. This was sufficient to bring down all diopside particles larger than 0.2μ. Solutions were drawn off with a micro pipette and solids combined into one centrifuge tube and recentrifuged. Liquid was again drawn off and combined with previous liquid. Separated solids were deposited at the bottom of a centrifuge tube and ready for counting. The liquid volume (∿45 ml) was evaporated down to ∿5 ml and rinsed into a clean centrifuge tube where it was combined with an equal volume of saturated oxalic acid. The resulting precipitate of gadolinium oxalate was allowed to digest for $\frac{1}{2}$ hour at 80°C and then centrifuged. The precipitate was shown by experiment to contain 100% of the gadolinium activity originally in solution. At this point both solid and liquid were in the same physical form for counting.

Measurement of the radioactivities of the separated solid and liquid phases was performed by a $1\frac{3}{4}$" x 2" NaI well detector. This was attached to a 400 channel pulse height analyzer equipped with digital readout onto paper tape. A scaler circuit was also implemented to record total counts received. A background count was included for each counting set and activites corrected accordingly.

After counting, the diopside separate was recovered and

weighed. A solid yield factor was computed by comparing this weight to the weight of solids originally placed in the capsule. Solid yields averaged about 95%. An activity yield factor was computed by summing the total activities of solid and liquid separate and comparing with the recorded counts of a standard tracer solution. Generally, solid yield and activity yield agreed within the errors for their calculation because in most experiments the tracer was highly preferred in the solid phase.

The efficiency of the separation procedure was also checked. The main concerns were contamination of liquid by tiny diopside particles and loss of liquid activity by adsorption. The latter was checked by manipulating a standard tracer solution plus carrier through the separation procedure and recounting. A liquid yield factor of 97% was obtained. In all the experiments a liquid yield factor of 100% was assumed. Small systematic errors may have resulted from this assumption. The former was checked by redissolving the gadolinium oxalate in 6 N nitric acid and filtering though 0.05μ millipore filter paper with water and $GdCl_3$ carrier. The filter papers were then counted for an activity due to trapped bits of diopside. In no case did such activity exceed 5% of the liquid activity.

Concentration ratios were expressed as counts ^{153}Gd/wt according to the following equation

$$\frac{\text{counts solid} - \text{Bkg.}}{\text{counts liq.} - \text{Bkg.}} \cdot \frac{\text{wt. liquid}}{\text{wt. solid}} \cdot \frac{1}{\text{solid yield}} = \frac{\text{Gd/wt. solid}}{\text{Gd/wt. liquid}}$$

Absolute values of concentration were obtained knowing the

original concentration of the starting solution.

Finally, solid products were examined optically and by x-ray diffraction for possible impurity phases. Apart from the above-mentioned tridymite, no other phase was observed except for wollastonite in some $CaCl_2$ solution runs probably formed by the reaction

$$CaCl_2 + SiO_2 + H_2O \rightleftharpoons Ca\ SiO_3 + 2HCl$$
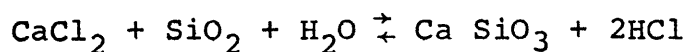
Establishment of an Equilibrium Condition

Direct measurements of gadolinium distributions in the solid phase using scanning electron microprobe or autoradiograph were not possible because of the small amounts of trace element (~5 ppm for most experiments) and the small grain sizes of run products ($1-20\mu$). Indirect methods were therefore required to 1) establish that the distribution was homogeneous, 2) show that equilibrium had been attained. Only if these two conditions were satisfied, could a study of Nernst distribution coefficients be initiated.

a) Nernst equilibration - The experimental variables which should alter Nernst-type distribution coefficients are given in column 1 of table 1. Column 2 lists those experimental variables which should not affect the equilibrium distribution. Column 2 variables are kinetic variables which should influence the rate at which equilibrium is attained but not its final value. Measured concentration ratios independent of all variables in column 2 were considered to represent the case of homogeneous, equilibrium distributions between solid and liquid phase. Homogeneous

Table 1.

Dependent and Independent Variables for Equilibrium Conditions

Dependent Variables	Independent Variables
Pressure	Solid/liquid Ratio
Temperatures	Grain Size
Composition of Phases	Run Duration
Trace Element Type	Trace Concentration (dilute solution obeyed)
	Reaction Type SDT vs. ODT
	Forward or Reverse Reactions

distributions in the supercritical liquid phase which existed at run conditions were assumed. Given the excellent mixing and transport properties of such a phase, this assumption was considered reasonable.

b) <u>Rayleigh equilibrium</u> - A possible alternate to Nernst equilibration is that for the case of non-homogenous trace concentrations in the solid. Such distributions result from a series of frozen-in surface equilibrations between a growing crystal and a liquid phase of changing composition. For each equilibration, the concentration at the mineral surface is assumed proportional to the concentration in the liquid phase. This proportionality constant is called the Rayleigh or logarithmic distribution coefficient (λ). Resulting crystals are zoned and only the outermost surface is in equilibrium with the final liquid. If this process is operative, measurement of distribution coefficients by bulk concentration techniques clearly leads to erroneous results with D.C. apparent > D.C. Nernst for D.C. > 1. Measurement of λ requires actual measurement of trace concentrations in mineral surfaces or data on phase abundances as a function of amount of crystallization. This type of data is difficult to obtain in this experimental system. Since this type of distribution requires simultaneous crystal growth, agreement of ODT and SDT series would not be expected. Also, reversal experiments would initially only involve outer surfaces of newly grown crystals and thus reversal results would not agree with original results measured by a bulk concentration technique.

c) <u>Non-equilibrium</u>.- For this situation, any trace element distribution is possible and results should be dependent on all

or some of the kinetic variables of column 2. Kinetically controlled results could lead to study of rate constants (diffusion constants) as well as rate-altering variables and their implicataions regarding mechanisms of Gd-substitution in diopside.
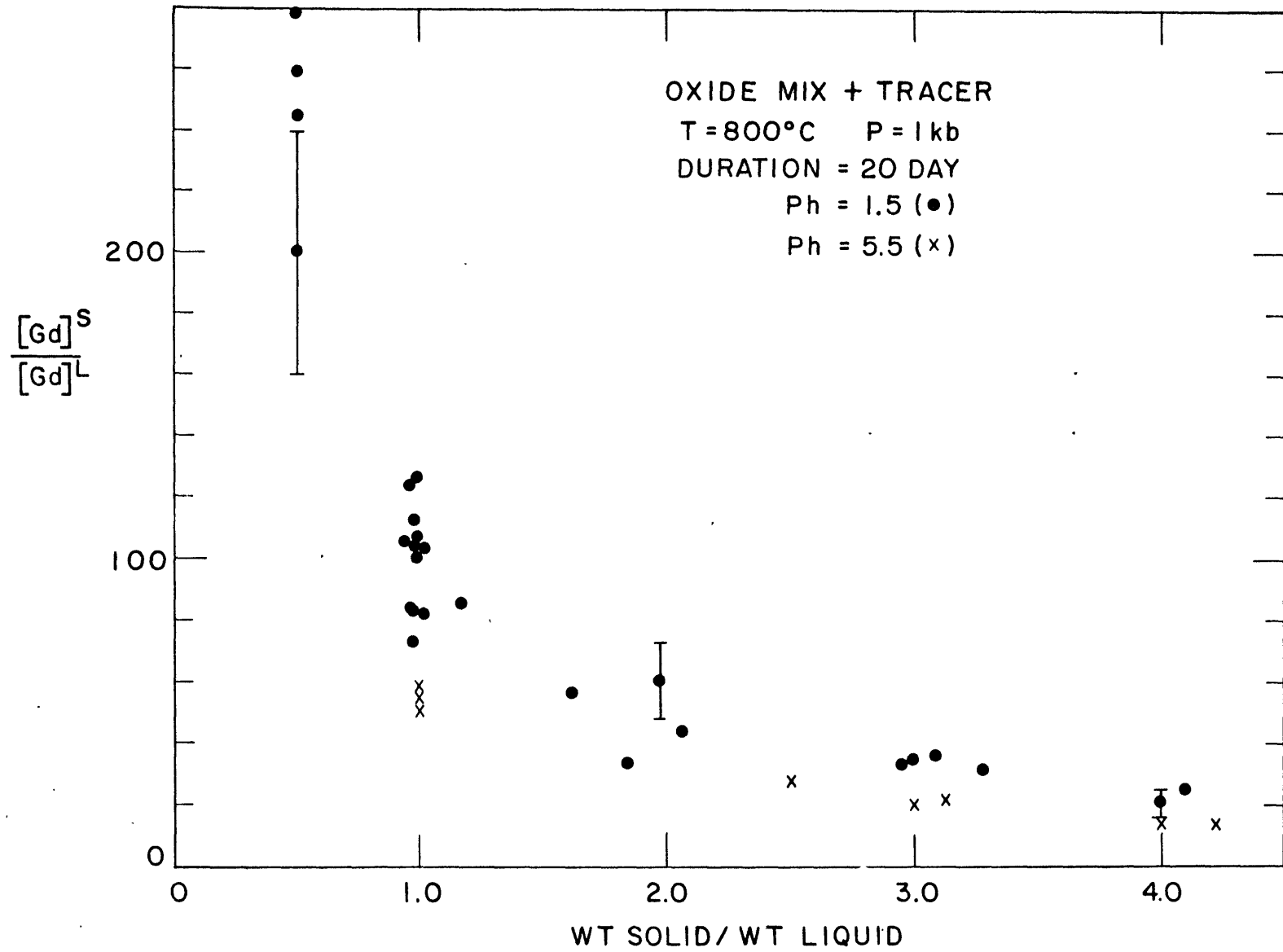
Experimental Results

Figures 1a, 1b represent results for the effect of solid/ liquid weight ratios on the measured Gd concentration ratios. Other possible variables such as temperature (800°C), pressure (1 kb), composition of phases, run duration (20 days), grain size (average radius = 10 μ), $[Gd]_{liq}^{orig}$ (5 ppm) were kept constant. Measured gadolinium concentration ratios of SDT or ODT products do not agree at identical values of solid/liquid ratio. Uptake in the solid is more pronounced for diopside synthesized from an oxide mix. In both the SDT and ODT series there is increased uptake in the solid at lower solid/liquid ratios. Most of these experiments were performed using initial solution pH's of 1.5. A few points marked (x) represent results at initial pH of 5.5. Error bars are drawn as ±20% and indicate the standard deviation between twin experiments from the same bomb. A standard deviation of ±30% approximates errors for all experiments at a particular set of conditions. These same errors are assumed for all the following results. Constancy of interfering variables is also strictly maintained in all of these controlled experiments.

Figure 2 shows the effect of grain size of SDT starting materials on the final concentration ratios. Grain sizes are reported as average grain sizes estimated by calibrated microscope

Figures 1a, 1b: Measured Gd concentration ratio as a function

of solid/liquid ratio; Oxide mix and previously
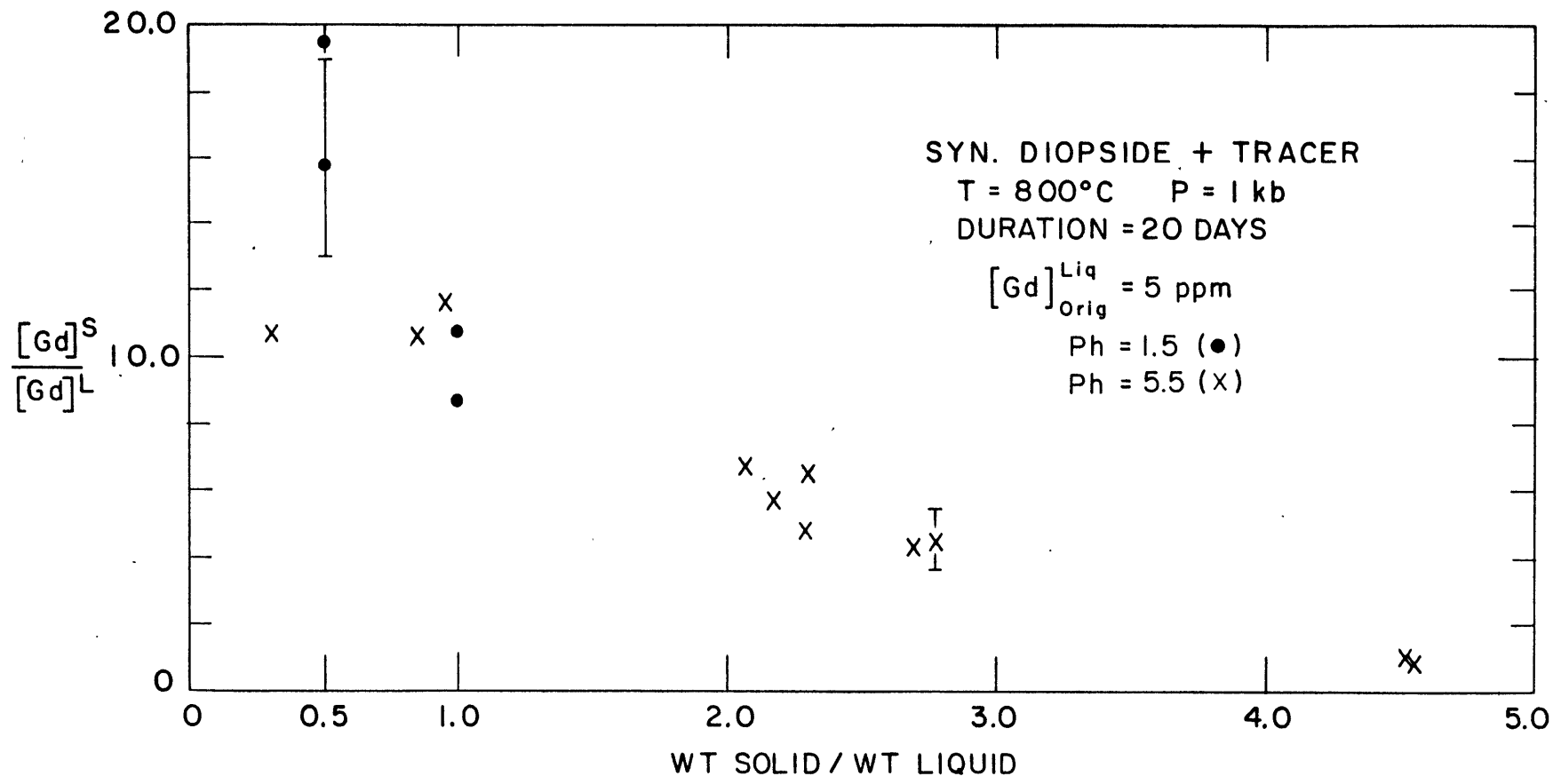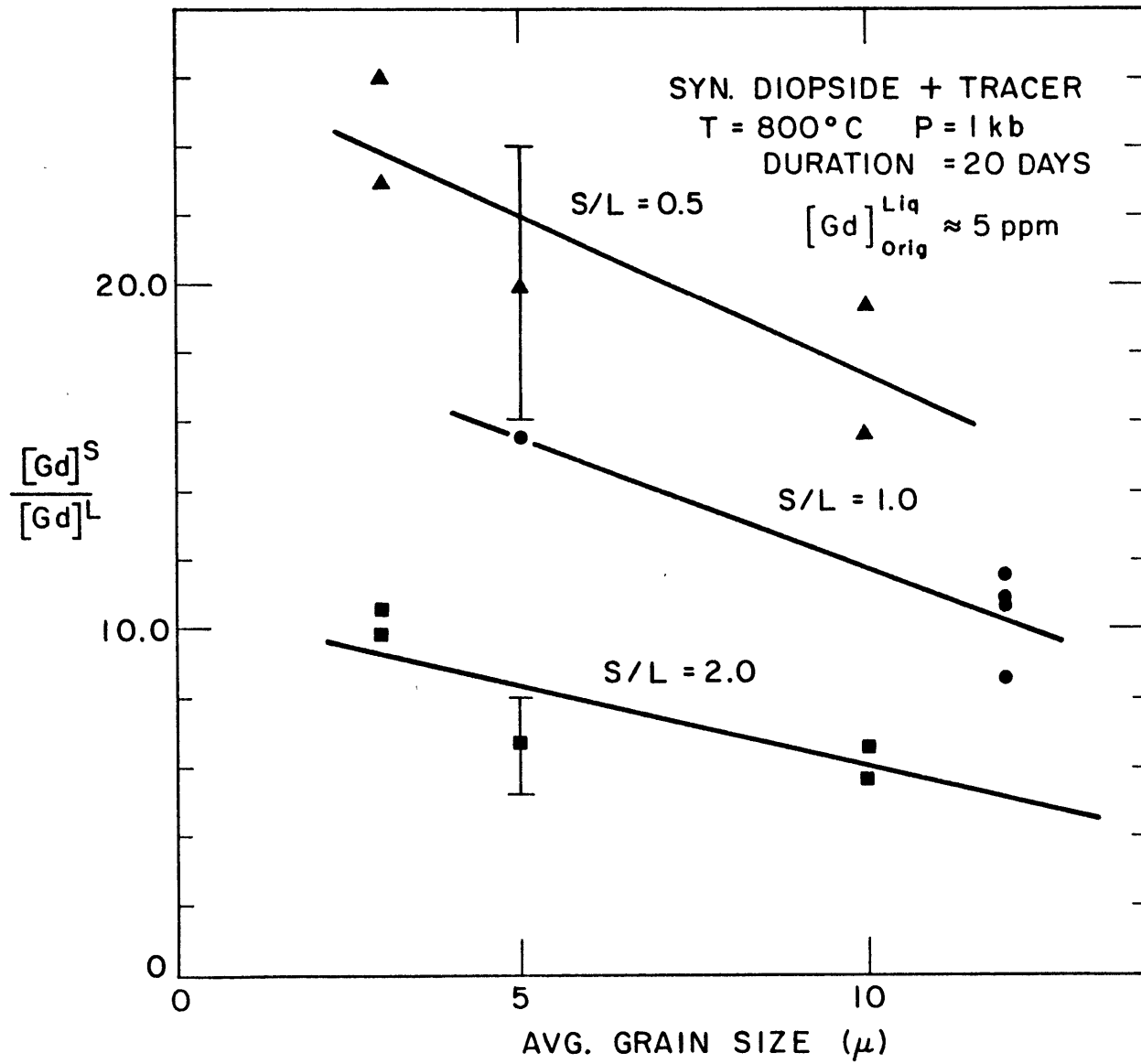
synthesized diopside.

OXIDE MIX + TRACER
T = 800°C   P = 1 kb
DURATION = 20 DAY
Ph = 1.5 (●)
Ph = 5.5 (×)

$\dfrac{[Gd]^S}{[Gd]^L}$

WT SOLID/ WT LIQUID

SYN. DIOPSIDE + TRACER
T = 800°C   P = 1 kb
DURATION = 20 DAYS

$[Gd]_{Orig}^{Liq}$ = 5 ppm

Ph = 1.5 (●)
Ph = 5.5 (×)

$\dfrac{[Gd]^S}{[Gd]^L}$

WT SOLID / WT LIQUID

Figure 2: Variation of measured concentration ratio as a function

of average grain size. Curves for S/L = 0.5, 1.0, 2.0.

All values for SDT case.

observations. Such estimates are to be regarded as qualitative.
Smaller starting grain size is more favorable for Gd incorpora-
tion in the solid. For the SDT results, grain size effect is
shown for a number of solid/liquid ratios. Combination of low
solid/liquid ratio and small grain size leads to the most pro-
nounced solid uptake. Oxide mixes finer than 10μ radius gave
$[Gd]_S/[Gd]_L > 200$ for S/L = 1.0. Errors in measurement of such
small amounts of activity in the liquid result in large variations
in measured ratios. All ratios >250 are therefore grouped as
"very large".

Results for the reversals of ODT and SDT reactions are given
in Table 2. Agreement between forward and reverse reactions for
the ODT and SDT cases is generally within a factor of two. Re-
versal results for the SDT case give concentration ratios which
are systematically larger than the forward reaction indicating
less tracer has gone into the liquid phase than expected. Con-
versely, ODTR results are systematically smaller, indicating more
tracer has entered the liquid phase than expected.

Figures 3a and b plot measured $[Gd]^S/[Gd]^{liq}$ as a function
of experiment duration. Rapid initial uptake of Gd by the solid
is noted for times of the order of 1 day. For both the ODT and
SDT series this initial uptake is reduced somewhat at 4 days and
subsequently either increases slowly (SDT) or remains fairly con-
stant (ODT).

Figures 4a,b,c show the effect of variations in trace concentration
on measured concentration ratios. Both series show little depen-
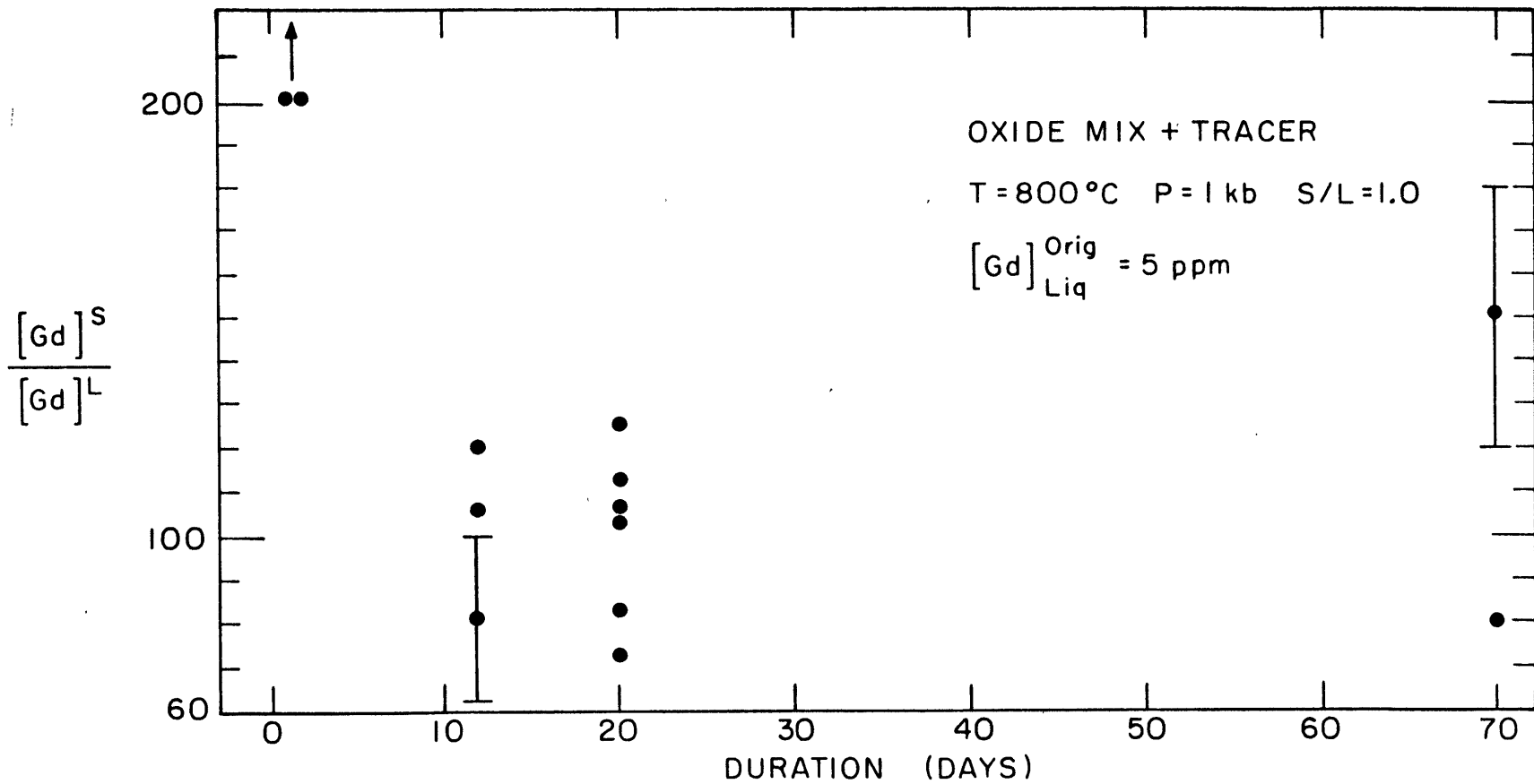dence on this variable over a substantial range of trace
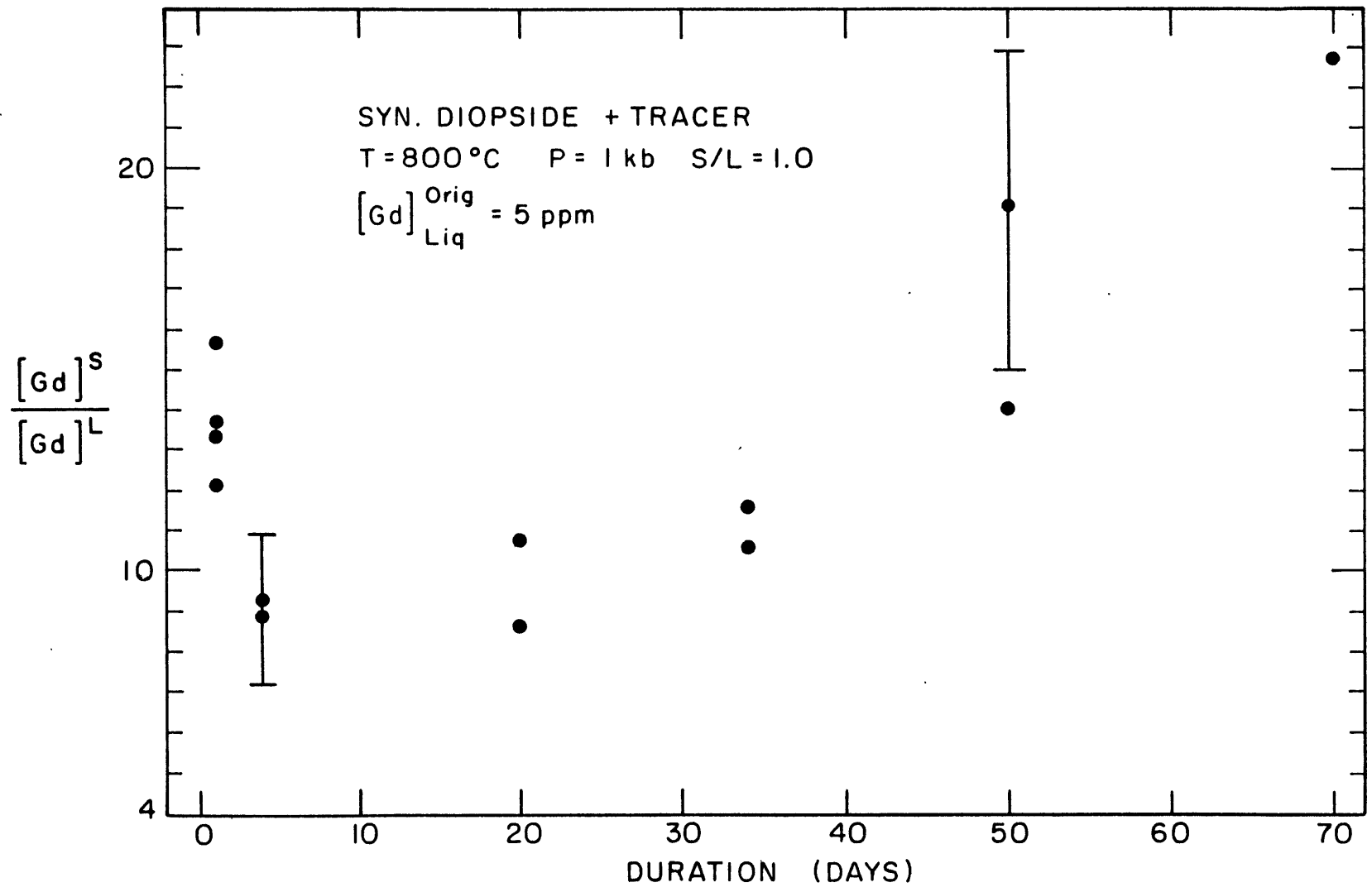
Table 2.

Results of Reversed Experiments

Exp. #	Conc. ratio forward	Conc. ratio reverse	Duration forward & reverse (days)	Forward ratio > reverse
ODT 5	15.1	15.7	17	—
ODT 7	16.6	8.30	10	Y
ODT 8	19.4	17.7	10	Y
ODT 11	21.9	34.2	6	N
ODT 12	11.4	8.50	6	Y
ODT 9	46.2	27.8	12	Y
ODT 69	72.0	32.5	20	Y
ODT 71	112	60.0	20	Y
ODT 25	23.6	10.4	20	Y
ODT 26	20.4	14.6	12	Y
ODT 28	33.5	32.3	20	—
ODT 29	32.0	31.7	20	—
ODT 85	8.20	6.00	20	Y
ODT 96'	8.90	10.8	20	N
ODT 97'	123	91.5	20	Y
SDT 15	15.5	8.70	20	Y
SDT 16	6.70	4.10	20	Y
SDT 25	14.8	20.9	20	N
SDT 24	10.6	14.4	20	N
SDT 21	10.6	24.0	34	N
SDT 22	11.5	18.0	34	N
SDT 49	2.88	4.21	20	N
SDT 50	0.92	1.63	20	N

Figures 3a, 3b: Ratio of $[Gd]_s/[Gd]_l$ as a function of experiment
duration. ODT and SDT cases.

OXIDE MIX + TRACER

T = 800°C   P = 1 kb   S/L = 1.0

$\left[Gd\right]_{Liq}^{Orig} = 5$ ppm

$\dfrac{\left[Gd\right]^S}{\left[Gd\right]^L}$

DURATION (DAYS)

SYN. DIOPSIDE + TRACER
T = 800 °C   P = 1 kb   S/L = 1.0

$[Gd]_{Liq}^{Orig} = 5$ ppm

$\dfrac{[Gd]^S}{[Gd]^L}$

DURATION   (DAYS)

Figures 4a, 4b: Gd conc. ratio as a function of original conc.

of Gd in tracer solution.

Plot showing $\dfrac{[Gd]^S}{[Gd]^L}$ versus $[Gd]^{Liq}_{Orig}$ (ppm).

SYN. DIOPSIDE + TRACER
T = 800°C   P = 1 kb
DURATION = 20 DAYS
S/L = 1.0
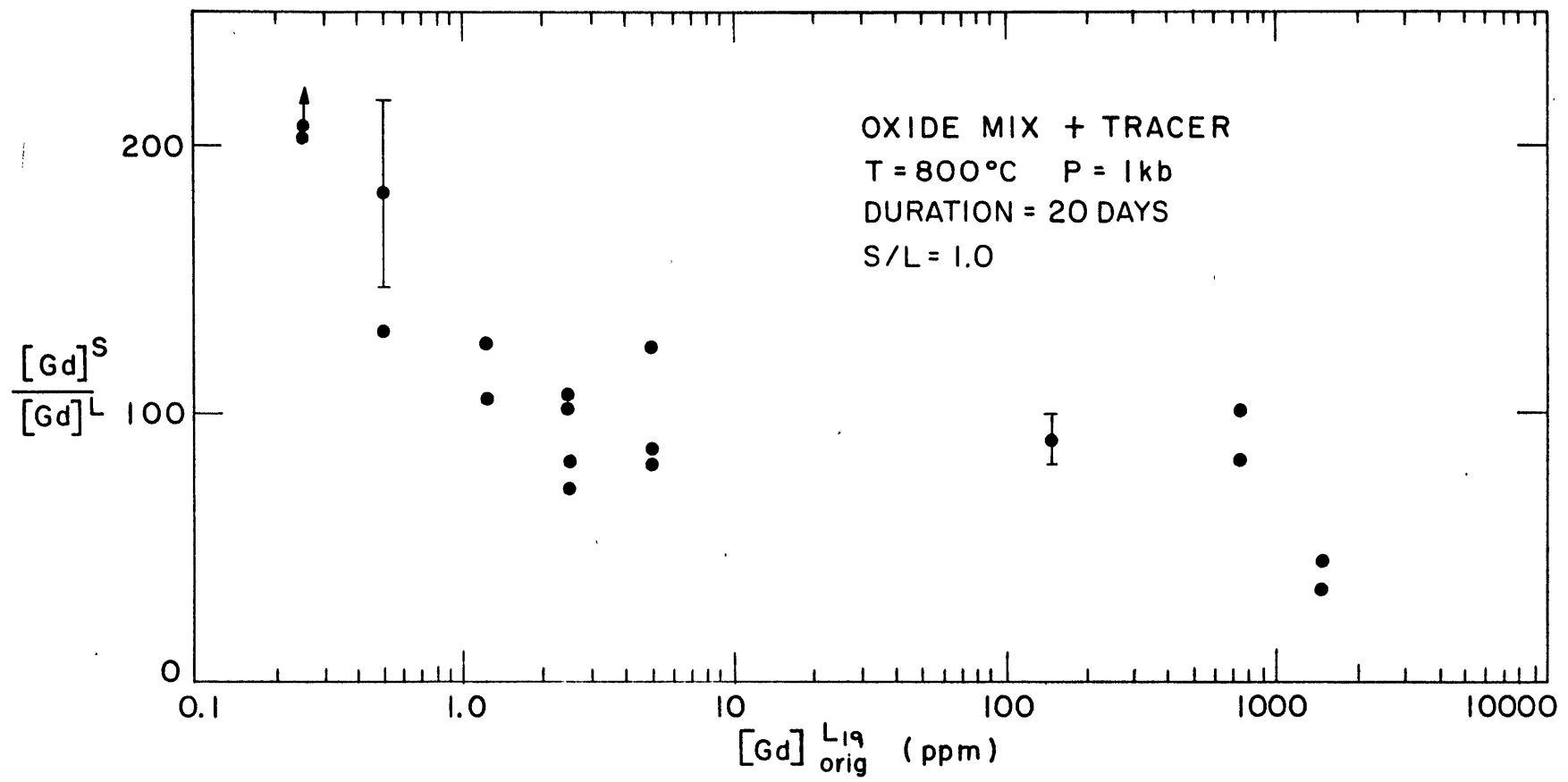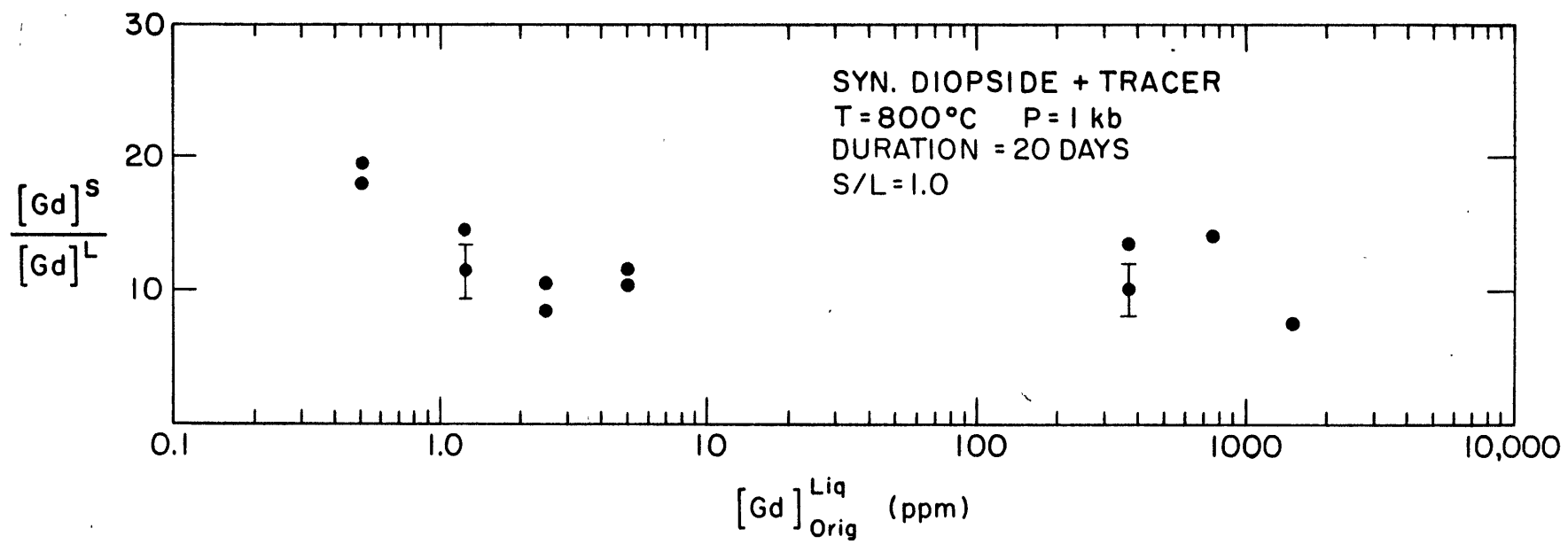
Figure 4c: Concentration of Gd in solid vs. conc. of Gd in
liquid for SDT and ODT experiments. Lines drawn
for constant D.C. = 10, 100.
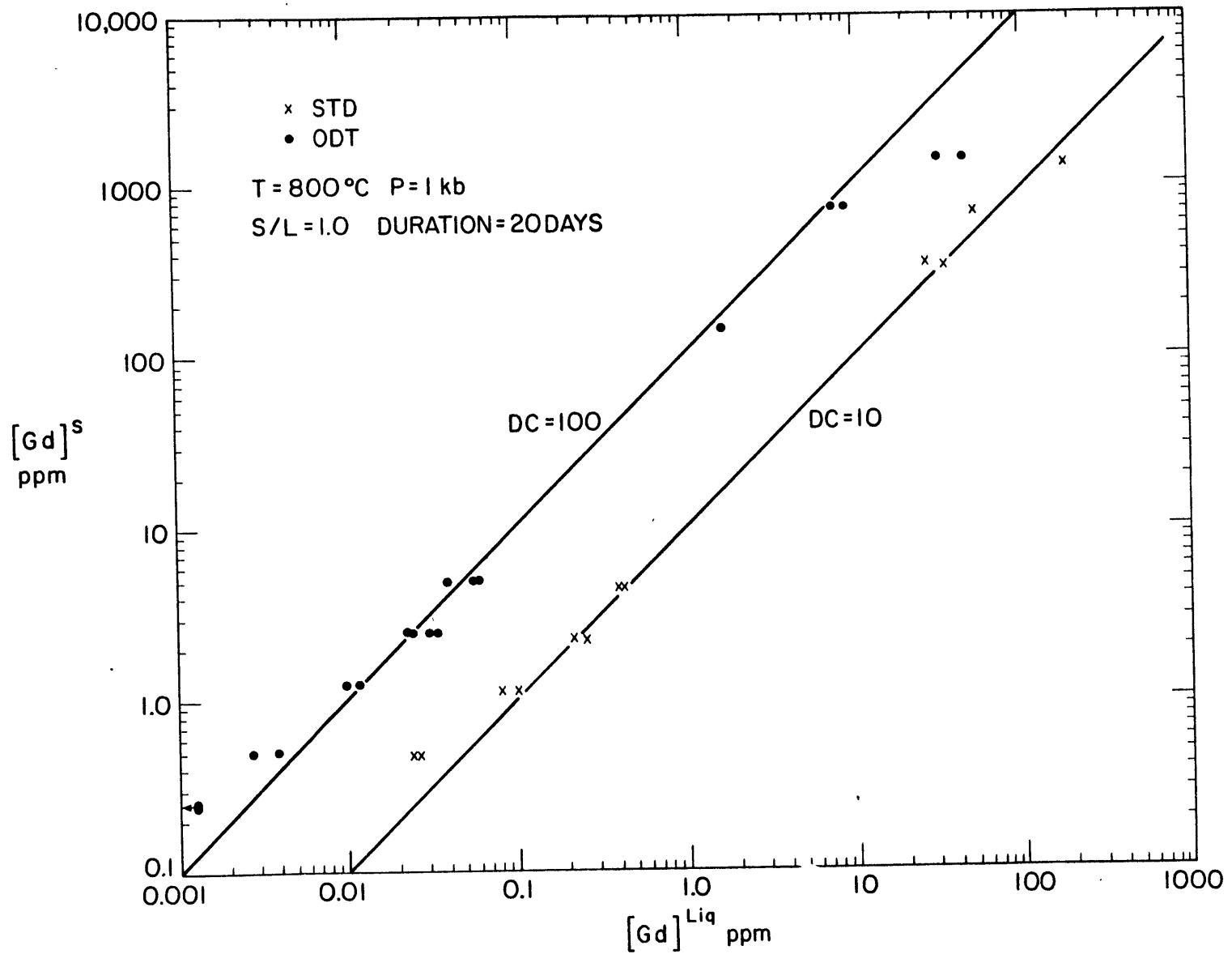
concentrations. There is some effect noted at the low end of the scale ($[Gd]_{orig}^{liq}$ < 1 ppm) and at the high end ($[Gd]_{orig}^{liq}$ = 1550 ppm). ODT values seem to fit a constant concentration ratio = 100 while SDT results are consistently around a value of 10.

Plotted on Figures 5a and 5b are results for variations of the liquid phase composition. Measured concentration ratios are shown as a function of $CaCl_2$ concentration of the liquid. The ODT series shows marked decrease of ratios as the molarity of $CaCl_2$ in the solution increases. A similar effect for the SDT case is not as obvious. Measured ratios for liquid solutions of 1M NaCl are also included and indicate increased uptake of Gd in the solid compared to pure water.

A few experiments were performed at 800°C, 2kb water pressure to study the effect of pressure on the Gd partitioning. This data is presented in Table 3 and indicates slight increases in $[Gd]^S [Gd]^{liq}$ at higher pressures. The effect of temperature on the Gd partitioning has been reported (Cullers et al., 1970. Increasing temperature (600-800°C) was found to increase measured concentration ratios.

Finally, the liquid phase composition was altered by inducing finite partial pressures of CO_2. This was accomplished by adding weighed amounts of oxalic acid dihydrate. Oxalic acid was pinch sealed in small platinum capsules which were placed inside the normal capsule containing diopside and tracer. During the experiment, oxalic acid decomposed to CO_2 and H_2O which escaped from the small capsule to mix with the rest of the

Figures 5a, 5b: Variation of measured Gd concentration ratios as a function of liquid phase composition. ODT and SDT cases.
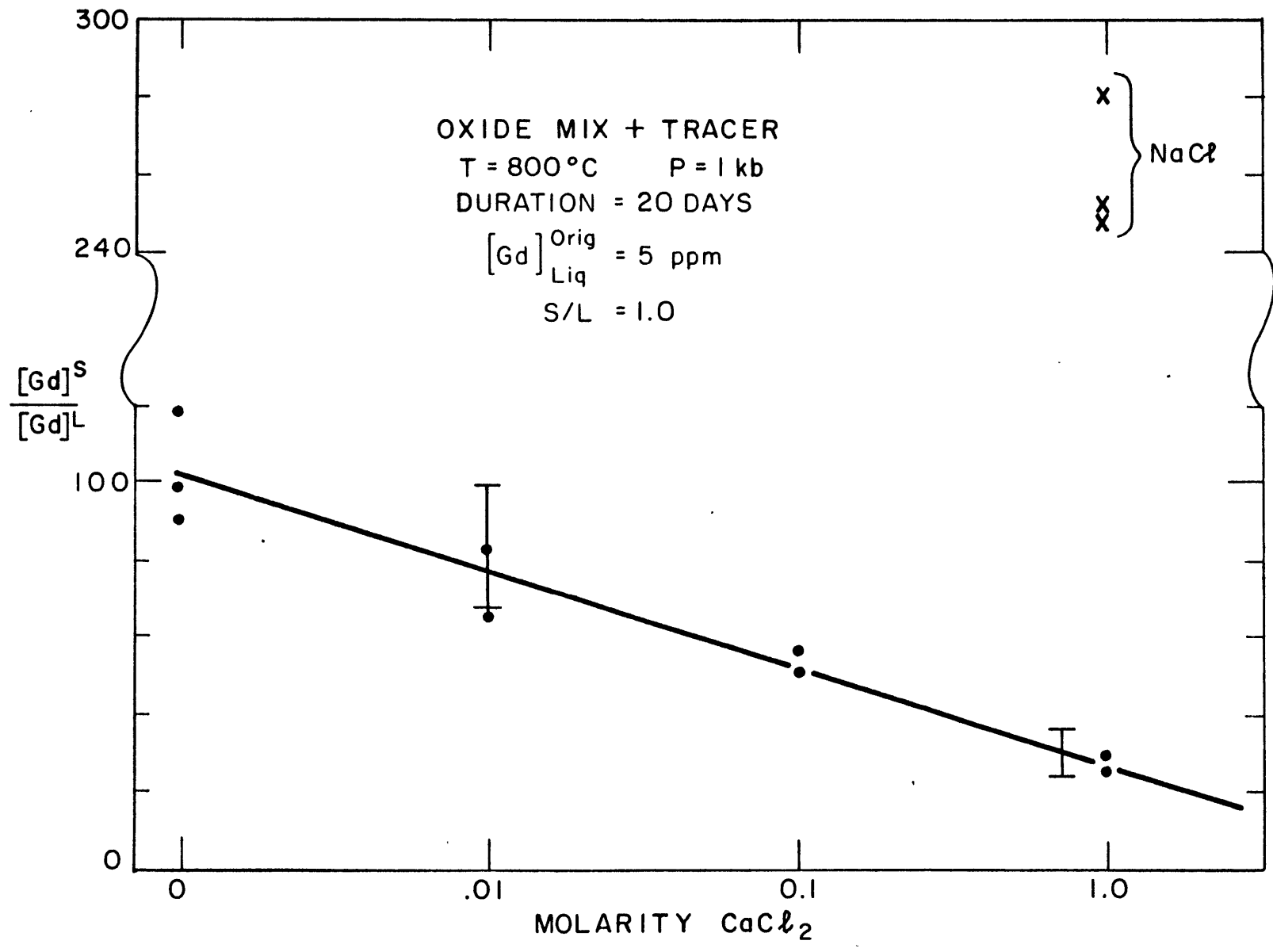
OXIDE MIX + TRACER
T = 800°C   P = 1 kb
DURATION = 20 DAYS
$\left[Gd\right]_{Liq}^{Orig}$ = 5 ppm
S/L = 1.0

NaCℓ

$\dfrac{[Gd]^S}{[Gd]^L}$

MOLARITY CaCℓ$_2$
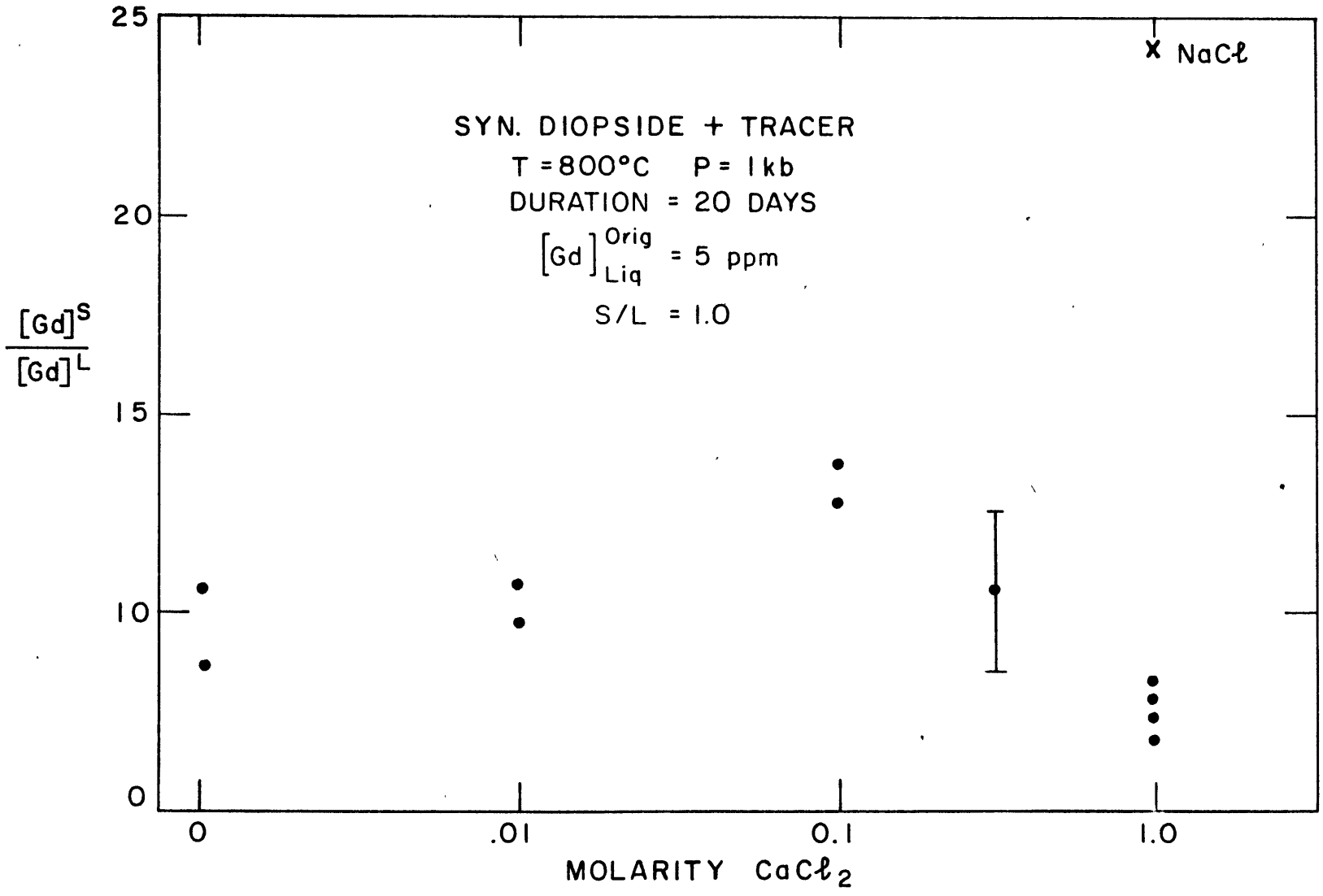
Table 3.

Pressure Effect

T = 800°C

Time = 20 days

S/L = 1.0

Exp.	Pressure	$[Gd]_s/[Gd]_{liq}$
SDT 43	2 Kb	17.0
SDT 44	2 Kb	15.3
SDT 46	2 Kb	15.7
SDT (avg)	1 Kb	10 ± 2
ODT 120	2 Kb	250
ODT 121	2 Kb	162
ODT (avg)	1 Kb	100 ± 20

charge solution. Possible decomposition products such as CO

or CH_4 are not stable in the range of P_{O_2} induced by the buf-

fering action of the steel bomb. (Holloway, Burnham and Milhol-

len, 1968). Estimated P_{O_2} for the 800°C experiments are of the

order of 10^{-14} - 10^{-18} bars (Eugster and Wones, 1962). During

quenching, CO_2 remains in the gas phase. Its large molar volume

at room temperature and atmospheric pressure causes considerable

internal pressures within the sealed capsule. Using capsule

sizes equivalent to those for the other experiments and S/L =

1.0, mole fractions greater than X_{CO_2} = 1.20 ($5mgCO_2/15mgH_2O$)

were found to burst the capsules. Use of Ag-Pd capsules did

not greatly improve upon this. Data for experiments with X_{CO_2} =

.120 is shown in Table 4. No effect of increased CO_2 content

on concentration ratios can be conclusively shown for the SDT

case. ODT values seem to be increased. Investigations at

higher values of CO_2 content will require larger capsule volumes,

a variable not investigated in this paper.

Discussion

Nature of Substitution: General Theory

Gadolinium should exist in the +3 valence state at the P_{O_2}

imposed by the experimental system. This poses problems for

substitution in minerals such as diopside in which there are no

triply-charged cations for isovalent exchange. Any postulated

substitution mechanism must involve some charge-compensating

scheme. Of the cations available in diopside for exchange with

Gd, Ca^{+2} has an ionic radius (.99 Å, Pauling) closest to that of

Table 4.

$$X_{CO_2} = .120 = 5mgCO_2/15mgH_2O$$

T = 800°C

P = 1 Kb

Time = 20 days

S/L = 1.0

Exp.	X_{CO_2}	$[Gd]_s/[Gd]_{liq}$
SDT 83	.120	11.6
SDT 84	.120	13.8
SDT (avg)	0	10 ± 2
QDT 136	.120	281
QDT 139	.120	286
QDT (avg)	0	>250 (finer grained mix)

Gd^{+3} (1.02 Å). Exchange of these two cations requires less distortion of the diopside structure than any other postulated cation exchange couple and is therefore energetically favored. Possible exchange reactions involving calcium and gadolinium are listed in Table 5.

Reaction (1) requires coupled substitutions of Gd^{+3} and a hydrogen ion replacing two calcium cations. Availability of H^{+} cations in the solution is critical to such a reaction. Reaction (2) involves substitution of two gadolinium ions for the calcium ions with the formation of cation vacancies in the solid. Large numbers of vacancies in the original solid would favor such a reaction. Finally, reaction (3) requires coupling of Gd^{+3} and Na^{+1} cations substituting for two Ca^{+2} ions. The Na^{+1} cation is similar in size (.95 Å) to Ca^{+2} and this reaction should be favored in systems with high sodium ion concentrations.
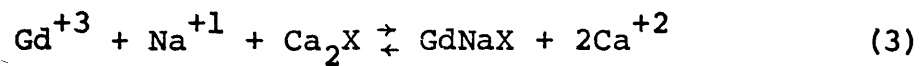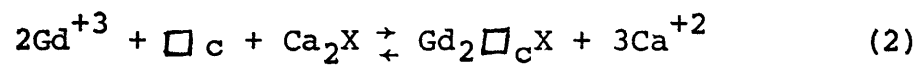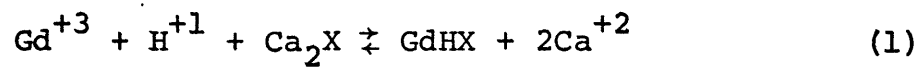
Postulated Mechanisms for Gd-Ca Exchange

SDT Case:

Step 1: This step is attained during the early part of the experiments and is controlled by the rate at which diopside reaches its equilibrium solubility in the liquid. Calcium ions are leached from the mineral surface leaving sites which can be occupied by Gd. For the SDT case, this surface controlled solubility-exchange involves only the outermost layers of the original diopside and the apparent D.C. measured as ratio of bulk concentrations of Gd in the phases is less than the true D.C. Nernst. Rate of uptake of Gd ions during this step is enhanced by any experimental variable which leads to increased surface leaching

Table 5

Likely Substitution Mechanisms

$$Gd^{+3} + H^{+1} + Ca_2X \rightleftharpoons GdHX + 2Ca^{+2} \qquad (1)$$

$$2Gd^{+3} + \square_c + Ca_2X \rightleftharpoons Gd_2\square_cX + 3Ca^{+2} \qquad (2)$$

$$Gd^{+3} + Na^{+1} + Ca_2X \rightleftharpoons GdNaX + 2Ca^{+2} \qquad (3)$$

X = remainder of diopside structure

$\square_c$ = cation vacancy

of calcium.

Step 2: Subsequent to uptake of Gd by step 1, further move-
ment of Gd in the solid is controlled by the rate of Gd diffu-
sion in the non-leached areas of the crystal (see appendix).
Existing concentration gradients of Gd after step 1, result in
diffusion of Gd into the crystal. As time proceeds, more Gd
is taken into the crystal from the liquid and D.C. apparent in-
creases and approaches D.C. Nernst.

ODT Case:

Step 1: The behavior of Gd in this system is complicated
by the simultaneous growth of diopside. The mechanisms of diop-
side growth include dissolution of reactants, transport of dis-
solved materials, nucleation of product (possibly through a
series of simple structured reaction intermediates). Description
of the precise behavior of Gd during these processes is beyond
the scope of this investigation. The following simplified view
of the behavior of Gd is consistent with the results of ODT
experiments. Under this simple model, a number of diopside sur-
faces may be exposed to the liquid phase as diopside first nu-
cleates and grows to its final size. The Gd content of the li-
quid will be changing as crystallization proceeds. Diopside
cores exchange with the original, most concentrated, Gd solutions
while the final partitioning between outermost rim and liquid
involves a much diluted Gd solution. Resulting Gd profiles in
such crystals might resemble those calculated for Rayleigh
equilibrium when logarithmic distribution coefficients are
greater than 1.0 (Albarede and Bottinga, 1972). For such

distributions D.C. apparent measured by bulk concentration ratios
is greater than D.C. Nernst. Experimental conditions which af-
fect the rate-controlling step of diopside growth would then be
expected to influence the amount of Gd uptake by the solid. On
the basis of experimental results for ODT reactions, it is postu-
lated that the rate controlling step for diopside growth, and
Gd uptake, is the dissolution of the oxides. Experimental con-
ditions which enhance the rate of dissolution of the oxides
should enhance the rate of Gd uptake in product diopsides (Fyfe,
Turner and Verhoogen, 1960).

Step 2: Since the postulated Gd concentration gradients
existing in the solid after step 1 put most of the Gd in the
center of the crystal. With time, Gd should diffuse out of the
crystal allowing further exchange between the aqueous phase and
the outermost rim of the grown diopside. As time proceeds,
D.C. apparent → D.C. Nernst.

Experimental Support of Postulated Mechanisms

Referral to experimental results for the time dependence of concentration ratios shows that from ~4 days on,,the SDT results agree with those expected for diffusion into the crystal. Anomalous behavior at <4 days may be due to surface crack trapping of Gd adsorbed at lower temperatures. By 4 days, these cracks have annealed out and the anomalously high solid concentrations reduced. By estimating the average grain size of the diopside and assuming that equilibrium is 99% attained at t = 70 days, it is possible to calculate a maximum value for the diffusion constant of Gd in diopside. The equation used is that for diffusion into spheres from a well-stirred solution of finite volume (Crank, 1956, eqn. 6.30) at t=0 the solid is assumed free of all diffusant. At t > 0 , the rate of uptake by the solid is always balanced by the rate of loss from the solution. Solution composition is assumed homogeneous. The calculated value for D_{max} is 2.5 x 10^{-15} cm^2 sec^{-1} (see appendix). Possible errors caused by non-sphericity of grains, nonisotropic diffusion in complex crystals, and poor estimates of grain size have been discussed (Lin and Yund, 1971) and should not contribute more than a factor of 3 error (see appendix). Literature values for some measured diffusion constants of ions in silicates are given in Table 6 for comparison.

Time dependence of ODT results is not clear. Postulated zoning in ODT product diopsides requires measured ratios to decrease with time as Gd diffuses from the concentrated center to the edge. In the SDT case most of the Gd is at the crystal surface with ready availability to the solution. Abruptness of

Table 6

Diffusion Constant Data

| Element	Host	Temp(C°)	Dcm^2sec^{-1}	References
Mg	fayalite	900	2×10^{-12}	Misener, 1972
Mg	fayalite	1100	3.7×10^{-11}	"
Na	orthoclase	800	8.8×10^{-11}	Foland & Giletti, 1972
K	orthoclase	800	9.5×10^{-14}	"
Na	phlogopite	800	6×10^{-11}	Giletti, 1972
K	phlogopite	800	1.5×10^{-13}	"
Rb	phlogopite	800	1.3×10^{-13}	"
Na	albite	850	8×10^{-11}	Sippel, 1963
Na	orthoclase	850	5×10^{-11}	"
Na	acmite	940	$<10^{-11}$	"
Na	orthoclase	800	$\sim 8 \times 10^{-13}$	Lin & Yund, 1972
K	orthoclase	600	1×10^{-10}	"
Mg	enstatite	25	$<10^{-17}$	Luce et al., 1971
Ca	β wollastonite	800	2×10^{-13}	Lindner, 1954
Ca	larnite	800	2×10^{-13}	"
Ca	α larnite	800	3.6×10^{-15}	"

changes in the Gd surface concentration caused by diffusion depend upon the sharpness of the concentration gradient of Gd between crystal surface and core. Changes in the concentration of the surface with time are immediately reflected in the solution concentrations according to the constant surface/liquid D.C. For ODT products all or much of the Gd is originally at the crystal center. If the concentration gradient for Gd near the diopside surface is small, the concentration of Gd at the crystal surface may not change greatly within 70 days time and the concentration of Gd in the liquid and bulk solid remain essentially constant. At greater times, as large amounts of Gd reach the crystal surface, the solution concentration would increase and measured $[Gd]_S/[Gd]_L$ would decrease.

Results for reversals of ODT and SDT experiments lend interesting support to the concentration gradient models for both cases. Figure 6 is a schematic representation of Gd behavior during ODTR and SDTR experiments.

SDT case: At the end of the forward reaction SDT, the concentration profile of Gd in the solid resembles that for diffusional transport after deposition as a thin surface film (Shewmon, 1963). At SDTR t>0, the surface layer re-equilibrates with pure water according to the constant diopside/water distribution coefficient for Gd. The surface layer is depleted of Gd compared to its content at the end of the SDT experiment. Likewise, the concentration of Gd in the liquid which is in equilibrium with this depleted layer is lower relative to its value at the end of the SDT run. If the number of atoms of Gd

Figure 6: Diagram illustrating hypothesized behavior of Gd

during reversal experiments for ODTR and SDTR

cases.
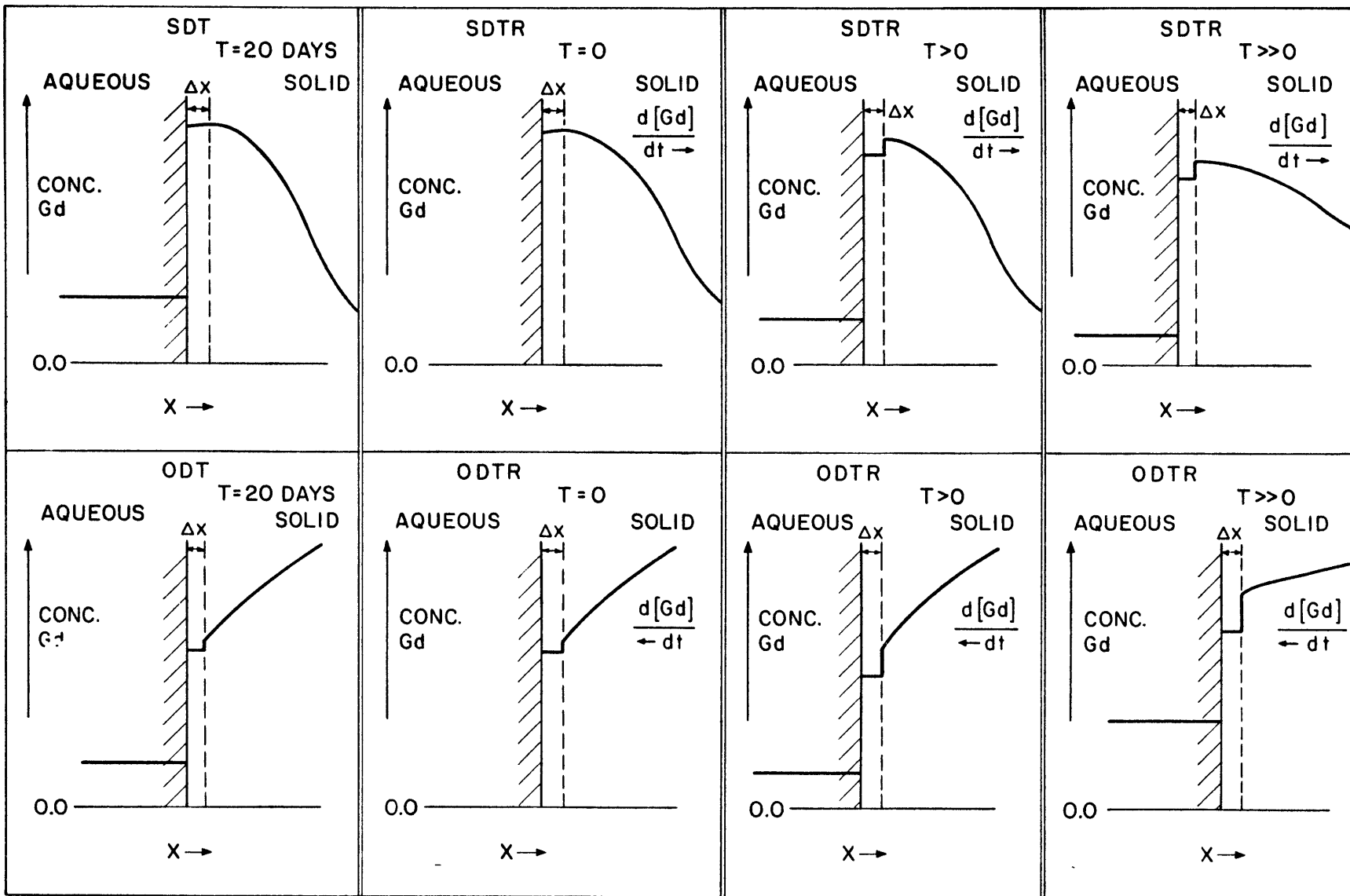
which are removed from the surface layer are small compared to the total number of Gd atoms in the solid, the concentration of Gd in the solid $\approx$ concentration of Gd in solid at the end of the SDT experiment. Measured $[Gd]_S/[Gd]_L$ at SDTR, $t>0$ should be larger than the value of SDT, $t=20$ days. At SDTR $t>0$ Gd has diffused into the center of the crystal. The surface layer of thickness ΔX has been depleted by diffusion but is replenished as some tracer enters the layer from the solution. As a result, concentration of Gd in the solid increases while liquid concentration decreases. Measured $[Gd]_S/[Gd]_L$ at SDTR, $t>70$ should be even larger than those for SDTR, $t>>0$.

ODT Case: At the end of the forward reaction ODT, the concentration profile of Gd in the solid resembles that for Rayleigh equilibrium, given a distribution coefficient >1 (Albarede and Bottinga, 1972). At ODTR, $t>0$ the surface layer of thickness ΔX reequilibrates with pure water and measured $[Gd]_S/[Gd]_L$ are larger than for ODT, $t = 20$ days by the same arguments used for SDTR, $t>0$. At ODTR, $t>>0$. Gd diffuses from the center of the crystal enriching the surface layer. The aqueous phase, which is in equilibrium with this surface is also enriched. The concentration of Gd in the solid decreases while the liquid concentration increases. Measured $[Gd]_S/[Gd]_L$ should then decrease relative to the values of ODTR, $t>0$ and eventually should become even lower than the values for ODT, $t = 20$ days.

The results for the effect of solid/liquid weight ratios on measured concentration ratios can give useful information

about the actual value of D.C. Nernst.

Consider first the SDT synthesis. Low solid/liquid ratios result in the leaching of more Ca ions from the solid to bring the liquid up to the equilibrium concentration of calcium. The thickness of the leached layer ΔX is increased. In the limiting case of large excesses of water, the leached layer increases to the point where the entire crystal is in contactwith the solution. If the partitioning between the leached layer and the solution is taken as the Nernst distribution coefficient, then $[Gd]_S/[Gd]_L$ for SDT synthesis is equal to D.C. Nernsc at very low solid/liquid ratios. From Figure 1b this value appears to be approaching 20 at S/L = 4.0. Equilibration with respect to Gd of solid and liquid can also occur by solid diffusion and at t = 70 days measured $[Gd]_S/[Gd]_L$ approach a value of 20 for SDT (Figure 3b).

Consider the ODT synthesis. Rate of growth from an oxide mix is greatly enhanced by addition of water to the system. The rate of solution of starting materials and/or their rate of transport to nucleation centers are increased (Fyfe, Turner and Shaw, 1951 and Verhoogen, 1958). Changes in the weight of water added to a closed system of solids + water determines the speed at which reactants may be dissolved. If hydrated forms of the oxides are important reaction intermediates in the growth process of diopside, the overall growth rate of diopside should be influenced by changes of water content. Rate of growth can influence the value of logarithmic distribution coefficients (McIntire, 1963). Successively formed layers may

not equilibrate with their coexisting liquids. For a loga-
rithmic distribution coefficient greater than 1.0, efficiency
of uptake by the solid should increase with the degree of
equilibration of successive layers and liquid. However, if
the growth rate becomes too rapid, the predominant mechanism
of uptake will be occlusion. In the limiting case of instan-
taneous precipitation (quench phase) all uptake is by occlu-
sion and $[Gd]_S/[Gd]_L$ becomes less than 1.0. Occlusion does
not appear to be important in the ODT experiments because at
S/L = 0.5 efficiency of solid uptake is still increasing
(Figure 1a). At very high S/L ratios, rate of growth is slowed
to a point where Gd zoning is homogenized by diffusion as fast
as layers are added. Values of $[Gd]_S/[Gd]_L$ for ODT syntheses
should then be expected to approach D.C. Nernst. From Figure
1a, the value of $[Gd]_S/[Gd]_L$ approaches 20 at S/L = 4.0.

From the above arguments, D.C. Nernst for Gd in the sys-
tem diopside/water is tentatively estimated at a value of 20.
Further experiments at low S/L (SDT) and high S/L (ODT) are
required to support this hypothesis. Longer duration diffu-
sion measurements for SDT and ODT would also support or refute
a D.C. $\approx$ 20.

As shown in Figure 2, smaller starting grain sizes of
previously synthesized diopside result in increased solid up-
take of Gd for experiments of equal duration. The solubility
of a particle is dependent on its size according to the so-
called surface tension effect. Small grains are unstable with
respect to larger grains because of the tendency of the system

to reduce its total surface area. For SDT runs, increased

solubility leads to greater leaching of calcium and resulting

greater uptake of Gd by solubility exchange of stage 1. For

oxide mix synthesis, smaller grain size of starting materials

increases rate of diopside formation by increasing the rate of

solution of oxides. Correlation of rapid growth and large Gd

uptake is noted.

The pressure effect noted at 2 Kb water pressure could be

explained using the argument of increased solution of solids

at higher solvent densities. Also, increased adsorption ef-

fects at higher pressures cannot be ruled out. According to

the shapes of adsorption isotherms for most solids, increasing

pressure initially causes dramatic increases in % adsorption.

At "high" (dependent on system) pressures adsorption becomes

much less dependent on P, presumably as the capacity of the

initially adsorbed monolayer is exceeded.

In his measurements of the effect of temperature on Gd

partitioning between silicates and water, Cullers found in-

creased uptake of Gd in diopside at higher temperatures. Since

equilibrium partitioning of Gd was assumed in his experiments

he calculated values for ΔH_{subst} from the slopes of his D.C.

vs. temp. plots. From the results of this study, it would

seem unlikely that equilibrium conditions were attained in his

system. His experiments were performed at larger solid/liquid

ratios (3.5-7.0) larger grain sizes (10-200 μ) and shorter

duration (10-20 days). For previously synthesized diopside of

this size range to equilibrate with a liquid via diffusion in

20 days time would require a diffusion constant of the order of 10^{-12} cm^2 sec^{-1}. This is equivalent to diffusion of Na in albite at 800°C (see Table 6). Results of this study and others (Sippel, 1963; Lindner, 1954; Misener, 1972) would indicate a much smaller diffusion constant for Ca diffusion in pyroxenes. Arguing for equilibration at lower temperatures becomes even more diffucult. More likely, what Cullers measured were kinetic effects in which rate of Gd uptake/unit time increased as the temperature increased.

An attempt was made to duplicate the results of Cullers starting with 80 mg of previously synthesized diopside (hydrothermal synthesis) and 20 mg of water in a large Pt capsule (1" long 3.5 mm I.D.). Gd concentration in the original liquid was 1500 ppm and the experiment duration = 20D. Grain sizes were 1-20μ. Results for two experiments gave values of 2.8 and 1.0 for $[Gd]_S/[Gd]_L$ as compared to Cullers' values of $\sim$50. These lower values agree well with data plotted on Figure 1b using diopside previously synthesized from an anhydrous oxide melt. The large differences in SDT results between this study and Cullers' remain to be resolved. Oxide mix synthesis results for similar conditions are in closer agreement (Cullers $\sim$50, this paper $\sim$20).

Changing the composition of the liquid phase during partitioning experiments can be informative with regard to the nature of possible substitution mechanisms.

According to reaction (1) of Table 5, increasing the hydrogen ion concentration in the liquid should cause more Gd to

enter the solid phase. Measured $[Gd]_S/[Gd]_{Liq}$ should there-fore increase with decreasing solution   pH. As noted in Figures la, lb starting solution pH's of 1.5 and 5.5 give similar results. Only at S/L ratios of 1.0 do the values for pH 5.5 experiments appear to be definitely lower than for pH 1.5 (ODT case only). Neutral pH at 800°, 1Kb is approximately 6.0(Ganeyev and Rumyantsev, 1970). At supercritical conditions the dielectic constant of water is greatly reduced and this has been correlated with reduced solvent density. Strong elec-trolytes like HCl are most severely affected and the measured dissociation constant for HCl at 800°, 1 Kb is of the order of 3×10^{-7} (Frank, 1956). In effect, the conditions of P and T buffer the system's pH by keeping most of the added HCl in molecular form. For original pH = 5.5, water becomes a stronger acid than HCl at run conditions (see appendix). For original pH = 1.5, HCl and H_2O are of comparable strength, i.e. pH $\approx$ that of neutral water $(10^{-6}$ M). For T = 800°C, P = 1 Kb the concentration of free hydrogen ions is essentially constant at orig. pH = 1.5, 5.5 and in large excess to the concentration of _free_ gadolinium ions $(Gd_{Tot} = 5$ ppm or 3.3×10^{-5} M. By this argument, little or no change in $[Gd]_S/[Gd]_L$ would be expected as a function of initial solution pH.

Reaction (2) of Table 5 should be favored if the concen-tration of gadolinium ions becomes small compared to the num-ber of vacancies already existing in the solid. All crystals have some equilibrium concentration of cation and anion vacan-cies; the vacancy concentration is strongly dependent

on temperature. This equilibrium concentration of vacancies

may be calculated if one has an estimate of the ΔH of forma-

tion of the defects (see appendix). From Figure 4, measured

$[Gd]_S/[Gd]_L$ increase at original gadolinium concentration <1 ppm.

This effect has been noted by other researchers studying alter-

valent substitution mechanisms (Nassau and Broyer, 1962; M.I.T.

Chem. Dept. Annual Report, 1969). The concentration of free

Gd ions in the solutions or the ΔH formation of defects in

diopside are not known, but a calculation can be performed by

assuming that all the Gd is dissociated (upper limit) and that

the ΔH of defect formation equals that for NaCl, i.e., 2 eV

(minimum ΔH). Maximum values of Gd^{+3} and cation vacancies

are therefore compared. The resulting calculations show that

for 20 mg diopside, 20 mg solution at 800°C the number of va-

cancies exceeds the number of Gd ions at a gadolinium concen-

tration of 40 ppm (see appendix). If either ΔH defect or the

% of Gd dissociated in soln were known, it would be possible

to rigorously calculate the other.

Reaction (3) of Table 5 should be favored if sodium ions

are added to the original solution. Results from Figure 5

show increased uptake of Gd by the solid for original solutions

1 M in NaCl. Solid products from these experiments as well as

diopsides run with 1 M NaCl but no Gd were analyzed for sodium

content by neutron activation analysis. Results are shown in

Table 7. A number of facts emerge from this table. a) sodium

does not have the preference for diopside that Gd exhibits,

b) slightly more Na enters diopside in the presence of Gd,

Table 7

Sodium-Gadolinium Correlations

(ppm)

Exp	$[Na]_{liq}^{orig}$	$[Gd]_{liq}^{orig}$	$[Na]_{solid}$	$[Gd]_{solid}$	$[Na]^{s}/[Na]^{liq}$	$[Gd]^{s}/[Gd]^{liq}$
SDT Blank	23,000	0	185	0	.008	0
SDT 41	23,000	5	250	4.76	.011	20
SDT 21	0	5	0	4.53	0	10
ODT Blank	23,000	0	250	0	.011	0
ODT 118	23,000	5	280	4.975	.012	200
ODT 116	23,000	5	297	4.975	.012	200
ODT 96'	0	5	0	4.95	0	100
ODT 97'	0	5	0	4.95	0	100

c) on an atomic basis, many more atoms of additional Na enter diopside per atom of additional Gd incorporated. Sodium-Gd coupling does not seem to be a very efficient means of increasing the bulk amount of incorporated Gd.

Reactions (1), (2), (3) of Table 5 all should be suppressed by addition of excess Ca^{+2} ion to the reaction solution. From Figure 5, this is clearly the case for ODT experiments but not so clear for SDT experiments. Excess Ca^{+2} ions in the solution should suppress the solubility of diopside by reducing the amount of Ca ions leached from the structure. Uptake of Gd during stage 1 solubility-exchange should therefore be reduced.

The influence of partial pressures of CO_2 in the volatile phase is an important geologic variable since diopsides are commonly found in metamorphosed carbonate-rich rocks. Also, carbonatite minerals contain large quantities of rare earths as well as other unusual elements. On the basis of rare-earth mineral studies of pegmatites some investigators believe rare-earths may migrate in solution as fluoride or carbonate complexes (Kosterin,1959; Ganeyev, 1962; Mineyev, 1963). Formation of Gd carbonate complexes in solution should hinder uptake by the solid and reduce measured $[Gd]_S/[Gd]_L$. Limited results of CO_2 experiments using oxalic acid are inconclusive but it is unlikely that rare earth carbonate complexes are stable at 800° 1 Kb. Fluoride complexes of rare earths can be completely hydrolyzed in 30 minutes at 1000°C (Warf, Cline Tevebaugh, 1954). If increased P_{CO_2} increases the solubility
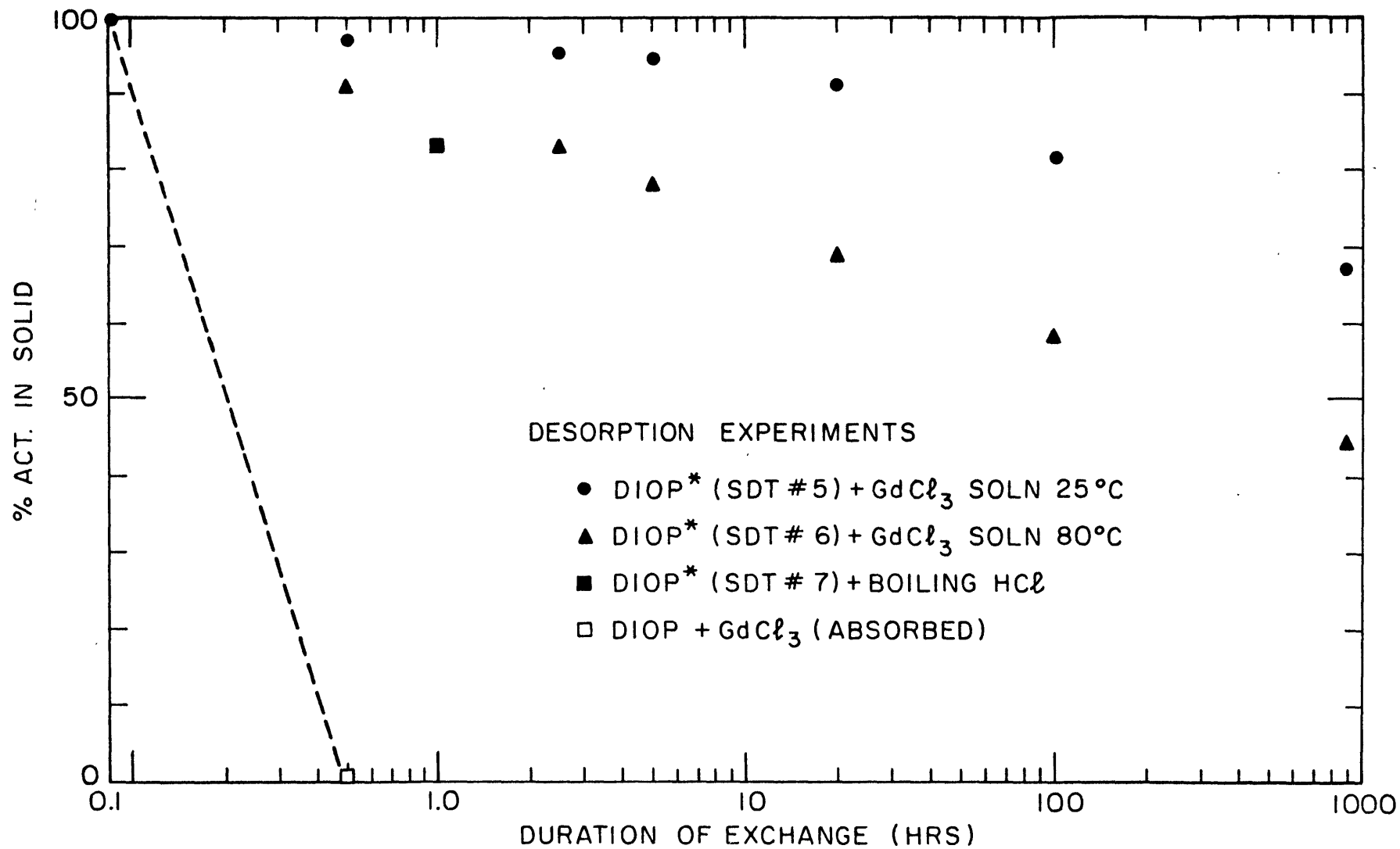
of diopside, measured $[Gd]_S/[Gd]_L$ should increase. It has been shown that at 25°C diopside is more soluble in CO_2-rich solutions (Keller, Balgord, Reesman, 1963).

Alternative Modes of Gd Uptake

In any study of partitioning of small amounts of material between phases, a major concern is the effect of possible impurity phases or non-substitutional takeup mechanisms. Such competing effects probably exist in any system and it is incumbent upon the investigator to show that their contributions are insignificant. The following discussion deals with some of the more obvious possible interferences and attempts to show how the previous results limit their importance.

Physical Adsorption: Gd^{+3} ions are strongly adsorbed onto surfaces at room temperature. Tracer solution deposited on diopside refused to yield any Gd to an aqueous solution at room temperature. Addition of .01M $GdCl_3$ carrier solution resulted in quantitative removal of the radioactive tracer, presumably by simple surface exchange. It was assumed, and later tested by the liquid yield experiment mentioned above, that addition of $GdCl_3$ carrier eliminated the effects of adsorption during quenching of experiments or subsequent separation procedures. The exchange properties of SDT run products in $GdCl_3$ solutions were measured and are presented in Figure 7. The tenacity with which the Gd is held by SDT products in the presence of $GdCl_3$ would argue against adsorption being a major effect. Adsorption is disfavored at high temperatures and does not explain the

Figure 7: Rates of desorption of Gd from tracer-doped SDT

products and from diopside containing only adsorbed

tracer.

DESORPTION EXPERIMENTS

- ● DIOP* (SDT #5) + GdCl₃ SOLN 25°C
- ▲ DIOP* (SDT #6) + GdCl₃ SOLN 80°C
- ■ DIOP* (SDT #7) + BOILING HCl
- ☐ DIOP + GdCl₃ (ABSORBED)

greater preference of diopside for Gd at high temperatures
(Cullers, 1970). Also adsorption would be expected to depend
on the surface properties (grain size, shape) rather than ad-
sorbant composition and this does not explain the high uptake
of Gd in diopside compared to quartz. An experimental run
using quartz instead of diopside gave a concentration ratio of
0.2.

Occlusion and Crack Trapping: Again, solid phase composi-
tion should not be an important variable if these processes are
important. The general reversability of the SDT and ODT reac-
tions would not be possible if these irreversible processes were
operative. The results for SiO_2, which offers no favorable
substitutional sites, probably represent expected magnitudes of
non-substitutional processes.

Formation of an Insoluble Gd-bearing Phase: If Gd is
partitioning between an aqueous solution and some small amount
of new Gd-bearing solid phase rather than diopside, then as
$[Gd]_{liq}^{orig}$ is increased, more of this phase precipitates and a
constant amount of Gd remains in solution, controlled by the
solubility of the new phase. Plots of concentration ratios vs.
$[Gd]_{liq}^{orig}$ would then have a strong positive slope reflecting the
constancy of Gd concentration in the liquid.

Partitioning with Other Impurity Phases: Special care was
taken in choice of pure starting materials and in mixing of
oxides to produce a diopside which was on composition. Run
products were checked by x-ray diffraction and optical methods.
Diopside synthesized from an oxide melt was cooled very slowly

to avoid formation of glass. Products of hydrothermal experiments equilibrated with pure water contained no spurious phases except a small amount (<.5 volume %) of silica beads identified as tridymite usually precipitated at one end of the reaction capsule. These were interpreted as formed by silica leaching of the charge followed by vapor transport and precipitation at the cooler end of the capsule. Any phase which grows contemporaneously with diopside will compete with diopside for Gd. The importance of this competition will depend on the amount of phase and the magnitude of its distribution coefficient with the aqueous phase. As noted, both of these factors are very small for the silica phase so the net result of a silica phase is that of a dilutent, giving measured $[Gd]^{diopside}/[Gd]_{liq}$ which are very slightly smaller than if the solid phase were 100% diopside. In the case of diopsides equilibrated with $CaCl_2$ salt solutions an additional solid phase can be produced according to the reaction

$$CaCl_2 + SiO_2 + H_2O \rightleftharpoons CaSiO_3\downarrow + 2HCl$$
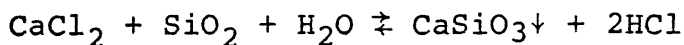
Up to 1 vol % of wollastonite is observed in run products from these experiments. Assuming a $[Gd]^{woll}/[Gd]_{liq}$ of 0 (an unlikely case for this Ca-bearing phase) the amount of wollastonite formed would not be enough to cause the measured decreases in $[Gd]^{diopside}/[Gd]_{liq}$ by the simple dilution effect. This effect may be contributory but is certainly minor. Measured concentration ratios for experiments substituting wollastonite for diopside were around 6-10. (See Table 8).

Table 8

Wollasonite Synthesis

T = 800°C $[Gd]_{liq}^{orig}$ = 5 ppm   Duration = 20 days

P = 1 Kb   S/L = 1.0

	$[Gd]_s/[Gd]_l$
OWT 1	6.99
OWT 2	7.9
OWT 3	7.4
OWT 4	6.8

Formation of Gd Complexes in Solution with Cl⁻ Anion: The
chloride anion is present in abundance in all the experimental
runs. Tracer is added as $GdCl_3$, solutions are acidified with HCl
and salt solutions added as chlorides. Addition of chloride
ion or some complex ion involving chloride to the solid phase
is considered unlikely because of the large size of such species
compared to sizes of possible substitutional sites. If gadoli-
nium chloride complexes form in solution, the complexed Gd
should be hindered from entering the solid, resulting in smaller
measured solid/liquid Gd concentration ratios. Complexing
could be used to explain the lowered ratios at high concentra-
tions of $CaCl_2$, but the variations with NaCl are in contradic-
tion to the expected trend. Also, no significant differences
were noticed as a function of HCl concentration. On the basis
of this data it would seem that the presence of chloride anion
in the solution has little effect on the partitioning of Gd.
If one wanted to press the explanation of the $CaCl_2$ effect as
due to complexing, a special mixed GdCa-Cl complex would have
to be postulated with no GdNa-Cl or GdH-Cl analogs.

Formation of Impurity Phases During Quenching: The ex-
perimental techniques and apparatus used did not permit with-
drawal of the liquid phase at experimental conditions. Rather,
experiments were rapidly quenched to room temperature and pres-
sure before phase separation and measurement. Treatment of
possible adsorption of liquid-phase Gd during quenching has been
discussed. Formation of new phases during quenching is an
additional problem which needs consideration. Such phases could

incorporate Gd which should belong in the liquid phase. The previous "equilibration" with diopside leaves only a small concentration of Gd in the liquid at quench time so uptake from the liquid during quench could increase the value of final measured concentration ratios. This effect is more serious than growth of impurities during a run because in the latter, diopside can compete very effectively for Gd but in the former it may behave as an inert phase.

Phases formed during a quench probably represent solids which have precipitated from solution as pressure and temperature are lowered. Solubility studies (Morey and Hesselgesser, 1951;   ) indicate that minerals like diopside or enstatite probably do not dissolve congruently but leach out silica in large excess of the other constituents. During early stages of dissolution, CaO and MgO may be leached more rapidly than silica (Luce et al., 1972) but at equilibrium, silica is the predominant dissolved species. The dissolved, and later precipitated, species is probably very silica rich with upper limits of possible solubility set at those for pure silica. For 800°C and 1 Kb this is around .3 wt % dissolved silica/wt of liquid phase (Morey and Hesselgesser, 1951).

The speed of the quenching and precipitate formation probably does not allow uptake by substitutional equilibrium. As noted above, silica has a very low preference for Gd under such conditions. An upper limit for a possible distribution coefficient for a silica-rich quench phase liquid = 1.0, representing simple entrapment of liquid phase. Using a distribution

coefficient of 1.0 and abundance of .3 wt % for the quench phase, one may calculate the effect on liquid concentrations and the final measured Gd concentration ratios. The results show a change in measured D.C. of less than 1% (see appendix). Increasing the quench/liquid distribution coefficient to 10 results in ~10% variation in final solid/liquid concentration ratio. It seems unlikely that the variation observed for $[Gd]_S/[Gd]_L$ with solid/liquid ratio and grain size can be ascribed to formation of quench phase unless D.C. quench/liquid is of the order of 100-1000. This could only be the case if Gd was intimately associated with silica while in solution, as some Gd-silica complex, and the two precipitated together. Again, the low $[Gd]_S/[Gd]_L$ values for the system silica/water would not support the existence of precipitated Gd-silica complexes.

Reaction with Capsule Walls: Platinum capsules were chosen because of their general chemical inertness and strength at experimental conditions. Remnant, non-exchangable radioactivites on capsule walls were measured for a few experiments and were always less than .1% of the total activity. As long as the capsule equilibrated with the liquid during the experiment, it should have no effect on Gd partitioning between diopside/liquid.

Additional Evidence for Substitution: Independent evidence for the substitutional nature of rare-earth incorporation in diopside can be obtained by electron spin resonance studies of rare-earth-doped single crystals. Interpretation of spectra requires some skill but such information can lead to the

understanding of distribution and symmetry of substitutional sites as well as charge balancing mechanisms. ESR studies have been performed on calcium tungstate grown from a melt containing Ce_2O_3 (Nassau, 1963). Results indicated that Ce occupied substitutional sites coupled with a cation vacancy or Na^{+1} impurity. ESR studies of Gd-doped diopside indicate that incorporation of Gd^{+3} is at a normal structural site (Cullers, personal communication).

Future Work

Possible future work on the kinetics of rare earth incorporation in diopside could include a detailed investigation of the effects of capsule size. No effect is expected since capsules should collapse to conform to the volume of the solution at experimental temperature and pressure. Larger capsule volumes would allow for measurements of X_{CO_2} over a large range using the oxalic acid technique. Other rare earths could be studied for differential rates of uptake as a function of ionic radius. Finally the effects of varying solid composition along the $CaMgSi_2O_6-FeMgSi_2O_6$ join could be investigated. Use of iron-bearing compounds would require strict oxygen buffering to control the Fe^{+2}/Fe^{+3} ratio. Presence of a competing altervalent cation Fe^{+3} can influence the partitioning of Gd^{+3} primarily in the case of substitution by vacancy formation (McIntire, 1963).

Conclusions

An experimental study of the partitioning of Gd cation in

the system diopside/water as a function of a number of experimental variables has led to the following conclusions:

1) Measured concentration ratios of Gd in the separated phases do not represent equilibrium partitioning of Gd between phases which have homogeneous distributions of Gd. Depending on the nature of the solid diopside (previously synthesized vs. simultaneous growth), Gd will be zoned in the solid with higher concentrations at the edges or center respectively.

2) Incorporation of Gd tracer in diopside is believed to involve a two-stage mechanism a) exchange of Gd for cations at the solid/liquid interface, b) modification of initial partitionings as Gd diffuses through the bulk of the crystal in response to existing concentration gradients. Conditions which increase the size of the leached layer relative to the size of the solid to be equilibrated or increase the rate of diopside growth from an oxide mix by increasing the rate of solution of the oxides, enhance the rate of uptake of Gd.

3) An estimated maximum value of the diffusion constant of Gd in diopside is equal to 2.5×10^{-15} cm^2 sec^{-1}.

4) Likely substitution mechanisms involve replacement of two calcium cations by a gadolinium cation coupled with hydrogen or sodium cation or exchange of 2 Gd^{+3} for 3 Ca^{+2} with the formation of a cation vacancy in the solid.

5) Care should be taken in attempting to study distribution coefficients by experimental methods. Nernst-type bulk equilibrations are difficult to attain in silicate/water systems because of slow diffusion rates.

6) Results support the observations of high rare-earth contents in calcium-bearing minerals correlated with trace element rich volatile phases (skarns, carbonatites).

Solid/Liquid Table

T = 800°C; P = 1 Kb; Grain Size = 10μ

Exp #	pH	[Gd]$^{liq.}_{orig.}$ (ppm)	Duration (days)	S/L	D.C.
ODT 25	1.5	5.0	12	4.10	23.6
ODT 26	1.5	5.0	20	3.96	20.4
ODT 5	5.5	5.0	17	4.00	15.1
ODT 6	5.5	5.0	17	4.22	14.2
ODT 28	1.5	5.0	20	3.00	33.5
ODT 29	1.5	5.0	20	2.96	32.0
ODT 18	1.5	5.0	12	3.27	30.8
ODT 19	1.5	5.0	12	3.09	35.0
ODT 10	5.5	5.0	12	3.13	21.4
ODT 42	5.5	5.0	20	3.03	20.7
ODT 9	5.5	5.0	12	2.51	27.8
ODT 16	1.5	5.0	20	1.85	32.6
ODT 24	1.5	5.0	20	1.98	60.8
ODT 27	1.5	5.0	12	2.07	43.2
ODT 17	1.5	5.0	20	1.62	56.1
ODT 49	5.5	5.0	20	1.00	55.5
ODT 15	5.5	5.0	20	1.01	53
ODT 48	5.5	5.0	20	1.00	55.7
ODT 20	1.5	5.0	12	0.95	106
ODT 45	1.5	2.5	20	1.03	103
ODT 55	1.5	2.5	12	1.03	81
ODT 62	1.5	1.25	20	1.00	107
ODT 63	1.5	1.25	20	1.00	126
ODT 67	1.5	2.5	20	0.99	104
ODT 69	1.5	2.5	20	0.98	72
ODT 71	1.5	5.0	20	0.99	112
ODT 74	1.5	5.0	20	0.98	125
ODT 76	1.5	5.0	20	1.18	85
ODT 77	1.5	5.0	20	1.00	82
ODT 34	1.5	5.0	20	0.50	200
ODT 35	1.5	5.0	20	0.50	291
ODT 38	1.5	2.5	12	0.50	259
ODT 39	1.5	2.5	12	0.50	244

SDT

Solid/Liquid Table

T = 800°C, Grains ∿ 10μ, P = 1 Kb

Exp #	pH	$[Gd]_{orig.}^{liq.}$ (ppm)	Duration (days	S/L	D.C.
SDT 5	5.5	5.0	17	4.55	0.81
SDT 6	5.5	5.0	17	4.53	0.87
SDT 7	5.5	5.0	20	2.70	4.38
SDT 8	5.5	5.0	20	2.78	4.45
SDT 9	5.5	5.0	31	2.17	5.70
SDT 10	5.5	5.0	31	2.29	6.25
SDT 11	5.5	5.0	20	2.30	4.8
SDT 21	5.5	5.0	34	0.985	10.6
SDT 22	5.5	5.0	34	0.995	11.5
SDT 27	1.5	2.5	20	1.01	8.6
SDT 28	1.5	2.5	20	1.01	10.7
SDT 65	1.5	2.5	20	0.510	15.7
SDT 66	1.5	2.5	20	0.492	19.5
SDT 11	5.5	5.0	20	0.292	10.6

SDT

Grain Size Table

T = 800°C; P = 1 Kb; Duration = 20 days; [Gd] = 2.5 - 5.0 ppm

Exp #	Avg Grain Size (μ)	S/L	D.C.
SDT 65	10	0.510	15.7
SDT 66	10	0.495	19.5
SDT 14	5	0.555	20.0
SDT 19	3	0.480	23.0
SDT 20	3	0.528	26.0
SDT 27	10	1.01	8.60
SDT 28	10	1.01	10.7
SDT 15	5	1.01	15.5
SDT 7	10	2.70	4.38
SDT 8	10	2.78	4.45
SDT 16	5	2.06	6.7
SDT 29	3	1.99	10.6
SDT 30	3	2.06	9.8

Run Duration Table

T = 800°C; Grains = 10μ; P = 1 Kb; pH = 1.5; S/L = 1.0

Exp #	Run Duration (days)	D.C.
SDT 63	1	13.4
SDT 64	1	14.6
SDT 96	1	13.5
SDT 97	1	12.0
SDT 94	4	8.9
SDT 95	4	9.1
SDT 27	20	8.6
SDT 28	20	10.7
SDT 21	34	10.6
SDT 22	34	11.5
SDT 85	50	13.5
SDT 86	50	18.7
SDT 51	70	22.8
ODT 112	1	>250
ODT 113	1	>250
ODT 20	12	106
ODT 55	12	81.0
ODT 30	12	120
ODT 45	20	103
ODT 67	20	104
ODT 69	20	72.0
ODT 71	20	112
ODT 74	20	125
ODT 77	20	82.0
ODT 83	70	152
ODT 84	70	80.0

Gd Concentration Table

T = 800°C; Duration = 20 days; P = 1 Kb; S/L = 1.0

exp #	[Gd]$^{liq.}_{orig.}$ (ppm)	ppm Solid	ppm Liquid	D.C.
ODT 64	0.25	>0.2488	<0.0012	>200
ODT 65	0.25	>0.2488	<0.0012	>200
ODT 110	0.50	0.4973	0.0027	183
ODT 111	0.50	0.4962	0.0038	129
ODT 62	1.25	1.238	0.012	107
ODT 63	1.25	1.240	0.010	126
ODT 75	2.50	2.476	0.024	103
ODT 55	2.50	2.470	0.030	81.0
ODT 67	2.50	2.476	0.024	104
ODT 69	2.50	2.466	0.0342	72.0
ODT 74	5.0	4.960	0.0397	125
ODT 76	5.0	4.942	0.058	85.0
ODT 77	5.0	4.940	0.060	82.0
ODT 115	150	148.4	1.60	90.0
ODT 81	750	741.1	8.90	83.0
ODT 82	750	742.6	7.40	100
ODT 88	1500	1456.4	43.60	33.0
ODT 89	1500	1467.8	32.20	46.0
SDT 69	0.50	0.4755	0.0245	19.4
SDT 70	0.50	0.4737	0.0263	18.0
SDT 67	1.25	1.1491	0.101	11.4
SDT 68	1.25	1.169	0.081	14.5
SDT 27	2.50	2.240	0.260	8.60
SDT 28	2.50	2.287	0.213	10.7
SDT 21	5.0	4.569	0.431	10.6
SDT 22	5.0	4.60	0.40	11.5
SDT 81	375	340.6	34.4	9.90
SDT 82	375	349.0	26.0	13.4
SDT 88	750	700.3	49.7	14.1
SDT 90	1500	1323.5	176.5	7.5

Liquid Comp. Table

T = 800°C; pH = 1.5; Grains = 10µ; P = 1 Kb; S/L = 1.0; 20 days

Run #	Salt	Conc (M)	D.C.
SDT 27	H_2O	0	8.6
SDT 28	H_2O	0	10.7
SDT 23	$CaCl_2$	.01	9.8
SDT 24	$CaCl_2$	.01	10.6
SDT 25	$CaCl_2$	0.1	14.8
SDT 26	$CaCl_2$	0.1	13.8
SDT 37	$CaCl_2$	0.5	14.5
SDT 38	$CaCl_2$	0.5	10.5
SDT 31	$CaCl_2$	1.0	7.8
SDT 32	$CaCl_2$	1.0	6.8
SDT 47	$CaCl_2$	1.0	7.4
SDT 48	$CaCl_2$	1.0	8.2
SDT 41	NaCl	1.0	22.3
ODT 96'	H_2O	0	89.8
ODT 97'	H_2O	0	123
ODT 108	$CaCl_2$	.01	85.7
ODT 109	$CaCl_2$	.01	65.0
ODT 100	$CaCl_2$	0.1	56.6
ODT 101	$CaCl_2$	0.1	51.7
ODT 102	$CaCl_2$	1.0	28.1
ODT 103	$CaCl_2$	1.0	27.8
ODT 106	NaCl	1.0	249
ODT 116	NaCl	1.0	248
ODT 117	NaCl	1.0	281
ODT 118	NaCl	1.0	212

Appendix

Diffusion Calculations

The equation used to calculate diffusion coefficients for the above experimental system is that given in Crank (1956 eqn. 6.30). It pertains to the diffusionally controlled uptake of solute from a well-stirred solution of limited volume into spherical particles. Concentration of the solution is assumed always uniform and spheres are initially free of solute.

$$\frac{Mt}{M\infty} = 1 - \sum_{n=1}^{\infty} \frac{6\alpha(\alpha+1)e^{-Dq_n^2 t/a^2}}{9+9\alpha+q_n^2\alpha^2}$$

Mt = total amount of solute in spheres after time t.

M∞ = total amount of solute in spheres after infinite time.

D = diffusion constant

a = particle radius

$$\alpha = \frac{3V}{4\pi a^3 K}$$

V = volume of solution

K = solid/liquid distribution coefficient.

qn = non-zero roots of

$$\tan q_n = \frac{3q_n}{3+\alpha q_n^2}$$

Values of qn are tabulated for various values of α and amounts of fractional uptake by the solute. The value of α is related to the final fractional uptake by the following derivation.

V = volume of liquid $K = \frac{Cs}{Cl}$ $C\infty$ = final conc. in solid

$\frac{4}{3}\pi a^3$ = volume of solid   Co = orig. conc. in lqiuid

final amt. in liquid + final amt. in solid = original amt. in liquid.

$$\frac{VC\infty}{K} + \frac{4}{3}\pi a^3 C\infty = VCo$$

$$M_\infty = \frac{4}{3}\pi a^3 C_\infty \qquad\qquad \alpha = \frac{V}{\frac{4}{3}\pi a^3 K}$$

$$C_\infty \left(\frac{V}{K} + \frac{4}{3}\pi a^3\right) = VC_0$$

$$C_\infty = \frac{VC_0}{\left(\frac{V}{K} + \frac{4}{3}\pi a^3\right)}$$

$$M_\infty = \frac{4}{3}\pi a^3 C_\infty = \frac{VC_0 \cdot \frac{4}{3}\pi a^3}{V + \frac{4}{3}\pi a^3 K/K}$$

$$M_\infty = \frac{VC_0}{1 + \frac{V}{\frac{4}{3}\pi a^3 K}}$$

$$M_\infty = \frac{VC_0}{1+\alpha}$$

$$\frac{M_\infty}{VC_0} = \frac{1}{1+\alpha} \tag{2}$$

for the sample calculation, the following values were used

$a = 5 \times 10^{-4}$ cm (microscopic estimate)

$t = 70$ days $= 6.05 \times 10^6$ sec

$\dfrac{[Gd]solid}{[Gd]liq} = 20$, $\dfrac{M_\infty}{VC_0} = .95$, so $\alpha = .05$

$\dfrac{Mt}{M_\infty} = .99$ for the limiting case assuming an equilibrium condition was established at 70 days.

$q_1 = 4.42$ from tables, with higher order terms neglected as they are small compared to experimental errors.

Solving equation (1) for D_{max} gives a value of $\sim 10^{-15} cm^2 sec^{-1}$ as the largest possible value since an equilibrium state was not reached at 70 days.

Lin and Yund (1971) discuss possible errors due to misestimates of average grain size, non sphericity of grains and non isotropic diffusion in complex crystal systems. They conclude

maximum expected errors from these sources should alter D by a factor of about 3. This allows for the effective radius to be a factor of 2 in error. Variation in solid/liquid ratio during their experiments was found to have no effect on the solid diffusion constants, in agreement with previous findings (Petrovic' and Skinner, 1971). The presence of high diffusivity paths along grain boundaries and microfissures cannot be ruled out but would required an even smaller value than the estimated D_{max} = $10^{-15} cm^2/sec$. The initial solubility-exchange surface equilibration postulated in this paper would be equivalent in effect to just such a high diffusivity path. It is expected that cumulative errors in the calculated D_{max} are heavily weighted to preference of an even smaller value of D_{max}.

There have been attempts to measure diffusion constants of ions in silicates and some of the results are presented in Table (6). Most of the data pertains to the alkali ions in open structures like feldspar or mica. Much less is known about altervalent ion diffusion. The data that exists suggests that values for altervalent diffusion may differ as much as a factor of 10 from values for isovalent ions of similar size (Shewmon, 1963). Also, diffusion is expected to be more size dependent in dense silicates like pyroxenes.

That the measured diffusion constant is really that of Gd and not some weighted mean of D_{Gd} and D_{Ca} is shown by the Nernst-Plank equation for the special case when one of the exchanging ions is present in trace concentrations. For altervalent ion exchange the net flux of each ion is a sum of the normal diffusional

flux determined by concentration gradients and an electrical flux proportional to electrical gradients

$$Ji = Ji(diff) + Ji(elect)$$

$$Ji = -Di(grad\ Ci + \frac{ZiCiF}{RT}\ grad\ \phi) \tag{3}$$

R = gas constant   Di = diffusion const.

F = Farraday's constant   Ci = conc.

Zi = ion charge ϕ = electrical potential gradient

electroneutrality in the crystal at all times requires

ZACA + ZBCB = conc. of fixed charges = const.

$$ZAgrad\ Ca + ZB\ grad\ CB = 0 \tag{4}$$

the number of equivalents of charge leaving = number entering the solid

$$ZAJA + ZBJB = 0 \tag{5}$$

for ions A and B of different charge

$$ZAJA = -ZADA\ (grad\ CA + \frac{ZACAF}{RT}\ grad\ \phi) \tag{6}$$

$$ZBJB = -ZBDB\ (grad\ CB + \frac{ZBCBF}{RT}\ grad\ \phi) \tag{7}$$

solving 6, 7 simultaneously and using substitutions from 4, 5 one arrives at the relationship

$$JB = -grad\ CB \cdot DAB \tag{8}$$

$$DAB = \frac{Z^2BDADBCB + Z^2ADADBCA}{DBZ^2BCB + DAZ^2ACA} \tag{9}$$

For the case where $CB \ll CA$, DAB = DB

Hydrogen Ion Concentration Calculations

For H_2O at P = 1 Kb, T = 800°C $K_w \simeq 10^{-12}$ $[H^+] = 1 \times 10^{-6}M$

For HCl at P = 1 Kb, T = 800°C $K_{diss} \simeq 3 \times 10^{-7}$

For Gd = 5 ppm = $3.3 \times 10^{-5}M$ Gd

pH = 1.5

$$[H^+]^{1\ bar}_{25°C} = [HCl]^{1\ Kb}_{800°} = 10^{-1.5}M = .31 \times 10^{-2}M$$

$$K_{diss} = \frac{[H^+][Cl^-]}{[HCl]-[H^+]}$$

a) assume $[H^+] \simeq [Cl^-]$

b) assume $[HCl] \gg [H^+]$

$$K_{diss} \simeq \frac{[H^+]^2}{[HCl]}$$

$$[H^+] = \sqrt{K_{diss} \cdot [HCl]}$$

$$\underline{[H^+] = 3.2 \times 10^{-5}\ M}$$

Neutral water $[H^+] = 1 \times 10^{-6}M$

Gd (100% diss) = $3.3 \times 10^{-5}M$

pH = 5.5

$$[H^+]^{1\ bar}_{25°} = [HCl]^{1\ Kb}_{800°} = 10^{-5.5} = .31 \times 10^{-6}\ M$$

$$K_{diss} = \frac{[H^+]^2}{[HCl]-[H^+]}$$

$$3 \times 10^{-7} = \frac{[H^+]^2}{(.31 \times 10^{-6})-[H^+]}$$

$$\underline{[H^+] = 1.9 \times 10^{-7}M}$$

Neutral water $[H^+] = 1 \times 10^{-6}\ M$

Gd (100% diss) $= 3.3 \times 10^{-5}M$

Vacancy Calculations

1. Assume vacancies are of Shottky type, i.e., $M_{1-\delta}X_{1-\delta}$ (Swalin, 1962).

2. Assume following equilibrium equation for Ca vacancy formation

$$CaMgSi_2O_6 \rightleftharpoons Ca_{1-\delta}MgSi_2O_{6-\delta} + V_{Ca} + V_O$$
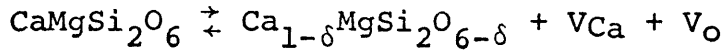
$$K_a = \frac{(^A Ca_{1-\delta}MgSi_2O_{6-\delta})\,(A_{V_{Ca}})\,(A_{VO})}{^A CaMgSi_2O_6}$$

3. Assume $^A Ca_{1-\delta}MgSi_2O_{6-\delta}$, $^A CaMgSi_2O_6 = 1$

$$K_a = (A_{V_{Ca}})(A_{VO}) = \delta V_{Ca} \delta V_O \cdot \gamma_{V_{Ca}} \gamma_{V_O}$$

4. Assume Henry's law behavior for vacancies so $\gamma_{V_{Ca}}$, γ_{V_O} = constants.

$$K' = (\delta_{V_{Ca}})(\delta_{V_O})$$

$$\delta x = \frac{\#\ \text{vacancies of X/crystal}}{\#\text{sites/crystal}}$$

$$K' = \delta\,V_{Ca}\,\delta V_O = e^{-\Delta G/Kt}$$

$$= e^{-\Delta H/Kt} \cdot e^{\Delta S/K}$$

5. Assume ΔS term is small for these solid-solid reactions

$$K' = e^{-\Delta H/Kt} = \delta\,V_{Ca}\,\delta\,V_O$$

$$\frac{\#\ \text{vacancies}}{cm^3} = \frac{\text{vacancies}}{xl} \cdot \frac{xl}{\text{sites}} \cdot \frac{\text{sites}}{cm^3}$$

$$= \delta \cdot \frac{\text{sites}}{xl} \cdot \frac{xl}{\text{sites}} \cdot \frac{\text{sites}}{cm^3}$$

$$= \delta \cdot \frac{\text{sites}}{cm^3}$$

$$[V_{Ca}] = \delta\,V_{Ca} \cdot \frac{\text{sites Ca}}{cm^3}$$

$$[V_O] = \delta\,V_O \cdot \frac{\text{sites O}}{cm^3}$$

$$[V_{Ca}][V_O] = \delta\,V_{Ca} \delta\,V_O \left(\frac{\text{sites Ca}}{cm^3}\right)\left(\frac{\text{sites O}}{cm^3}\right)$$

$$= e^{-\Delta H/Kt}\left(\frac{\text{sites Ca}}{cm^3}\right)\left(\frac{\text{sites O}}{cm^3}\right)$$

6. Assume pure crystal so $[V_{Ca}] = [V_O]$

$$[V_{Ca}]^2 = e^{-\Delta H/Kt} \left(\frac{sites\ Ca}{cm^3}\right) \left(\frac{sites\ O}{cm^3}\right)$$

20 mg $CaMgSi_2O_6$ $\qquad$ $\rho = 3.3$ grms/cm^3

$.092 \times 10^{23}$ sites Ca/cm^3

$.553 \times 10^{23}$ sites O/cm^3

7. Assume $\Delta H \approx$ typical value for shottky defect formation in ionic crystals

≈ 2 eV

$K = 8.616 \times 10^{-5}$ eV/deg

$T = 800°C = 1073°K$

$e^{-\Delta H/Kt} = 4 \times 10^{-10}$

$[V_{Ca}]^2 = (4 \times 10^{-10})(.553 \times 10^{23})(.092 \times 10^{23})$

$[V_{Ca}] = .45 \times 10^{18}$ vacancies/cm^3

$\qquad = 2.71 \times 10^{15}$ vacancies/20 mg diopside

20 mg of 40 ppm Gd solution = 3.12×10^{15} atoms of Gd

Effects of Quench Phase

For ease of illustration consider the following hypothetical values

    1) orig. wt. of Gd in the system = 100 grms

    2) wt diopside = wt. liquid = 20 grms

    3) $[Gd]^{diop}/[Gd]^{liq} = 100$

    4) $[Gd]^{quench}/[Gd]^{liq} = 1.0$

    5) .3 wt % of diopside dissolves in liquid = .06 grms

Step # 1 - Partitioning of Gd between diopside/liquid

    $[Gd]^{diop} = 100[Gd]^{liq}$

    x = grms of Gd in diopside

$$\frac{x}{19.94} = 100 \ (\frac{100-x}{20.06})$$

x = 99.004 grms of Gd in diopside

$$[Gd]^{diop} = \frac{99.004}{19.94} = 4.9651 \text{ grms Gd/grm diopside}$$

100-x = .9960 grms of Gd in liquid

$$[Gd]^{liq} = \frac{.9960}{20.06} = .049651 \text{ grms Gd/grm liquid}$$

Step #2 - Partitioning of Gd between quench/liquid

$$[Gd]^{quench} = [Gd]^{liq}$$

x = grms of Gd in quench phase

$$\frac{x}{.06} = \frac{.9960-x}{20.0}$$

x = .00298 grms of Gd in quench

$$[Gd]^{quench} = \frac{.00298}{.06} = .04966 \text{ grms Gd/grm quench}$$

.9960-x = .99302 grms of Gd in liquid

$$[Gd]^{liq} = \frac{.99302}{20} = .04966 \text{ grms Gd/grm liquid}$$

$$[Gd]^{total}_{solids} = \frac{\text{grms Gd}^{diop} + \text{grms Gd}^{quench}}{\text{wt. solid}} = \frac{99.004 + .00298}{20.0} =$$

4.9503 grms Gd/grm solid

$$D.C. = \frac{[Gd]^{total}_{solids}}{[Gd]^{liq}} = \frac{4.9503}{.04966} = 99.705$$

$$\Delta D.C.^{(\%)} = \frac{100.0 - 99.705}{100} \times 100 = .295\%$$

For case of $[Gd]^{quench}/[Gd]^{liq} = 10$

similar calculations give $\Delta D.C.$ (%) = 2.4%

Bibliography

Albarede, F., Bottinga, Y., Kinetic disequilibrium in trace element partitioning between phenocrysts and host lava. Geochim. Cosmochim. Acta 36, 141-156 (1972).

Crank, J., The mathematics of diffusion. London: Oxford University Press (1956).

Cullers, R.L., Medaris, L.G., Haskin, L.A., Gadolinium: Distribution between aqueous and silicate phases. Science 169, 580-583 (1970).

Eugster, H.P., Wones, D.R., Stability relations of the ferruginous biotite, annite. Jour. of Pet. 3, 82-125 (1962).

Foland, K.A., Giletti, B.J., Na, K and Rb diffusion in orthoclase (abs). A.G.U. tran. 53, no. 4, 557 (1972).

Franck, E.U., Hochverdichteter wasserdampf III, Z. Phys. Chem. N.F. Bd 8 Hf 3/4, 190-206 (1956).

Fyfe, W.S., Turner, F.J., Verhoogen, J., Metamorphic reactions and metamorphic facies, G.S.A. Mem #73 (1968).

Ganeyev, I.G., On the possible transport of matter in the form of complicated complex compounds. Geochem. Int. 1042-1049 (1962).

Ganeyev, I.G., Rumyantsev, V.N., Some properties of water at elevated pressures and temperatures. Geochem. Int. 708-715 (1969).

Holloway, J.R., Burnham, C.W., Millhollen, G.L., Generation of H_2O-CO_2 mixtures for use in hydrothermal experimentation. Jour. of Geophys. Res. 73, 6598-6600 (1968).

Keller, W.D., Balgord, W.D., Reesman, A.L., Dissolved products of

pulverized silicate minerals and rocks: part 1. Jour. Sed.

Pet. 33, 191-204 (1963).

Kosterin, A.V., The possible modes of transport for the rare

earths by hydrothermal solutions, Geochemistry Int. 381-387

(1959).

Lin, T.H., Yund R.A., Potassium and sodium self-diffusion in al-

kali feldspar, Contr. Mineral. and Petrol.34 177-184 (1972).

Lindner, R., Studies on solid state reactions with radiotracers,

J. Chem. Phys. 23, 410-411 (1955).

Luce, R.W., Bartlett, R.W., Parks, G.A., Dissolution kinetics of

magnesium silicates, Geochim. et Cosmochim. Acta 36, 35-50

(1972).

Masuda, A., Kushiro, I., Experimental determination of partition

coefficients of ten rare earth elements and barium between

clinopyroxene and liquid in the synthetic silicate system

at 20 kilobar pressure. Contr. Mineral. and Petrol. 26, 42-

49 (1970).

McIntire, W.L., Trace element partition coefficients - a review

of theory and applications to geology. Geochim. et Cosmochim.

Acta 27, 1209-1264 (1963).

Mineyev, D.A., On the behavior of lanthanides during alteration

of rare earth minerals. Geochem. Int. 684-693 (1962).

Misener, D.J., Cationic diffusion in Fe-Mg olivines at elevated

pressure and temperature (abs), Am. Geophys. Union Trans.541,

(1972).

Morey, G.W., Hesselgesser, J.M., The solubilities of some minerals

in superheated steam at high pressures, Econ. Geol. 46, 821-835 (1951).

Nassau, K., Calcium Tungstate III, IV, Trivalent rare earth substitution and the theory of coupled substitution, J. Phys. Chem. Solids 24, 1503-1517 (1963).

Onuma, N., Higuchi, H., Wakita, H., Nagasawa, H., Trace element partition between two pyroxenes and the host lava, Earth and Planet. Sci. Letters   47-51 (1958).

Petrovic' R., Skinner, B.J., Alkali ion exchange reaction between alkali feldspars and hydrothermal solutions: replacement vs. cation exchange (abs). G.S.A. Bull. 3, no. 7, 669 (1971).

Schnetzler, C.C., Philpotts, J.A., Partition of rare-earth elements between igneous matrix material and rock-forming mineral phenocrysts II, Geochim. et Cosmochim. Act 34, 331-340 (1970).

Shaw, C.W., Ph.D. thesis, U. Cal., 1955.

Shewmon, P.G., Diffusion in solids, McGraw-Hill (1963).

Sippel, R.F., Sodium self diffusion in natural minerals, Geochim. et Cosmochim. Acta 27, 107-120(1963).

Swalin, R.A., Thermodynamics of Solids, John Wiley & Sons, Inc. (1962).

Wager, L.R., Mitchell, R.L. Distribution of trace elements during strong fractionation of basic magma - a further study of the Skaergaard intrusion. Geochim. et Cosmochim. Acta 1, 129-208 (1951).

Warf, J.C., Cline, W.D., Tevebaugh, R.D., Pyrohydrolysis in the determination   of fluoride and other halides, Am. Chem. Soc. Anal. Chem. 26, 342-346 (1954).

Zielinski, R.A., Frey, F.A., Gough Island: Evaluation of a

    fractional crystallization model, Contr. Mineral. and Petrol.

    <u>29</u>, 242-254 (1970).

Biographical Note

Robert A. Zielinski was born in New York City on November 9, 1945. In 1952 his family moved to New Jersey and he graduated with honors from Fair Lawn New Jersey high school in 1963.

In September of that year he began studies towards a chemistry degree at Rutgers University - Newark campus. In 1964 he transferred to the main campus in New Brunswick, N.J. and graduated magna cum laude in 1967. While at Rutgers, he was elected to the chemistry and german honor societies and Phi Beta Kappa. He was also chosen as a Henry Rutgers scholar and received an award from the Merck company for his chemistry scholarship.

After a summer research job at Brookhaven National Labs., he began his studies in geochemistry at M.I.T. During his first year he was awarded an N.S.F. traineeship and subsequently was supported as a research and teaching assistant in the geology department.

Mr. Zielinski is a member of the American Chemical Society, the American Geophysical Union and Sigma Xi.

Acknowledgements